



UTDRO/STARS21 RESEARCH DAY 2024 *PROGRAM GUIDE*

UTDRO RESEARCH DAY – PROGRAM GUIDE

Table of Contents

Welcome Message	2
Keynote Speaker	3
Research Day Program	4 – 9
Abstracts (Oral)	10 – 34
Abstracts (Poster)	35 – 74
Abstracts	75 – 84

UTDRO RESEARCH DAY – CO-CHAIRS WELCOME

On behalf of the organizing committee, welcome to the University of Toronto, Department of Radiation Oncology (UTDRO) & STARS21 Research Day 2024!

UTDRO is excited to partner with the STARS21 Program once again this year, showcasing and celebrating the extraordinary work of our trainees who are undertaking radiation oncology, medical physics, radiotherapy, and basic radiation sciences in our department. We hope that this program will initiate thoughtful dialogue and foster new collaborations within the UTDRO & STARS21 clinical and academic communities. This Research Day is aimed at providing a cross-section of our research accomplishments and highlighting the diverse and innovative work in which our trainees have been involved over the past year.

We also welcome Dr. Cynthia Ménard, MD as our keynote speaker. Dr. Ménard is the Head of the Department of Radiation Oncology, Hospital Centre of the University of Montreal (CHUM) and is a full clinical professor, University of Montreal. She will give a Keynote Presentation on “Portraits from Data: Empowering Strides in Cancer Care”.

Finally, we would like to extend a special thanks to our UTDRO Chair, Dr. Laura Dawson as well as all faculty members, and UTDRO staff for their continued support and participation. We hope that you enjoy the program!

Sincerely,



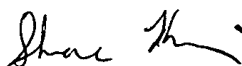
Michael Milosevic, MD, FRCPC
Professor and Vice Chair of Research, UTDRO



William T. Tran, MRT(T), MSc, PhD
Associate Professor, UTDRO



Anne Koch, MD, PhD, FRCPC
Associate Professor and
Co-Director, STARS21 Program



Shane Harding, PhD
Assistant Professor and
Co-Director, STARS21 Program

UTDRO RESEARCH DAY – KEYNOTE SPEAKER

Keynote Speaker:

Dr. Cynthia Ménard, MD



Dr. Cynthia Ménard received the M.D. degree from the University of Calgary, AB, Canada, in 1996. She completed her residency in radiation oncology at the University of Alberta, Edmonton, in 2001. She is currently the Chief of the Department of Radiation Oncology at the University of Montreal Hospital Center (CHUM), a Professor at the University of Montreal, and a Researcher at the CHUM Research Center. She is also a TECHNA member at the University of Toronto.

Previously, she was a Clinician Scientist in the Radiation Medicine Program at Princess Margaret Hospital, Toronto, ON, Canada, and an Associate Professor in the Department of Radiation Oncology at the University of Toronto. She pursued postgraduate research training as a Fellow in the Radiation Oncology Branch at the National Cancer Institute (NIH) until 2003.

Her research interests include radiation therapy through the development, validation, and clinical application of MRI techniques to radiation treatment planning, response assessment, and treatment adaptation. She has specifically invested her efforts in improving radiotherapy for patients with prostate cancer.

UTDRO/STARS21 PROGRAM SCHEDULE

Time	Session	Speakers	
8:30 – 9:00	Registration (30 mins)		
9:00 – 9:15	Cody Hall Welcome Remarks	Laura Dawson , UTDRO Chair Anne Koch/Shane Harding , Co-Directors of STARS21	
Cody Hall	Oral Presentations 1 (5 mins talk + 2 mins Q&A) Judges: Scott Bratman, Jay Detsky Moderator: Benjamin Lok		
# & Time	Title	Presenters	
#O1 9:15 – 9:22	Therapeutic Targeting of the TGF β Co-receptor Neuropilin-1 (NRP1) Attenuates the Contribution of M2-polarized Macrophages to Radiation-induced Lung Fibrosis	Lena Gockeln , <i>STARS21</i> Supervisor: Verena Jendrossek	
#O2 9:22 – 9:29	PRDX4 Loss Triggers Release of Cytosolic DNA and Inflammatory Gene Upregulation in Pancreatic Cancer	Emily Poulton , <i>STARS21</i> Supervisor: Marianne Koritzinsky	
#O3 9:29 – 9:36	Prospective Study of Local Relapse Patterns After MR-assisted Salvage HDR Prostate Brachytherapy	John Hudson , <i>Fellow</i> Supervisor: Hans T Chung	
#O4 9:36 – 9:43	Risk Factors for Developing Radiation Related Late Toxicities After Treatment for Head and Neck Cancers and Impact on Survival	John Mohan Mathew , <i>Fellow</i> Supervisor: Philip Wong, Jolie Ringash	
#O5*** 9:43 – 9:50	Clinical Outcomes of 3 vs 4 Fractions of MRI-guided Brachytherapy in Locally Advanced Cervical Cancer	Elizabeth Chuk , <i>Fellow</i> Supervisor: Kathy Han	
#O6 9:50 – 9:57	Dosimetric Predictors of Radiation Pneumonitis in Locally Advanced Non-Small Cell Lung Cancer Patients with Artificial-Intelligence Screened Interstitial Lung Disease	Hannah Bacon , <i>Oncology Resident</i> Supervisor: Andrew Hope, Patricia Lindsay	
Poster Discussion 1 (3 mins talk + 2 mins Q&A)			
# & Time	Title, Screen # – Poster #	Presenters	Judges
#P1-6 10:00 – 10:05	Investigating Micro-Environmental Changes in a Syngeneic Radio-Recurrent Prostate Cancer Model S1 – #P1	Stephanie White , <i>STARS21</i> Supervisor: Stanley Liu	David Kirsch Scott Bratman
	Characterizing the Microcirculatory System Using Light: Towards Studying the Effects of High-Dose Radiation Therapy in the Tumor Microcirculatory System S2 – #P2	Hector Alejandro Contreras Sanchez , <i>STARS21</i> Supervisor: Alex Vitkin, Edward Taylor	Anthony Lausch Catherine Coolens
	Cumulative Incidence of Sarcoma Brain Metastases: Report from a High-Volume Cancer Center S3 – #P3	Ayah Erjan , <i>Fellow</i> Supervisor: David Shultz	Jennifer Kwan Yat Tsang

	Pituitary Adenomas Treated with Gamma Knife Radiosurgery: A Retrospective Analysis within University Health Network S4 – #P4	Inhwa Kim, Oncology Resident Supervisor: Derek Tsang, Michael Yan	Jay Detsky Jennifer Croke
	MR-guided HDR brachytherapy boost in localized prostate cancer – results of a Phase II trial S5 – #P5	Carlton Johnny, Fellow Supervisor: Peter Chung	Phil Wong Jelena Lukovic
	Clinical Outcomes of Neuroendocrine Carcinoma of the Cervix: Retrospective Review from a Large Academic Cancer Center S6 – #P6	Jason Fernandes, Oncology Resident Supervisor: Jennifer Croke	Adam Gladwish Nauman Malik
#P7-12 10:10 – 10:15	The Contribution of Inflammasomes and cGAS-STING in RT-Induced Cell Fate S1 – #P7	Cindy Ha, STARS21 alumni Supervisor: Shane Harding	David Kirsch Scott Bratman
	Machine Learning based Quality Assurance Optimization of Breast Radiation Therapy Peer Review S2 – #P8	Christy Wong, MSc in Medical Biophysics Supervisor: Tom Purdie	Anthony Lausch Catherine Coolens
	Dosimetric Outcomes of SBRT to Ultracentral Lung Tumors: Lessons from the SUNSET Trial S3 – #P9	Rohan Salunkhe, Fellow Supervisor: Meredith Giuliani	Jennifer Kwan Yat Tsang
	Artificial Intelligence for Identification of Radiation-Related Toxicities from the Electronic Health Records of Patients with Head and Neck Cancer S4 – #P10	Faisal Alfadli, Oncology Resident Supervisor: Philip Wong	Jay Detsky Jennifer Croke
	Validating MR Hypoxia Detection in Prostate Cancer using pimonidazole and GLUT1 S5 – #P11	Martin Swinton, STARS21 Supervisor: Ananya Choudhury	Phil Wong Jelena Lukovic
	Prognostic Value of Baseline 18-FDG/PET Parameters for Disease Burden in Small Cell Lung Cancer S6 – #P12	Hillary Ho, BSc in MRS Supervisor: Benjamin Lok	Adam Gladwish Nauman Malik
#P13-18 10:20 – 10:25	Deciphering Radioresistance Mechanisms in Head and Neck Cancer: A Genome-Wide CRISPR Exploration S1 – #P13	Jacqueline Law, STARS21 Supervisor: Fei-Fei Liu	David Kirsch Scott Bratman
	Serial 4DPET/4DCT Imaging to Predict Long-term Response after Chemo-radiotherapy for Locally-advanced Non-small Cell Lung Cancer S2 – #P14	Daniel Tong, Fellow Supervisor: Jean-Pierre Bissonnette, Alex Sun	Anthony Lausch Catherine Coolens
	Exploring Family Physician Training Needs to Improve Cancer Patient Care S3 – #P15	Marissa Sherwood, Oncology Resident Supervisor: Meredith Giuliani	Jennifer Kwan Yat Tsang

	Reduction of Radiation Induced Bone Fracture Incidence Using Bone Avoidance Objectives for Radiotherapy Planning of Lower Extremity Soft Tissue Sarcoma: Retrospective Chart Review S4 – #P16	Hiba Othman, Fellow Supervisor: David Kirsch	Jay Detsky Jennifer Croke
	Therapeutic Index Improvement with Use of Rectal Spacer and Focal HDR Boost for Localized Prostate Cancer in an MR-guided Brachytherapy Setting S5 – #P17	Pradnya Chopade, Fellow Supervisor: Alejandro Berlin	Phil Wong Jelena Lukovic
	Investigating PLOD2 as a Therapeutic Target to Overcome Metastasis in Radiorecurrent Prostate Cancer S6 – #P18	Gavin Frame, Graduate Student Supervisor: Stanley K. Liu	Adam Gladwish Nauman Malik
10:25 – 10:55	Morning Break (30 minutes)		
Cody Hall	<u>Oral Presentations 2</u> (5 mins talk + 2 mins Q&A) Judges: Anne Koch, May Tsao Moderator: Catherine Coolens		
# & Time	Title	Presenters	
#07 10:55 – 11:02	Age As A Predictor For Vertebral Compression Fracture Following Spine Stereotactic Body Radiotherapy In Elderly Patients	Adrian Wai Chan, Fellow Supervisor: Jay Detsky	
#08 11:02 – 11:09	Impact of Post-operative Radiotherapy Neck Volume on Unstimulated Saliva Flow in Oral Cavity Squamous Cell Carcinoma	Claire Rooney, Fellow Supervisor: Andrew McPartlin	
#09 11:09 – 11:16	Treatment Toxicity And Outcomes Following Definitive Radiotherapy For Patients With Early-Stage Non-Small Cell Lung Cancers And Pre-Existing Interstitial Lung Disease – A Systematic Review	George Li, Oncology Resident Supervisor: Alexander Louie	
#O10 11:16 – 11:23	Outcomes and Characteristics of Patients Receiving Pre-operative Versus Post-operative Radiotherapy for Sinonasal Squamous Cell Carcinoma	Revadhi Chelvarajah, Fellow Supervisor: Ezra Hahn	
#O11 11:23 – 11:30	Stereotactic Ablative Radiotherapy for Ultra-Central Lung Tumors: Local Control and Toxicity from a Seventeen-Year Single-Institution Experience	Amir Safavi, Oncology Resident Supervisor: Meredith Giuliani	
#O12 11:30 – 11:37	Predictors of Vertebral Compression Fracture Following Spine Stereotactic Body Radiotherapy	Laura Burgess, Fellow Supervisor: Arjun Sahgal	
11:40 – 12:25 (35 mins talk + 10 mins Q&A)	<u>Keynote Address</u> Portraits from Data: Empowering Strides in Cancer Care	Cynthia Ménard, University of Montreal Introduction: Mike Milosevic	
12:25 – 1:25	Great Hall	Lunch (60 minutes)	

Poster Discussion 2 (3 mins talk + 2 mins Q&A)

# & Time	Title	Presenters	Judges
#P19-24 1:25 – 1:30	Computational and Experimental Investigation of the Applicability of X-ray PDT Using Gold Nanoclusters S1 – #P19	Catherine Coolens (present on behalf of: Etain Davidson, Medical Biophysics Supervisor: Catherine Coolens)	Alex Vitkin Ed Taylor
	Quantification of the Tumor Microvascular Response to Stereotactic Body Radiation Therapy Using Optical Coherence Tomography Angiography and Dynamic Contrast-enhanced MRI S2 – #P20	Jeff Zabel, STARS21 Alumni, PhD Student Supervisor: Alex Vitkin	Humza Nusrat Jeff Winter
	Leveraging Hybrid PET/MR Imaging to Distinguish Progression from Radionecrosis Post-radiosurgery S3 – #P21	Michael Maddalena, Medical Biophysics Graduate Student Supervisor: Catherine Coolens	Adam Gladwish David Hodgson
	Molecular Heterogeneity in Radiation Resistance and Metastatic Ability of NSCLC S4 – #P22	Marina Martínez Cruz, STARS21 Supervisor: Barbara Grüner	Shane Harding Kathy Han
	Spatial Dynamics of Cell States and the Tumour Microenvironment in Glioblastoma S5 – #P23	Phoebe Lombard, STARS21 Supervisor: Bradly Wouters	Mike Milosevic Jay Detsky
	Elucidating the Drivers of Tumour Hypoxia: a Focus on PDAC S6 – #P24	Ji Zhang, Graduate Student Supervisor: Brad Wouters	May Tsao Anne Koch
#P25-30 1:35 – 1:40	Investigating Interstitial Fluid Pressure: Analyzing Drug Transport through Cross Voxel Exchange Model and Dynamic Contrast Enhanced MRI S1 – #P25	Janny Kim, PhD in Medical Biophysics Supervisor: Catherine Coolens	Alex Vitkin Ed Taylor
	Automated Segmentation of Pancreatic Tumour Vascular in Optical Coherence Tomography Images S2 – #P26	Héctor A. Contreras-Sánchez (present on behalf of: Elham Abouei, Researcher Supervisor: Alex Vitkin)	Humza Nusrat Jeff Winter
	Prostate External Beam Radiation Therapy Treatment Planning on Deep Learning Enhanced Diagnostic CT Imaging S3 – #P27	Aly Khalifa, PhD Student Supervisor: Thomas Purdie	Adam Gladwish David Hodgson
	CRISPR Screen of Druggable Targets in Small Cell Lung Cancer Identified ATM Inhibitor (AZD1390) as a Radiosensitizer S4 – #P28	Bell Wu, PhD Candidate Supervisor: Benjamin Lok	Shane Harding Kathy Han
	Synthesis and Characterization of Auger Electron (AE)-Emitting [197Hg]Hg-NS4-TCO-Panitumumab Radioimmunoconjugates S5 – #P29	Arthur Chu, STARS21 Supervisor: Raymond Reilly	Mike Milosevic Jay Detsky
	Identifying Immune Resistance Mechanisms in Locally Advanced Anal Cancer - Preliminary Results from the GRECIAN Study S6 – #P30	Robert Samuel, STARS21 Supervisor: Adel Samson	May Tsao Anne Koch

#P31-36 1:45 – 1:50	Characterization of a Dual-Energy CT Protocol for Radiation Treatment Planning S1 – #P31	Heather Young, Physics Resident Supervisor: Hedi Mohseni	Alex Vitkin Ed Taylor
	Evaluation of EZFluence for 2-field Breast Tangents Field-in-field Planning S2 – #P32	Jie (Jane) He, Physics Resident Supervisor: Mithunan Modchalingam	Humza Nusrat Jeff Winter
	Evaluation of Bladder Filling Variability for Cervical Cancer Patients Undergoing Radical Radiotherapy S3 – #P33	Claire Nelder, STARS21 Supervisor: Cynthia Eccles	Adam Gladwish David Hodgson
	Investigating NRF2-Mediated Radioresistance in HPV-Negative Head and Neck Squamous Cell Carcinoma Preclinical Models S4 – #P34	Aakshi Puri, PhD Student supervised by a UTDRO supervisor Supervisor: Scott Bratman	Shane Harding Kathy Han
	DNA Methylation Subgroup and CNV Mediates Response to Radiotherapy in Chordoma S5 – #P35	Andrew Ajisebutu, STARS21 Supervisor: Gelareh Zadeh	Mike Milosevic Jay Detsky
#P37-42 1:55 – 2:00	Comparison of Online Adaptation Strategies for Patients with Prostate Cancer Undergoing MR-Guided Radiation Therapy Using Dose Accumulation S1 – #P36	Iymad Mansour, Physics Resident Supervisor: Jeff Winter	Alex Vitkin Ed Taylor
	Physical Dose Validation of Dynamic Treatment for Gamma Knife Radiosurgery S2 – #P37	Benjamin Tham, Physics Resident Supervisor: Catherine Coolens	Humza Nusrat Jeff Winter
	Liver Cancer Volume Changes during MR Guided SBRT S3 – #P38	Aisling Glynn, Fellow Supervisor: Laura Dawson	Adam Gladwish David Hodgson
	Investigating the Role of Macrophages in Small Cell Lung Cancer to Enhance Immunotherapy Efficacy S4 – #P39	Jalal Mahmoud Kazan, Fellow Supervisor: Benjamin Lok	Shane Harding Kathy Han
	Investigating The Cell-Free Hydroxymethylome Of Small Cell Lung Cancer Patients Receiving Chemoradiation S5 – #P40	Janice Li, STARS21 Supervisor: Geoffrey Liu, Benjamin Lok	Mike Milosevic Jay Detsky

Cody Hall

Oral Presentations 3 (5 mins talk + 2 mins Q&A)

Judges: Anthony Lausch, Humza Nusrat

Moderator: Alexandra Rink

# & Time	Title	Presenters
#O13*** 2:05 – 2:12	Temporal Changes in Functional Magnetic Resonance Imaging for Cervical Cancer During Chemoradiotherapy	Mohammed Abdul-Latif, STARS21 Supervisor: Yat Man Tsang
#O14 2:12 – 2:19	Prognostic Factors for Local Failure and Overall Survival in Patients with Epidural Disease at the Cauda Equina Following Stereotactic Body Radiotherapy: A Clinical, Anatomic and Dosimetric Analysis	Sondos Zayed, Fellow Supervisor: Eric Tseng
#O15 2:19 – 2:26	Advancing OARs Dosimetric Accuracy in Cervical Brachytherapy: Near-to-Target-Aware Segmentation via Deep Learning	Ruiyan Ni, STARS21 + Graduate Student Supervisor: Alexandra Rink

#O16 2:26 – 2:33	Elekta Hounsfield Unit Calibration and 3D Printed Phantom for CBCT-Based Dose Calculation	June Cheng Baron , <i>Physics Resident</i> Supervisor: Catherine Neath
#O17 2:33 – 2:40	Quantifying Conventional and MR-Conditional Ionization Chamber Response in Clinical 1.5T and 0.35T MR-Linac Beams	Nathan Orlando , <i>Physics Resident</i> Supervisor: Arman Sarfehnia
#O18 2:40 – 2:47	Evaluating 3D Vane Sequence on Elekta Unity MR-Linac for ITV Contouring	Lingyue Sun , <i>Physics Resident</i> Supervisor: Brige Chugh
2:47 – 3:17	Afternoon Break (30 minutes)	
Cody Hall	Oral Presentations 4 (5 mins talk + 2 mins Q&A) Judges: Shane Harding, David Hodgson Moderator: Gang Zheng	
# & Time	Title	Presenters
#O19 3:20 – 3:27	Multicentre Prospective Validation of Integrated Molecular Classification of Meningiomas and Prediction of Recurrence Risk Using DNA Methylation	Alex Landry , <i>STARS21</i> Supervisor: Gelareh Zadeh
#O20 3:27 – 3:34	HPV-Seq Is Prognostic In p16-Positive Oropharyngeal Cancer (OPC): Independent Validation In A Large Prospective Cohort And A Secondary Analysis Of NRG-HN002	Eric Stutheit-Zhao , <i>Oncology Resident</i> Supervisor: Scott Bratman
#O21 3:34 – 3:41	Uncovering the Mechanism of HDAC3-Mediated Radiosensitization in Small Cell Lung Cancer	Ujas Patel , <i>STARS21 Alumni</i> Supervisor: Benjamin Lok
#O22 3:41 – 3:48	Cross-Cancer Analysis Reveals Distinct Pattern of Immune Modulation during Curative Radiotherapy: Preliminary Findings from the SCIPER Study	Badr Id said , <i>Oncology Resident</i> Supervisor: Michael Milosevic
#O23 3:48 – 3:55	Comparison of the Localisation of Phototheranostic PORPHYOSOME Nanoparticles in Rodent and Nonrodent Models of Prostate Cancer	Michael Valic , <i>STARS21</i> Supervisor: Gang Zheng
#O24 3:55 – 4:02	Determining DNA Damage Sensitivity and Synthetic Lethal Vulnerabilities of FBXO11 Loss in Small Cell Lung Cancer	Tony Yu , <i>STARS21</i> Supervisor: Benjamin Lok
#O25 4:02 – 4:09	Early Apparent Diffusion Coefficient (ADC) Changes During Concurrent Chemoradiation: An Imaging Biomarker for Treatment Response and Recurrence Prediction in Glioblastoma	Daniel Palhares , <i>Fellow + STARS21</i> Supervisor: Arjun Sahgal
4:10 – 4:25	Closing Remarks	Michael Milosevic , UTDRO Vice-Chair of Research
4:30 – 6:00	Great Hall	Wine and Cheese Social + Award Presentation

UTDRO/STARS21 RESEARCH DAY ABSTRACTS – ORAL PRESENTATIONS

Oral Presentations: Section 1

01 Therapeutic Targeting of the TGF β Co-receptor Neuropilin-1 (NRP1) Attenuates the Contribution of M2-polarized Macrophages to Radiation-induced Lung Fibrosis

Lena Gockeln, Anette Haak, Irene Bocci, Sandra Curras Alonso, Juliette Soulier, Charles Fouillade, Arturo Londoño-Vallejo, Martin Stuschke, Verena Jendrosseck, Florian Wirsdörfer

PURPOSE

Radiation-induced lung fibrosis (RILF) constitutes a dose-limiting side effect of thoracic radiotherapies, with limited treatment options. The underlying pathogenesis remains incompletely understood, but it is assumed that a sophisticated network of resident cells, immune cells (e.g., M2-polarized macrophages) and soluble mediators fosters the inflammatory and fibrotic lung tissue alterations. In this context, TGF β is considered as a pro-fibrotic key mediator. Here, we aimed to study the relevance of the TGF β co-receptor neuropilin-1 (NRP1) in radiation-induced lung fibrosis, with focus on the macrophage compartment.

METHOD

To unravel the relevance of NRP1 for RILF pathogenesis, a murine whole thorax irradiation model was applied. C57BL/6 mice received a single dose (12.5 Gy) whole thorax irradiation (WTI) and were additionally treated in the fibrotic phase (from week 16 post WTI onwards) with a small peptide inhibitor (A7R) for pharmacologic targeting of NRP1. At 25-30 weeks post irradiation, the fibrosis degree was assessed. Based on single cell RNA sequencing data and histological analyses, we identified pulmonary macrophages as potential target cells of NRP1 inhibition, which were further analyzed by histological and RT-qPCR analyses in A7R-treated mice. The effect of A7R on the M2 polarization of macrophages was investigated in detail in a surrogate in vitro model with bone marrow-derived macrophages (BMDMs).

RESULT

Treatment with the NRP1 inhibitor A7R ameliorated the degree of fibrosis, the expression of pro-fibrotic markers and TGF β protein levels in irradiated lungs. In vivo, NRP1 inhibition reduced the organization of pro-fibrotic M2-polarized macrophages in clusters and the mRNA expression of the M2 polarization marker arginase-1. In vitro, NRP1 was highly expressed on M2-like BMDMs and NRP1 inhibition mitigated the expression of M2 markers upon IL-4 stimulation. These results imply that NRP1 promotes the M2-polarization and organization of macrophages in RILF pathogenesis and that pharmacologic inhibition of NRP1 counteracts fibrosis development.

CONCLUSION

Based on our current investigations, we conclude that NRP1 has diverse therapeutically targetable functions in RILF pathogenesis, which include, but are not limited to the M2 polarization of pulmonary macrophages. Patients receiving thoracic radiotherapies might thus benefit from therapeutic targeting of NRP1 to attenuate normal tissue toxicities, ultimately allowing for the application of curative treatment doses.

UTDRO/STARS21 RESEARCH DAY ABSTRACTS – ORAL PRESENTATIONS

Oral Presentations: Section 1

02

PRDX4 Loss Triggers Release of Cytosolic DNA and Inflammatory Gene Upregulation in Pancreatic Cancer

Emily Poulton, Lucie Malbeteau, Marianne Koritzinsky

PURPOSE

Pancreatic Ductal Adenocarcinoma (PDAC) poses a formidable clinical challenge, urging the development of targeted therapies against its vulnerabilities¹. Elevated reactive oxygen species (ROS) levels in cancer cells creates dependence on ROS detoxification, offering a potential target². The peroxiredoxin (PRDX1-6) family of proteins metabolize hydrogen peroxide (H₂O₂), and our group unveiled that targeting PRDX4 in pancreatic cancer cells increases ROS and DNA damage, reduces proliferation, and increases survival of tumour-bearing mice³. Interestingly, other DNA damaging treatments, such as radiation, have been shown to prompt the release of DNA into the cytosol, triggering inflammatory immune responses mediated by the cGAS/STING pathway^{4,5}. The overarching goal of my project is to uncover whether disruption of redox balance results in immunogenic cytosolic DNA and determine whether this can be coupled with radiation to enhance pro-inflammatory immunity signalling in pancreatic cancer cells.

METHOD

Doxycycline-inducible shRNA was used to knockdown (KD) PRDX4 in human PDAC cells, and cytosolic DNA was observed through immunofluorescence (IF) using an antibody targeting double-stranded DNA. Cells were treated with 8Gy of radiation followed by IF to assess the differences between groups. Next, we used RT-qPCR of inflammatory genes to assess mRNA upregulation post-PRDX4 depletion. To determine whether the cGAS/STING pathway is involved in mediating inflammatory genes upon PRDX4 loss, we used siRNA and specific inhibitors for cGAS (G140) and STING (H151) and assessed the consequences on genes previously tested using RT-qPCR.

RESULT

Strikingly, IF experiments showed notable accumulation of cytosolic double-stranded DNA post-PRDX4 depletion and 8 Gy of radiation. Differences emerge between these conditions, with radiation inducing increased micronuclei formation and PRDX4 loss resulting in heightened levels of free cytosolic DNA. Cytosolic DNA release is observed as early as 2 days following PRDX4 loss and continues to be detected for more than 8 days. Additionally, it appears as though PRDX4 loss triggers release of more cytosolic DNA overall compared to 8Gy radiation.

Moreover, we have pinpointed that PRDX4 depletion significantly increases inflammatory genes including CCL5, CCL20, CXCL10, ISG54, and OAS1. Inhibition and KD of cGAS or STING significantly reduces upregulation of these same targets, revealing that this upregulation is partially dependent on cGAS/STING pathway. However, the data also indicate that other DNA sensing mechanisms are involved following PRDX4 loss.

CONCLUSION

Previous research has demonstrated that radiation stimulates the release of immune-activating cytosolic DNA, primarily in the form of micronuclei⁴. We have uncovered that disturbing redox homeostasis through PRDX4 loss similarly triggers the release of cytosolic DNA, although in a different form. Additionally, in the absence of PRDX4, specific inflammatory genes are upregulated, partially through the cGAS/STING pathway. This is relevant within the context of pancreatic cancer where radiation as monotherapy shows striking resistance⁶. We herein unveil that perturbation of redox homeostasis presents a novel approach to activating innate immunity signalling in hard-to-treat cancer cells and shows potential for enhancing tumor cell death when combined with radiation therapy.

UTDRO/STARS21 RESEARCH DAY ABSTRACTS – ORAL PRESENTATIONS

Oral Presentations: Section 1

03

Prospective Study of Local Relapse Patterns After MR-assisted Salvage HDR Prostate Brachytherapy

John M Hudson, Gerard Morton, Andrew Loblaw, Chia-Lin Tseng, Moti Paudel, Melanie Davidson, Matt Wronski, Masoom Haider, Andrea Deabreu, Hans T Chung

PURPOSE

Salvage high dose rate (HDR) prostate brachytherapy (BT) is a treatment option for patients with intra-prostatic recurrent prostate cancer after prior radiation. This study explores the relapse patterns and dosimetry of the patients who had recurrent/persistent disease on post-salvage mpMRI follow-up after whole-gland (WG) or focal-gland (FG) MR-assisted salvage HDR prostate brachytherapy.

METHOD

Eligible patients had a biopsy and staging confirmed localized prostate cancer who relapsed >30 months after primary BT and/or external radiotherapy. Ultrasound (US)-based HDR BT was performed with either cognitive fusion and/or deformable registration between a diagnostic mpMRI and US images. FG prescription dose was 27Gy in 2 fractions, 1-2 weeks apart, to the dominant intra-prostatic lesion (DIL) with a 3-5mm expansion. WG prescription dose was 21Gy to the entire prostate and 27Gy to the DIL if present (3-5mm expansion) in 2 fractions. All patients underwent pre- and 1–2-year post-salvage mpMRI to assess response. Adjuvant androgen deprivation therapy (ADT) was not used. We analyzed the subset of patients with recurrent/persistent disease on the post-salvage mpMRI (PIRADS \geq 4). Deformable registration between the post-salvage DIL and the original plan was performed using MIMvista software to calculate the received dosimetry of the treated site and identify geometric patterns of recurrence.

RESULT

Sixty patients (median 73 years) were treated with salvage HDR (WG n=30, FG n=30). The overall median (range) pre-salvage HDR PSA for both cohorts was 4.24 ng/ml (0.63-11.63). The median time of the post-salvage mpMRI was 429 days (WG n=28, FG n=27). Sixteen recurrent/persistent lesions were identified: WG (n = 9): in-field = 6 (median V100 = 96%, median D90 = 33.2Gy), marginal = 3 (V100 = 62%, D90 = 23.3Gy), distant = 0; FG (n = 7): in-field = 3 (V100 = 99% D90 = 36.9Gy), marginal = 3 (V100 = 44%, D90 = 14.0Gy), distant = 1 (V100 = 17% D90 = 12.6Gy).

CONCLUSION

Our salvage FG and WG BT results suggest that most recurrent/persistent lesions on the post-salvage mpMRI were infield despite optimal dosimetric coverage (V27, D90). Alternate strategies for treatment intensification may need to be considered. Marginal recurrences were undercovered, which may suggest inadequate margins. Distant intra-prostatic recurrence was minimal in both cohorts, though this was likely limited by the timing of the mpMRI at 1-2 years post-salvage.

UTDRO/STARS21 RESEARCH DAY ABSTRACTS – ORAL PRESENTATIONS

Oral Presentations: Section 1

04 Risk Factors for Developing Radiation Related Late Toxicities After Treatment for Head and Neck Cancers and Impact on Survival

John Mohan Mathew, Jolie Ringash, Melanie Woodside, Jie Su, Scott Bratman, B.C. John Cho, Ezra Hahn, Ali Hosni Abdalaty, Andrew Hope, John Kim, Andrew McPartlin, Brian O' Sullivan, C. Jillian Tsai, John Waldron, Jennifer Kwan, Anna Spreafico, David Goldstein, Shao Hui Huang, Philip Wong.

PURPOSE

Identification of severe radiation-related late toxicity (RLT) risk factors in patients treated for head and neck cancers (HNCs) could guide mitigation strategies and follow-up routines. Impact of RLT on long term overall survival (OS) is also not well studied in HNC survivors.

We investigate potential predisposing factors and association with long term outcomes for patient with severe RLTs.

METHOD

We performed a retrospective case-control study, using data from our institutional prospective data systems. We included HNC patients treated from 2003 – 2020 who received radiation (RT) \geq 50 Gy without any treatment failure. Cases with either documented RTOG grade 3-4 RLT (\geq 6 months post-RT) in the data system, or referral to a specialized radiation late effects clinic were combined as RLT group. Those without documented RLT and follow-up of at least 2 years served as controls. In cases with multiple RLTs, the date of RLT was recorded at the 1st occurrence. Baseline characteristics were compared between cases and controls. Actuarial rates of LT and OS were calculated using competing risk and Kaplan-Meier methods, respectively. Multivariable logistic regression analyses (MVA) were performed to identify risk factors (odds ratio, OR) for RLT and prognostic factors (hazard ratio, HR) for OS.

RESULT

Our analysis included 4797 patients (1048 cases and 3749 controls), with a median follow-up of 5.5 years. The most common RLTs observed were: osteoradionecrosis (n=355), dysphagia +/- feeding tube dependence (n=196) and fibrosis (n=140) which represented two thirds (66%) of RLT. MVA identified the following potentially modifiable risk factors (OR) for RLT: use of non-IMRT technique [2.4 (1.9-3.0) p <0.001], neck RT [unilateral neck RT: 2.2 (1.5-3.2) p<0.001, bilateral neck RT 2.7 (1.9-3.9) p<0.001], >2Gy per fraction [1.5 (1.04-2.1) p=0.028], chemotherapy use [1.3 (1.1-1.6) p=0.009] and smoking at diagnosis [OR 1.2 (1-1.4) p=0.048]. Additional non modifiable risk factors include younger age [OR 0.99 per year (0.98-1.00) P=0.016], female sex [1.3 (1.1-1.5) p=0.01], advanced stage [TNM-7 stage II vs I: OR 1.6 (1.1-2.4) p=0.016, III vs I: 1.50 (1.01-2.2) p=0.045 and IV vs I: 1.7 (1.2-2.5) p=0.008 respectively] and primary site (vs oropharynx) [nasopharynx (OR 1.5 (1.2-2) p=0.001, oral cavity (2.3 (1.8-2.9) p<0.001) and hypopharynx (1.9 (1.3-2.7) p=0.002].

MVA for OS showed that RLT patients had higher mortality risk vs control group [HR 1.3 (1.1-1.6) p=0.001] after adjusting previously identified RLT risk factors and performance status.

CONCLUSION

We found non IMRT treatment technique, neck irradiation, dose per fraction >2 Gy, use of chemotherapy and being a smoker at diagnosis as significant modifiable risk factors. This information could be used to guide patient discussion, and select patients for RLT monitoring. If confirmed by prospective studies, these results could be used to develop risk-based treatment approaches and/or clinical trials of RLT prevention.

UTDRO/STARS21 RESEARCH DAY ABSTRACTS – ORAL PRESENTATIONS

Oral Presentations: Section 1

05 Clinical Outcomes of 3 vs 4 Fractions of MRI-guided Brachytherapy in Locally Advanced Cervical Cancer

Elizabeth YH Chuk, Candice Yu, Aba Anoa Scott, Zhihui Amy Liu, Michael Milosevic, Jennifer Croke, Anthony Fyles, Jelena Lukovic, Alexandra Rink, Akbar Beiki-Ardakani, Jette Borg, Jason Xie, Kitty Chan, Heather Ballantyne, Julia Skliarenko, Jessica L. Conway, Robert A. Weersink, Kathy Han

PURPOSE

MR-guided brachytherapy (MRgBT) is an essential component of the management of locally advanced cervical cancer, leading to excellent local control rates. However, MRgBT is also resource intensive. This study aimed to compare disease and toxicity outcomes in patients with locally advanced cervical cancer treated with a less resource intensive regimen of 24 Gy/3 fractions (Fr) versus the conventional 28 Gy/4Fr.

METHOD

This retrospective study included consecutive patients with FIGO 2018 stage IB-IVA cervical cancer treated with definitive chemoradiation between April 2014 - March 2021 in a large academic cancer centre. Patients with histologies other than squamous cell carcinoma, adenocarcinoma or adenosquamous carcinoma; those who did not receive cisplatin; or those who received palliative intent treatment were excluded. MRgBT fractionation transitioned gradually during the study period from 28 Gy/4Fr to 24 Gy/3Fr due to resource constraints and to improve patient experience.

Patient, tumour and treatment parameters, disease status and treatment-related toxicities were extracted from medical records. Continuous variables were compared using Wilcoxon's rank sum test; categorical variables, using Chi-squared test. Disease-free survival (DFS) was estimated using the Kaplan-Meier method and compared using the logrank test. Cumulative incidence of local failure (LF), and grade 2+ gastrointestinal (GI), urinary (GU) and vaginal toxicity were estimated using the cumulative incidence function with death as a competing risk, and compared using the Gray's test. For LF, distant metastasis was also counted as a competing risk. Statistical analyses were performed in R version 4.0.2. All tests were two sided, and p values < 0.05 were considered statistically significant.

RESULT

Of the 241 patients included for analysis, 101 (42%) received 24 Gy/3Fr and 140 (58%) received 28 Gy/4Fr. There were no significant differences in the distribution of histology, T category, or FIGO 2018 stage between the 2 groups. The 24 Gy/3Fr group was older, and had smaller tumor size at diagnosis and CTVHR at brachytherapy. The CTVHR D90% were similar between the 2 groups. The 24 Gy/3Fr group had significantly lower rectal D2cm3, small bowel D2cm3, bladder D2cm3 and ICRU rectovaginal point dose compared to the 28 Gy/4Fr group.

With a median follow up of 3.2 (range 0.2-9.2) years, there were 14 local, 41 regional nodal and 51 distant failures in 63 (26%) patients (simultaneous failures at different sites included). There were no significant differences between the 24 Gy/3Fr vs 28 Gy/4Fr group in 3-year DFS (77% vs 68%, p = 0.21), 3-year cumulative incidence of LF (5% vs 7%, p = 0.57), grade 2+ GI toxicity (11% vs 20%, p = 0.13), or grade 2+ vaginal toxicity (14% vs 17%, p = 0.48), respectively. The 3-year cumulative grade 2+ GU toxicity rate was significantly lower in the 24 Gy/3Fr group compared to the 28 Gy/4Fr group (9% vs 23%, respectively, p = 0.03).

CONCLUSION

Cervical cancer patients treated with 24 Gy/3Fr had similar DFS, LF, GI and vaginal toxicity rates, and lower grade 2+ GU toxicity rate compared to those treated with 28 Gy/4Fr. A less resource-intensive brachytherapy fractionation schedule of 24 Gy/3Fr is a safe alternative to 28 Gy/4Fr for definitive treatment of cervical cancer.

UTDRO/STARS21 RESEARCH DAY ABSTRACTS – ORAL PRESENTATIONS

Oral Presentations: Section 1

06 Dosimetric Predictors of Radiation Pneumonitis in Locally Advanced Non-Small Cell Lung Cancer Patients with Artificial-Intelligence Screened Interstitial Lung Disease

Hannah Bacon, Nicholas McNeil, Tirth Patel, Mattea Welch, Xiang Y. Ye, Andrea Bezjak, Benjamin H. Lok, Srinivas Raman, Meredith Giuliani, John Cho, Alexander Sun, Geoffrey Liu, Sonja Kandel, Chris McIntosh, Tony Tadic, Andrew Hope, Patricia Lindsay

PURPOSE

Purpose: Radiation pneumonitis (RP) is a common and potentially severe complication following radiotherapy for locally advanced non-small cell lung cancer (NSCLC). We previously reported on an artificial intelligence (AI) algorithm to identify patients with radiographic features of interstitial lung disease (ILD), and demonstrated that these patients are at greater risk of developing severe grade ≥ 3 (G3+) RP. In this work we evaluate dosimetric predictors of G2+ and G3+ RP in patients identified by our AI-ILD algorithm.

METHOD

Methods: All locally advanced NSCLC patients treated with conventionally-fractionated definitive radiotherapy at our institution from 2006-2021 with full dosimetric information available were assessed. RP data were prospectively collected and retrospectively reviewed. Dose volume histogram (DVH) data and clinical data were extracted from an institutional database. A convolutional neural network was previously developed and validated to identify patients with radiographic ILD. Planning CT scans for the retrospective cohort were used as input to the algorithm, with AI-ILD score as an output. AI-ILD scores above our established threshold were labeled as AI-ILD+. Univariate correlations between RP and dosimetric parameters including MLD (mean lung dose), Dx (minimum dose to x% volume) and Vx (% volume receiving at least xGy dose) were calculated using Spearman coefficients (R).

RESULT

Results: 498 patients were available for analysis. Of these, 141 (28%) were identified as AI-ILD+. Grade 2-5 RP was reported in 17%, 4.8%, 0% and 0.60% of all patients respectively. Grade 2-5 RP was reported in 14%, 7.1%, 0%, and 1.4% of AI-ILD+ patients respectively, compared to 18%, 3.9%, 0% and 0.28% of AI-ILD- patients. There was a higher MLD in the AI-ILD+ cohort (mean 16Gy, median 16Gy, IQR 13Gy-19Gy) compared to the AI-ILD- cohort (mean 15Gy, median 15Gy, IQR 12Gy-18Gy). Our previous multivariable analysis incorporating MLD showed a significant correlation between G3+ RP and AI-ILD status. When cohorts were dichotomized by AI-ILD threshold, we identified higher correlations between dosimetric parameters and G2+ and G3+ RP in AI-ILD+ patients. The Spearman coefficient (R) for the correlation between MLD and G2+ RP in AI-ILD+ patients was $R=0.25$ ($p=0.0015$), compared to $R=0.092$ ($p=0.041$) in AI-ILD- patients. Similarly for V20 and G2+ RP, $R=0.25$ ($p=0.0016$) for AI-ILD+ patients, compared to $R=0.092$ ($p=0.040$) for AI-ILD- patients. AI-ILD- patients demonstrated no significant correlations between MLD or V20 and G3+ RP. For AI-ILD+ patients, both MLD ($R=0.17$, $p=0.020$) and V20 ($R=0.14$, $p=0.044$) were significantly correlated with G3+ RP.

CONCLUSION

Conclusion: In summary, our AI-ILD algorithm identifies a subset of patients who have a greater correlation between dosimetric parameters and the development of G2+ and G3+ RP. This may motivate the application of lower dose constraints in this population to mitigate the increased risk of severe RP.

UTDRO/STARS21 RESEARCH DAY ABSTRACTS – ORAL PRESENTATIONS

Oral Presentations: Section 2

07 Age As A Predictor For Vertebral Compression Fracture Following Spine Stereotactic Body Radiotherapy In Elderly Patients

Adrian Wai Chan, K. Liang Zeng, Sten Myrehaug, Hany Soliman, Chia-Lin Tseng, Hanbo Chen, Eshetu G Atenafu, Arjun Sahgal, Jay Detsky

PURPOSE

Stereotactic body radiotherapy (SBRT) for spinal metastases improves local control and provides a higher rate of pain relief compared with conventional external beam radiotherapy (cEBRT). There is limited data on the risk of vertebral compression fracture (VCF) after spine SBRT and its predictors in the elderly. We aim to evaluate the risk of VCF, local failure (LF) and OS in the elderly patients treated with spine SBRT.

METHOD

A prospectively maintained institutional database of over 900 patients and 2300 vertebral segments treated with spine SBRT was reviewed. The primary endpoint was the VCF rate. Secondary endpoints included MRI-based LF and OS. Age as a continuous variable was used with binary partitioning methods to determine an age cut-off where the risk of VCF may start to increase.

RESULT

252 patients (580 segments) aged 70 or above were included. The median (range) age was 75.8 (70 – 90.3) years old. The rates of VCF at 12-month and 24-month were 8.4% and 12.4% respectively. VCF risk was similar between ages 70-75, 75-80 and 80-85 and ranged from 9.8% – 13.3% at 2 years. In those over 85.8, the risk of VCF jumped significantly to 30.3% at 2 years (95% CI: 14-38.7%, $p=0.0461$). On multivariable analysis, age ≥ 85.8 (HR = 2.3, 96% CI (1.12-4.54), $p=0.0220$), pre-existing vertebral body collapse (HR = 2.0, 96% CI (1.13-3.44), $p=0.0169$) and CTV D80 EQD2 ($\alpha/\beta=10$) ≥ 44 Gy (HR = 3.1, 96% CI (1.64-5.88), $p = 0.0005$) remained independent predictors for VCF. The median OS of the entire cohort is 20.3 months (95% CI: 14.7 – 25.2). Aged ≥ 85.8 is a predictor of poorer overall survival on multivariable analysis. The median OS of patients who were ≥ 85.8 -year-old or <85.8 -year-old were 14.3 months and 20.35 months respectively ($p=0.0375$). The age at treatment did not influence the local control.

CONCLUSION

Spine SBRT in elderly patients is safe and effective, with no increased risk of VCF until patients are 86 years and older (27% compared to 12% in younger patients). Overall, elderly patients treated with spine SBRT had reasonable overall survival, which suggests that a durable local control brought by SBRT will still be beneficial for this group of patients. These data may help to inform patient selection, counselling of treatment benefit or risks and decision of prophylactic vertebroplasty in the elderly.

UTDRO/STARS21 RESEARCH DAY ABSTRACTS – ORAL PRESENTATIONS

Oral Presentations: Section 2

08 Impact of Post-operative Radiotherapy Neck Volume on Unstimulated Saliva Flow in Oral Cavity Squamous Cell Carcinoma

Claire Rooney, Shao Hui Huang, Erin Watson, Michael Glogauer, Jie Su, Ali Hosni, Jonathan Irish, David Goldstein, John de Almeida, Scott Bratman, John Cho, Ezra Hahn, Andrew Hope, John Kim, Brian O'Sullivan, Jolie Ringash, Jillian Tsai, John Waldron, Anna Spreafico, Andrew McPartlin

PURPOSE

Hyposalivation is a common sequelae of oral cavity carcinoma (OSCC) surgery and post-operative radiotherapy (PORT). The relative contribution of both treatment modalities to long term xerostomia is poorly described. Quantification of the effect of bilateral neck PORT on saliva dysfunction can inform decisions regarding adjuvant PORT volumes. We compare change in unstimulated salivary function, measured via 3-minute modified Schirmer test (MST), in OSCC patients following an ipsilateral neck dissection (IND) stratified by PORT neck volumes.

METHOD

We reviewed a prospectively assembled cohort of OSCC patients who underwent IND with intensity modulated PORT between 2005-21 and who had a routine 3-minute MST measurement pre-RT and 6 and/or 12 months post-PORT. Change in saliva flow and prevalence of hyposalivation, (defined as MST <25mm) was compared by PORT neck volumes (bilateral vs unilateral/no). Multivariable linear regression analysis (MVA) was performed to identify predictors for hyposalivation.

RESULT

A total of 165 patients were eligible; 88 (53%) bilateral, 66 (40%) ipsilateral, and 11 (7%) no neck PORT. Baseline characteristics were similar between groups, except more N2b/N2c with bilateral PORT (60% vs 31%, $p<0.001$). Similar proportions had baseline hyposalivation after surgery prior to PORT (26% vs 28%, $p=0.97$). The median absolute change in MST (mm) compared to baseline was greater in the bilateral vs ipsilateral/no neck PORT at 6 (21 vs 5) and 12 (21 vs 0) months (both $p<0.001$). Hyposalivation occurred more in bilateral vs ipsilateral/no neck PORT at 6 months (90% vs 54%) and 12 months (90% vs 44%) (both $p<0.001$). MVA identified bilateral neck PORT and higher smoker pack-years as predictors for hyposalivation at 6/12 months (Table 1).

CONCLUSION

About a quarter OSCC patients have baseline unstimulated salivary hypofunction following IND prior to PORT. Rates of hyposalivation at 6- and 12-months post-PORT nearly doubles following bilateral neck PORT compared to unilateral or no neck PORT. Incidence of hyposalivation following bilateral PORT was stable at 6 and 12 months, suggesting little long term recovery of function. Further investigation with correlation of irradiation dosimetry to the salivary gland structures may help guide dose optimization strategies.

UTDRO/STARS21 RESEARCH DAY ABSTRACTS – ORAL PRESENTATIONS

Oral Presentations: Section 2

09

Treatment Toxicity And Outcomes Following Definitive Radiotherapy For Patients With Early-Stage Non-Small Cell Lung Cancers And Pre-Existing Interstitial Lung Disease – A Systematic Review

George J. Li, Melissa Sam Soon, Hanbo Chen, Gabriel Boldt, Houda Bahig, Patrick Cheung, David A. Palma, Christopher J. Ryerson, Suresh Senan, Alexander V. Louie

PURPOSE

Patients with interstitial lung disease (ILD) who develop lung cancer represent a unique challenge, as they are at a higher risk for serious toxicity from surgery, radiotherapy, and many systemic therapies. The aim of this study is to provide an up-to-date analysis on toxicities and outcomes associated with definitive radiotherapy in patients with ILD and early-stage non-small cell lung cancer (ES-NSCLC).

METHOD

We performed a systematic review in accordance with PRISMA guidelines. The PubMed (MEDLINE), EMBASE, and Cochrane Library databases were searched from inception until February 2024. Studies that included patients who underwent definitive radiotherapy alone for ES-NSCLC were included. All forms of radiotherapy, including proton and carbon ion therapy were included. Data including treatment-related toxicity, local control rates, and overall survival were collected and analyzed.

RESULT

Of the 3096 records reviewed, 24 studies were included for full data abstraction, with a minority (n = 4) being prospective. In total, 705 patients with stage 1-2 NSCLC were included, including both surgical and non-surgical candidates. Seventeen studies utilized photon-based radiotherapy (XRT), 4 carbon ion radiotherapy (CIRT), and 3 proton beam therapy (PBT), with each modality contributing to 81% (n = 574), 13% (n = 90), and 6% (n = 41) of included patients, respectively. Prescribed doses in BED10 ranged from 43 Gy to 180 Gy for XRT, and up to 300 Gy (RBE) for CIRT. Reporting of ILD subtype, severity, and pulmonary function testing were variable. Idiopathic pulmonary fibrosis accounted for 21% (n = 147) of patients, while a specific subtype was not reported for 71% (n = 502) of patients. Within the 11 studies reporting severity data, the majority of patients (65%) had mild ILD as defined by authors, while 26% and 9% had moderate and severe ILD, respectively. Eight studies reported median forced vital capacities ranging from 82-97% of predicted, and 5 reported median diffusing capacities for carbon monoxide ranging from 42-56% of predicted. The prevalence of severe (grade 3-5) treatment-related respiratory toxicity was 16.7% for XRT, 12.2% for CIRT, and 9.7% for PBT, while treatment-related mortality was 9.6% for XRT, 0% for CIRT, and 2.4% for PBT. The most commonly reported risk factor for respiratory toxicity (n = 6) was higher volume of lung receiving at least 5 Gy (V5), with two studies reporting cutoffs of 11.2% and 18%. Estimated local control at 3-years was 75.9%. Estimated overall survival at 3-years was 44.3%, with a median of 30.6 months.

CONCLUSION

There is a high risk of treatment-related toxicity and mortality for patients with ILD who receive definitive radiotherapy for treatment of ES-NSCLC. Future studies would benefit from consistent reporting of ILD details, which may help in risk stratification in this challenging clinical scenario.

UTDRO/STARS21 RESEARCH DAY ABSTRACTS – ORAL PRESENTATIONS

Oral Presentations: Section 2

10 Outcomes and Characteristics of Patients Receiving Pre-operative Versus Post-operative Radiotherapy for Sinonasal Squamous Cell Carcinoma

Revadhi Chelvarajah, Shao Hui Huang, Jie Su, Jolie Ringash, Ian Witterick, John de Almeida, Eric Monterio, Anna Spreafico, John Waldron, Brian O’Sullivan, Ali Hosni, Scott Bratman, MD, John Cho, Andrew Hope, John Kim, Andrew McPartlin, Jillian Tsai, Li, Tong, Wei, Xu, Ezra Hahn

PURPOSE

Resectable sinonasal squamous cell carcinoma (SNSCC) is often managed by surgery +/- post-operative radiation (postop-RT), guided by surgical pathology. In our institution, pre-operative radiation (preop-RT) has been used in select cases after multidisciplinary input due to advantages of lower dose and smaller/better defined volumes, especially important for disease adjacent to optic structures. We report our experience with preop-RT in SNSCC, focusing on oncologic outcomes and patient selection.

METHOD

All newly diagnosed SNSCC treated with preop-RT or postop-RT from 2005 to 2021 were included. SNSCC treated with surgery alone was excluded. Clinical characteristics and outcomes were compared between preop-RT vs postop-RT cohorts. Actuarial rates of overall survival (OS), disease-free survival (DFS), locoregional control (LRC), local control (LC), distant control (DC), and late toxicity were estimated.

RESULT

A total of 71 patients were eligible: 25 received preop-RT and 46 postop-RT. The preop-RT cohort comprised more ethmoid sinus primary sites (32% vs 0%, $p < 0.001$) and more T3-T4 diseases

(versus T1-2) at presentation (96% vs 65%, $p < 0.04$; mean tumor size 62 cc vs 49 cc, $p = 0.02$). The remaining baseline characteristics were similar between the preop-RT vs postop-RT cohorts. The reasons

for preop-RT included reduction of dose and volume of critical organs ($n = 16$, 64%), avoidance of orbital exenteration ($n = 2$, 8%), maximizing the likelihood of achieving clear resection margins ($n = 5$, 20%) and

other ($n = 2$, 8%). All patients in the preop-RT cohort received 50 Gy/25f to the primary site, and 7 received a simultaneous boost to 60 Gy for gross/equivocal nodal disease to spare a neck dissection

($n = 4$, 57%), or high-risk surgical regions with a high likelihood of a R1 resection based on a pre-RT discussion with the surgical team ($n = 3$, 43%). Patients in the postop-RT cohort received 60-70 Gy/30-35f.

Eight (32%) preop-RT patients had a pathological complete response (pCR). Five (20%) patients in the preop-RT cohort had local failure (1 residual, 4 recurrence) vs 16 (35%) in the postop-RT cohort. The

median follow-up was 5.5 and 5.2 years for the preop-RT and postop-RT cohort, respectively. Oncologic outcomes at 5 years including overall survival (76% vs 65%, $p = 0.91$), locoregional control (78% vs 64%, $p = 0.11$) and late toxicity (0.18 [0.05 - 0.36] vs 0.12 [0.04 - 0.23], $p = 0.39$) were similar between preop-RT and postop-RT cohorts respectively.

CONCLUSION

Nearly 1/3 of patients with SNSCC treated with preop-RT achieved a pCR. Preop-RT was associated with similar oncologic outcomes as postop-RT despite larger tumor sizes with higher T-categories. In the setting of collaborative multidisciplinary care in a high-volume center, pre-op RT in the management of locally advanced SNSCC is a reasonable option in select patients to minimize dose to optic structures, reduce the radiated volume, and improve margin clearance.

UTDRO/STARS21 RESEARCH DAY ABSTRACTS – ORAL PRESENTATIONS

Oral Presentations: Section 2

11

Stereotactic Ablative Radiotherapy for Ultra-Central Lung Tumors: Local Control and Toxicity from a Seventeen-Year Single-Institution Experience

Amir H. Safavi, Anna T. Santiago, Cynthia Torres, Srinivas V. Raman, Benjamin H. Lok, Andrew J. Hope, Andrea Bezjak, Alexander Y. Sun, Grace Wu, Jean-Pierre Bissonnette, John Cho,, Meredith E. Giuliani

PURPOSE

Stereotactic ablative radiotherapy (SABR) for ultra-central lung tumors can be associated with morbidity and mortality. We report local control (LC) and toxicity following SABR (≤ 8 daily fractions) with planning target volumes (PTV) overlapping trachea, proximal bronchial tree (PBT), esophagus, and/or pulmonary artery and vein (PA/PV).

METHOD

One hundred thirty-four of 1771 (7.6%) patients receiving lung SABR (January 2006-May 2023) were included from a prospective institutional database. In total, 141 ultra-central lung tumors (75% primary NSCLC, 25% metastases, no nodes) were analyzed. Primary outcomes were LC and incidence of grade (G) 3-5 CTCAE V5.0 toxicity. Secondary outcomes were overall survival (OS), progression-free survival (PFS), regional (RC) and distant control (DC), and incidence of G2+ pneumonitis. Dosimetry and LC were compared pre (2007-2017, 67 tumors) and post (2018-2023, 74 tumors) SUNSET (NCT03306680) inception.

RESULT

Median follow-up was 23.0 months (2.0-165.0). Median tumor size was 2.1 cm (0.8-6.0). Sixty-five (62.5%) patients with primary NSCLC were medically inoperable. PTV overlapped trachea in 7.1%, PBT 67.4%, esophagus 2.1%, PA 47.5%, and PV 12.8%. Tumor abutted PBT in 36.2% and PA/PV in 29.8%. No endobronchial invasion was noted. The most common prescription (89.4%) was 60 Gy/8 fractions (BED10 59.5-123.6 Gy). Prescription isodose line (IDL) (median: 87% [68.0-99.0]) was $\leq 90\%$ for 96 tumors (68.1%). Median PTV D99 and D95 were 96.2% (38.1-99.2) and 100.0% (70.9-108.4). PTV D99 $\geq 90\%$ was achieved for 87.9% of tumors. PTV D95 $\geq 100\%$ was achieved for 66.7% of tumors. Median PTV average dose was 109.2% (100.2-125.0). PTV Dmax (median: 119.8% [104.8-149.2]) was $\leq 120\%$ for 72 tumors (51.1%). Median Dmax,EQD2(a/b=3) (Gy) for trachea was 9.6 (0.1-138.5), PBT 124.6 (0.8-178.9), esophagus 22.2 (3.0-92.2), and PA/PV 135.6 (72.7-143.7). Median lung V20 was 8.8% (1.0-21.0). Five-year LC was 91.9% (95%CI:86.3-97.8). Tumor size (subdistribution hazard ratio (sHR)=1.50; 95%CI:1.01-2.23; p=.044), PTV (sHR=1.01; 95%CI:1.01-1.02; p<.001), and PET SUVmax (sHR=1.07; 95%CI:1.01-1.14; p=.021) predicted local failure. Two patients (1.5%) experienced G3-5 toxicities: 1) one with G3 pneumothorax/pneumopericardium, G3 pneumonitis, and G5 aspiration post 60 Gy/8 fractions, 2) another with G5 heart failure exacerbation post 24 Gy/1 fraction. Median OS was 46.0 months (95%CI:35.0-67.0). For patients with primary NSCLC, median PFS was 75.0 months (95%CI:35.0-NR) and 5-year RC and DC were 70.7% (95%CI:60.2-83.0) and 80.9% (95%CI:72.5-90.3). Incidence of G2+ pneumonitis was 12.9%. Multiple tumors (sHR=6.13; 95%CI:2.37-15.8; p<.001), lung V20 (sHR=1.12; 95%CI:1.01-1.23; p=.025), and systemic therapy use (sHR=5.70; 95%CI:1.88-17.3; p=.002) predicted G2 pneumonitis. Pre- to post-SUNSET, PTV D99, PTV D95, and prescription IDL increased while PTV average dose, PTV Dmax, and lung V20 decreased (Wilcoxon rank-sum tests p<.05). LC and Dmax,EQD2(a/b=3) for organs-at-risk remained similar pre- and post-SUNSET.

CONCLUSION

SABR, planned over 8 fractions with limited organ-at-risk hotspots and moderate PTV Dmax, has high LC and low toxicity for well-selected patients with ultra-central lung tumors.

UTDRO/STARS21 RESEARCH DAY ABSTRACTS – ORAL PRESENTATIONS

Oral Presentations: Section 2

12

Predictors of Vertebral Compression Fracture Following Spine Stereotactic Body Radiotherapy

Laura Burgess, K Liang Zeng, Eshetu G Atenafu Hanbo Chen, Sten Myrehaug, Hany Soliman, Jay Detsky, Chia-Lin Tseng, Pejman Maralani, Arjun Sahgal

PURPOSE

Spine stereotactic body radiotherapy (SBRT) provides excellent local control and pain response in the treatment of spinal metastases. The most common complication following spine SBRT is vertebral compression fracture (VCF). A number of clinical, radiographic and dosimetric risk factors for VCF have been identified including age, pre-SBRT fracture, spinal deformity, lytic disease and radiation dose. We hypothesized that these risk factors for VCF vary between those that have pre-SBRT VCF and those that do not. We set out to review outcomes and identify how predictors vary with pre-existing fracture.

METHOD

A retrospective review of a prospectively maintained institutional database of patients treated with SBRT for spinal metastases performed. The primary outcome was VCF. Clinical, dosimetric and radiographic factors were reported with descriptive statistics. The cumulative incidence of VCF was estimated competing risk analysis method. The impact of covariates was estimated with Cox proportional hazards model.

RESULT

From 2008 – 2022, 744 patients and 1813 spinal segments treated with spine SBRT. The median age at the time of treatment was 64.9 years. Slightly more men were treated than women (52.3%). Only 19.1% had a baseline pre-SBRT VCF. The most common dose fractionations were 24Gy in 2 (42.8%) and 28Gy in 2 (24.1%) with most patients treated in the de novo setting (68.0%). Of the 1813 spinal segments treated, there were 253 VCFs. Of these, 85 (33.6%) had pre-SBRT fractures and 168 (66.4%) did not. The cumulative incidence of VCF at 24 months was 12.0%, but varied between iatrogenic VCF (9.9%) and with tumor progression (22.0%).

On multivariate analysis (MVA), tumor progression (HR 2.26, 95% CI 1.17-3.07, $p < 0.01$), pre-SBRT VCF (HR 2.05, 95% CI 1.45-2.88, $p < 0.01$), mechanical pain (HR 1.89, 1.23-2.90, $p < 0.01$), older age at treatment (HR 1.014, 95% CI 1.001-1.03, $p < 0.03$), fewer segments treated (HR 0.76, 95% CI 0.64-0.90, $p < 0.001$), higher CTV D90 EQD2 (HR 1.006, 95% CI 1.001-1.01, $p < 0.03$) and no previous conventional RT to that segment (HR 2.03, 95% CI 1.27-3.24, $p < 0.01$) increased the risk of VCF. Looking only at those with a pre-SBRT fracture, tumor progression (HR 2.17, 95% CI 1.31-3.58, $p < 0.01$), no previous stabilization (HR 1.91, 95% CI 1.04-3.51, $p < 0.04$), involvement of the posterior elements (HR 2.32, 95% CI 1.17-4.80, $p < 0.03$), fewer segments treated (HR 0.72, 95% CI 0.56-0.92, $p < 0.01$) and higher CTV D90 EQD2 (HR 1.04, 95% CI 1.01-1.08, $p < 0.01$) increase the risk of progression of VCF. This contrasts to the factors that increase the risk of developing a new VCF: tumor progression (HR 2.63, 95% CI 1.77-3.91, $p < 0.01$), no previous conventional RT (HR 2.20, 95% CI 1.05-4.63, $p < 0.04$), higher dose per fraction (HR 1.11, 95% CI 1.03-1.19, $p < 0.01$), higher CTV D90 EQD2 (HR 1.01, 95% CI 1.001-1.013, $p < 0.03$).

CONCLUSION

The incidence of VCF varies as do the predictors of VCF with baseline pre-SBRT VCF or no pre-SBRT VCF.

UTDRO/STARS21 RESEARCH DAY ABSTRACTS – ORAL PRESENTATIONS

Oral Presentations: Section 3

13

Temporal Changes in Functional Magnetic Resonance Imaging for Cervical Cancer During Chemoradiotherapy

Mohammed Abdul-Latif, Amani Chowdhury, Hannah Tharmalingam, Peter Hoskin, Yatman Tsang

PURPOSE

Locally advanced cervical cancer (LACC) is managed with radical chemoradiotherapy (CRT) and brachytherapy. Local control rates are excellent, however distant relapse continues to impact survival. Risk-stratification using imaging biomarkers could be used to improve patient treatment and follow-up.

Functional magnetic resonance imaging (fMRI) can characterise biological properties of LACC. Parameters derived from fMRI include apparent diffusion coefficient (ADC from diffusion weighted imaging (DWI)), vascular permeability (Ktrans, from dynamic contrast enhanced MRI (DCE)) and the transverse relaxation rate ($R2^*$, calculated from blood oxygen level dependant (BOLD) MRI). These imaging parameters have potential as predictive and prognostic biomarkers for patients receiving CRT for LACC. This study aims to investigate temporal changes in fMRI parameters across CRT.

METHOD

A prospective cohort study in which patients undergoing CRT for LACC were imaged with fMRI prior to CRT (S1), halfway (S2) and on the final day of CRT (S3). fMRI sequences performed were T2-weighted MRI, DWI (ADC), DCE (Ktrans) and BOLD ($R2^*$) MRI. The median (e.g. ADCmed), lower (e.g. ADClow) and upper (e.g. ADChigh) quartiles for each parameter, in addition to percentage changes between scans (e.g. ΔADC_{S1-S2}). Tumour volume reduction rate (TVRR) between S1, S2 and S3 and response at 3 months after treatment (Complete response (CR) or partial response (PR)) was measured.

RESULT

Thirteen patients were included for analysis. The mean age was 57. 11 patients completed all three trial scans, whilst only 1 patient missed S2 and 1 missed S3. At three months follow-up imaging, 10 patients achieved a CR whilst 3 a PR.

Overall, ADC, Ktrans and $R2^*$ increased from S1 to S3 (Figures 1 and 2, $p < 0.05$). ADC, Ktrans and $R2^*$ at S1 are positively skewed, reducing in skewness from S1 to S3 ($p < 0.05$). Higher ADCmed at S1 was associated with lower ΔADC_{S2S3} and ΔADC_{S1S3} ($r = -0.71, -0.65$ respectively).

Higher $R2^*$ med at S1 was negatively correlated with $\Delta R2^*_{S1S3}$ ($r = -0.65, p < 0.05$), and at S3 positively correlated with $\Delta R2^*_{S1S3}$ ($r = 0.76, p < 0.02$).

TVRR was higher between S2 and S3 compared to S1 and S2 ($p < 0.05$), with volume at S1 correlating with volume at S3 ($r = 0.72, p < 0.02$). Only ADClow correlated with TVRR, with increasing $\Delta ADC_{lowS1S2}$ associated with increased TVRRS1S2.

Analysis of the three patients with PR showed they exhibited low (below median) ΔADC_{S1S3} despite having low ADC at S1 and S3. They also exhibited high (above median) $\Delta R2^*_{S1S3}$, with high $R2^*$ at S3 and low Ktrans at S1.

CONCLUSION

LACC receiving CRT is characterised by increasing ADC, Ktrans and $R2^*$ across treatment, reflecting a shift from hypercellular tumour towards more necrotic and hypoxic disease. Features identified in patients with PR indicate persisting hypercellularity despite CRT, with increasing hypoxia.

Identifying these changes may serve as predictors for poor response, providing opportunities to modify treatment during CRT or brachytherapy to mitigate this.

UTDRO/STARS21 RESEARCH DAY ABSTRACTS – ORAL PRESENTATIONS

Oral Presentations: Section 3

14

Prognostic Factors for Local Failure and Overall Survival in Patients with Epidural Disease at the Cauda Equina Following Stereotactic Body Radiotherapy: A Clinical, Anatomic and Dosimetric Analysis

Sondos Zayed, Mark Ruschin, Eshetu G. Atenafu, Deepak Dinakaran, Hanbo Chen, Jay Detsky, Hany Soliman, Sten Myrehaug, Arjun Sahgal, Chia-Lin Tseng

PURPOSE

The relationship between spine SBRT outcomes and the extent of malignant epidural disease (MED) compression of the cauda equina has yet to be reported. Our objective was to determine clinical, anatomic and dosimetric predictive factors for local failure (LF) and overall survival (OS) in a cohort of patients with spine metastases and epidural disease at the level of the cauda equina.

METHOD

Consecutive patients with cauda equina MED treated with SBRT, between January 1, 2008 and July 1, 2023, were identified and retrospectively reviewed from a prospectively maintained institutional database. MED parameters including linear dimensions, surface area, and volume ratios relative to the spinal canal, lumbar stenosis grading systems, clock position and various dosimetric factors were analyzed for their predictive value for LF post-SBRT and OS. Covariates with a P-value ≤ 0.20 on univariate analysis were selected for multivariable analysis (MVA), and those statistically significant ($P < 0.05$) were included in the final model.

RESULT

Ninety-five individual spinal segments (79 patients) with cauda equina MED were identified, of which 69 (73%) were intact and 26 (27%) post-op. Forty-one (43.2%) received 24 Gy in 2 fractions (fr), 27 (28.4%) received 30 Gy in 4 fr, 22 (23.2%) received 28 Gy in 2 fr and 5 (5.2%) received 30 Gy in 5 fr. Median follow-up and median time to LF were 16.3 (IQR 6.7-32.0) months and 4.7 (IQR 2.2-12.1) months, respectively. The cumulative incidence of LF at 6, 12, and 24 months was 12.7%, 12.7% and 17.4% respectively. OS at 6, 12, and 24 months was 79.6%, 58.4% and 40.7% respectively. In the intact cohort only (69/95), factors predictive of a higher risk of LF on MVA were chemotherapy naive (HR 8.197, 95% CI 2.198-30.303, $P=0.0017$), MED greater than one third of the circumference of the spinal canal (HR 9.632, 95% CI 1.863-49.806, $P=0.0069$), and lower V50Gy Equivalent Dose in 2Gy Fractions (EQD2) to the MED volume (HR 1.049, 95% CI 1.018-1.081, $P=0.0014$). These factors retained significance on MVA for LF when combined with the post-op (26/95) cohort ($P=0.0047$, 0.0272, 0.0024, respectively). In the intact cohort only, MVA identified oligometastatic disease (HR 0.381, 95% CI 0.190-0.764, $P=0.0065$) and MED limited to a single spinal level (HR 0.405, 95% CI 0.182-0.902, $P=0.0269$) as prognostic for OS. Oligometastatic disease and MED limited to a single spinal level also retained significance as predictors for OS on MVA when combined with the post-op (26/95) cohort ($P < 0.0001$, 0.0182, respectively).

CONCLUSION

We identified chemotherapy naive, MED encompassing more than one third of the circumference of the spinal canal, and lower V50Gy EQD2 to the epidural disease volume, as novel predictive factors for higher LF post-SBRT for MED at the cauda equina. Consideration for more aggressive management with decompressive surgery in those with MED spanning greater than a third of the spinal canal circumference and dose escalation to the thecal sac organ-at-risk may improve outcomes.

UTDRO/STARS21 RESEARCH DAY ABSTRACTS – ORAL PRESENTATIONS

Oral Presentations: Section 3

15

Advancing OARs Dosimetric Accuracy in Cervical Brachytherapy: Near-to-Target-Aware Segmentation via Deep Learning

Ruiyan Ni, Elizabeth Chuk, Kathy Han, Jennifer Croke, Anthony Fyles, Jelena Lukovic, Michael Milosevic, Benjamin Haibe-Kains, Alexandra Rink

PURPOSE

Deep learning has been previously used to improve efficiency in contouring organs at risk (OARs) and targets in radiotherapy. In cervical HDR brachytherapy, only OARs closest to the target are considered in treatment planning, driven by the highest dose to 2 cubic centimeters (D2cm³). Thus, accuracy in distal OAR does not translate to change in treatment planning or dosimetric impact. This study introduces a distance-penalized (DP) loss function to guide the network's attention toward the near-to-target OAR regions. A novel geometric metric, weighted Dice Similarity Coefficient (wDSC), is introduced as a surrogate for D2cm³ accuracy. Geometric, dosimetric and clinical acceptance evaluations were conducted.

METHOD

170 T2-weighted MR scans (56 patients) with clinical contours were split into training (45 patients, 150 scans) and testing (11 patients, 20 scans) subsets. A distance map, which emphasized errors close to HR-CTV, was used to penalize two commonly used loss functions, cross-entropy (CE) loss and DiceCE loss. A U-Net architecture was employed for model training. The novel metric, wDSC, emphasizes the accuracy of proximal OAR regions to HR-CTV by incorporating a weighted factor in the original volumetric DSC (vDSC). Dosimetric accuracy was quantified as the absolute difference between the D2cm³ calculated from the auto-contours and the clinical values. The D2cm³ of the auto-contour was generated by applying the clinical plan to auto-contours. Linear regression was performed, and the Pearson correlation coefficient (r) was used to quantify the strength of the relationship between the D2cm³ difference and five evaluation metrics (wDSC and four standard metrics). Clinical acceptability tests were performed, where a physician rated and revised the auto-contours. The dose parameters before and after revision were compared.

RESULT

The wDSC showed a moderate correlation with D2cm³ accuracy ($r=-0.55$), outperforming standard geometric metrics. Models using DP loss functions constantly yielded higher wDSCs compared to their respective non-DP counterparts. A statistically significant improvement was found in the small bowel with p -values=0.008 (CE group) and 0.017 (DiceCE group). DP loss models also achieved a reduced mean D2cm³ difference and smaller standard deviation, indicating an enhanced dosimetric accuracy. Small bowel in the CE group demonstrated a statistically significant difference (p -value=0.012). The clinical acceptability tests revealed that most bladder and rectum contours and approximately half of the sigmoid and small bowel contours were clinically accepted. Physician revisions on the auto-contours had little effect on D2cm³ (mean difference<0.02Gy).

CONCLUSION

We developed a DP loss function to guide the model for accurate near-to-target OAR segmentation in MR-guided cervical brachytherapy. The model with the proposed loss showed improved geometric and dosimetric performance. A new geometric metric, wDSC, was introduced and validated to be a better indicator of D2cm³ accuracy. Contour revision by the physician showed little dosimetric impact.

UTDRO/STARS21 RESEARCH DAY ABSTRACTS – ORAL PRESENTATIONS

Oral Presentations: Section 3

16

Elekta Hounsfield Unit Calibration and 3D Printed Phantom for CBCT-Based Dose Calculation

June Cheng Baron, Catherine Neath

PURPOSE

To evaluate the Elekta XVI Hounsfield unit (HU) calibration and to develop a process for dose calculation using cone-beam imaging, providing a pathway for post-treatment QA and adaptive radiotherapy.

METHOD

HU calibration was performed according to the manufacturer's procedure using the Catphan 504 phantom. Resulting image quality parameters were evaluated according to our institution's routine imaging QA procedure.

Two phantoms were evaluated for the purposes of generating a CBCT to electron density (CBCT-to-ED) curve: the Gammex 467 tissue characterization phantom and a custom 3D printed phantom made to accommodate the tissue mimicking inserts from the Gammex 467 phantom. The 3D printed phantom was created to have dimensions similar to a human head and body to simulate in vivo scatter associated with cone-beam imaging.

HU calibration in conjunction with the resulting CBCT-to-ED curve were used to calculate dose using CBCT images of the head, thorax and pelvis. CBCT-derived dose was compared to planning CT-derived dose using gamma analysis in 3D Slicer.

RESULT

HU calibration was successfully performed. Implementation of the HU calibration did not affect image quality parameters such as low contrast visibility, spatial resolution or spatial geometry. Without an HU license, CBCT values vary with mA-s. Installing an HU license, even without applying a calibration, was found to reduce this dependence. Applying a calibration resulted in measured HU versus reference HU close to unity.

CBCT values for tissue mimicking inserts were found to vary depending on the phantom used to hold the inserts, with the Gammex 467 phantom producing low contrast between different tissue densities and the 3D printed phantom producing much higher contrast. Since the 3D printed phantom better approximates human anatomy, it was used to generate two final CBCT-to-ED curves, one for the head and pelvis where there are no large regions of low density tissue, and one for the thorax where there are large regions of low density tissue.

Gamma analysis of CBCT-derived dose distributions used a 10% global threshold and 3%/3mm passing criteria. Passing rates of $\geq 97\%$ were observed for head and pelvis plans. For the treatment to the thorax, passing rates were lower (95.3%) despite applying the associated low density CBCT-to-ED curve.

CONCLUSION

Accurate dose calculation can be performed using CBCT-derived electron densities in the head and pelvis using HU calibration and a CBCT-to-ED curve generated using an anatomical tissue characterization phantom. Further work is necessary to produce robust dose calculations involving the lungs. This provides a pathway for post-treatment QA, adaptive radiotherapy and dose accumulation.

UTDRO/STARS21 RESEARCH DAY ABSTRACTS – ORAL PRESENTATIONS

Oral Presentations: Section 3

17

Quantifying Conventional and MR-Conditional Ionization Chamber Response in Clinical 1.5T and 0.35T MR-Linac Beams

Nathan Orlando, Jennie Crosby, Carri Glide-Hurst, Wesley Culberson, Brian Keller, Arman Sarfehnia

PURPOSE

Air-filled ionization chamber response in the magnetic resonance (MR) field of MR-linear accelerator (MR-linac) devices is influenced by the Lorentz force applied on charged particles set in motion within the field. Quantifying this chamber response in terms of a magnetic field quality conversion factor, k_B,Q , is necessary for accurate output calibration of MR-linac systems. While Monte Carlo simulations have determined k_B,Q values for numerous ionization chamber models, experimental validation is still required. The purpose of this work was to experimentally quantify both conventional and MR-conditional ionization chamber response for 1.5T Elekta Unity and 0.35T ViewRay MRIdian MR-linac systems.

METHOD

Eleven commercially available ionization chamber models along with seven equivalent MR-conditional ionization chamber models from manufacturers including Standard Imaging, IBA, and PTW were evaluated. Experimental determination of k_B,Q utilized a cross-calibration method against a reference Standard Imaging Exradin A1SL ion chamber. The ratio of absorbed dose measured with the reference A1SL chamber under reference conditions (10 x 10 cm² field size at depth of 10 cm) to corrected output measured with each test chamber at the same point of measurement allowed for determination of k_B,Q . The angular dependence of the magnetic field quality conversion factor was assessed for the 1.5T Elekta Unity system by measuring k_B,Q with the chamber axis and static magnetic field direction aligned at cardinal angles (0°, 90°, 180°, 270°).

RESULT

Magnetic field quality conversion factor, k_B,Q , values measured using our experimental cross-calibration method largely agreed to within uncertainty to Monte Carlo simulation data and experimental data where available. Comparing equivalent conventional and MR-conditional ionization chamber models, we obtained an average absolute percent difference in k_B,Q of $0.20 \pm 0.20\%$ and $0.16 \pm 0.15\%$ for the Elekta Unity and ViewRay MRIdian systems, respectively. Overall experimental uncertainty ($k=1$) in determining the magnetic field quality conversion factor for the Elekta Unity and ViewRay MRIdian systems was 0.71% and 0.72%, respectively. Investigation of the angular dependence of this correction factor demonstrated that the impact of the magnetic field on charge collection was minimized with the chamber axis parallel or anti-parallel to the magnetic field.

CONCLUSION

This work provides critical experimental validation of Monte Carlo simulated magnetic field quality conversion factors. k_B,Q values determined using our experimental method will serve as an important reference for MR-linac reference dosimetry protocols, and ultimately represent an important step towards accurate output calibration of MR-linac systems. Agreement of k_B,Q values within uncertainty for corresponding standard and MR-conditional ionization chamber models demonstrates the suitability of these conventional models for use in MR-linac reference dosimetry.

UTDRO/STARS21 RESEARCH DAY ABSTRACTS – ORAL PRESENTATIONS

Oral Presentations: Section 3

18

Evaluating 3D Vane Sequence on Elekta Unity MR-Linac for ITV Contouring

Lingyue Sun, Liam Lawrence, Ryan Oglesby, Mohammad Kazem, Angus Lau, Brige Chugh

PURPOSE

To investigate if a radial stack-of-stars sequence (“3D Vane”) on the Elekta Unity MR-Linac can accurately capture the full range of tumor motion, and if the MR images can be reliably used for internal target volume (ITV) contouring.

METHOD

A Modus QUASARTM MRI4D motion phantom was programmed to conduct user-specified displacements in the superior-inferior (SI) direction. Three scenarios were assessed: 1) a static 3cm diameter spherical tumor insert positioned at the center of the imaging field of view, 10mm superiorly off center, and 10mm inferiorly off-center; 2) a 3cm diameter spherical tumor insert with sinusoidal motion of 4mm, 5.3mm, and 10mm amplitude and 4s period; and 3) patient-specific 3D printed tumor inserts with patient-specific displacements for three gastrointestinal patients who had periodic breathing motion and two head-and-neck patients who had swallowing motion. Patient-specific motion displacements were extracted from cine MRI using a correlation-based object tracking method. A T1-weighted 3D Vane scan was acquired on the Unity MRL for all evaluation cases. Contrast agent-filled tumors for all cases were contoured three times on the 3D Vane image in the Monaco treatment planning system to examine the reproducibility of contouring using a built-in edge detection tool. The contoured volumes and SI extent of motion were compared to expected values. The expected volumes were calculated based on the known tumor insert volume and programmed displacements.

RESULT

For scenario 1, the contoured tumor volumes were within 1.2% of expected volumes, and the SI size of the contoured tumor was consistent with the expected 3cm length. For scenario 2, the contoured tumor volumes were systematically smaller than expected, and such deviation increased with increasing motion amplitude. The SI dimension of the contour was overall 2mm smaller than expected. For gastrointestinal patients in scenario 3, the contoured volumes were 14% to 18% smaller than expected, and only 70% to 75% of the programmed motion was observed. The most superior 3mm and most inferior 0 to 1.5mm tumor motion were not easily observed. This was likely because 1) the tumor stayed at those most extreme positions for a relatively short period of time; 2) the acquisition slice thickness was 5mm (reconstructed images had a slice thickness of 1.5mm). For head-and-neck patients, the tumor motion due to swallowing was not easily observed.

CONCLUSION

3D Vane scans can faithfully represent static spherical tumors. For GI patients with period breathing motion, a planning target volume margin of at least 3mm may be needed for an ITV contoured on the 3D Vane scan to ensure full dose delivery to the tumor volume undergoing periodic motion. For tumors with non-periodic motion (e.g., swallowing), 3D Vane scans may not reliably capture the motion.

UTDRO/STARS21 RESEARCH DAY ABSTRACTS – ORAL PRESENTATIONS

Oral Presentations: Section 4

19 Multicentre Prospective Validation of Integrated Molecular Classification of Meningiomas and Prediction of Recurrence Risk Using DNA Methylation

Alexander P. Landry, Justin Z. Wang, Vikas Patil, Andrew Ajisebutu, Jeff Liu, Rebeca Yakubov, Ramneet Kaloti, Aaron Cohen-Gadol, Christopher Wilson, Mohammed Zazoue, Zeel Patel, Chloe Gui, Olivia Singh, Qingxia Wei, Sheila Mansouri, Yosef Ellenbogen, Parnian Habibi, Stephen Yip, Serge Makarenko, Farshad Nassiri, Gelareh Zadeh

PURPOSE

Meningiomas have significant heterogeneity between patients and even within each WHO grade, making prognostication challenging. We previously developed and retrospectively validated a DNA methylation-based predictor of recurrence risk and integrated molecular groups (MG) of meningiomas. For this study we utilize prospectively collected cases to confirm the utility of these molecular tools in prognosticating meningioma patients and informing selection for adjuvant radiotherapy (RT) and compare these to WHO grade.

METHOD

Genome-wide DNA methylation profiles were generated with the Illumina EPICArray. Clinical data elements including progression-free survival (PFS) were extracted from the medical records and corroborated with neuroimaging. The performance of our methylation-based predictor and MG were compared with WHO grade using generalized boosted regression modelling by generating time-dependent receiver operating characteristic (ROC) curves and computing area under the ROC curves (AUCs) along with their 95% confidence interval using bootstrap resampling with 10000 resamples.

RESULT

173 meningiomas treated from 2018-2021 were included. Most patients were female (66%) and median age was 59. The cohort was enriched for WHO grade 2 (34%) and 3 (14%) meningiomas. Most cases received a gross total resection (56%). DKFZ classification confirmed the molecular diagnosis of meningioma for all cases. Meningiomas could be dichotomized into low-risk (Immunogenic, NF2-wildtype) or high-risk MG (Hypermetabolic, Proliferative). There was a significant increase in methylation-based risk scores and decrease in PFS with higher WHO grade and more aggressive MG. Using Cox proportional hazards modelling, increasing methylome recurrence risk was independently associated with a significantly increased hazard of recurrence (HR 4.16, 95% CI 2.14-8.09). Both the methylome-based predictor and MG had substantially improved performance in predicting 5-year PFS compared to WHO grade alone (Δ AUC = 0.10-0.23). Following results of methylation modeling, 59 cases (34%) were prescribed adjuvant RT prospectively following surgery.

CONCLUSION

DNA methylation modelling and molecular classification outperform conventional WHO classification in outcome prediction in an independent, prospectively collected cohort of meningiomas enriched for clinically aggressive cases and may be effectively used for real time prognostication, patient counselling, and referral for adjuvant RT.

UTDRO/STARS21 RESEARCH DAY ABSTRACTS – ORAL PRESENTATIONS

Oral Presentations: Section 4

20 HPV-Seq Is Prognostic In p16-Positive Oropharyngeal Cancer (OPC): Independent Validation In A Large Prospective Cohort And A Secondary Analysis Of NRG-HN002

Eric Y Stutheit-Zhao, Jonathan Harris, Jinfeng Zou, Zhen Zhao, Yangqiao Zheng, Shlomo A Koyfman, Jason W Chan, Mark W McDonald, Pencilla Lang, Dukagjin M Blakaj, Robyn Banerjee, MD, Melissa Young, Shao Hui Huang, Kathy Han, John N Waldron, Richard C Jordan, Pedro Torres-Saavedra, Quynh-Thu Le, Sue S Yom, Scott V Bratman

PURPOSE

HPV circulating tumor DNA (ctDNA) is a liquid biopsy biomarker that could evaluate treatment response and risk stratify patients after (chemo)radiotherapy ([C]RT). However, HPV ctDNA is undetectable at baseline in up to 15% of pts and needs prospective validation. HPV next-generation sequencing (HPV-seq) offers both genotyping and ultrasensitive quantification of HPV ctDNA. We validated HPV-seq, testing pre-specified hypotheses: (1) pre-RT HPV ctDNA correlates with gross tumor volume (GTV); (2) undetectable post-RT HPV ctDNA predicts favorable 2-year locoregional control (LRC) and progression-free survival (PFS).

METHOD

We analyzed pre- and post-RT HPV ctDNA in 2 cohorts of non-metastatic p16+ OPC. Cohort 1 (n=237): single-institution prospective study, standard RT/CRT; HPV ctDNA at pre-RT and ~3 mo post-RT. Cohort 2 (n=126): secondary endpoint of NRG-HN002, a phase II trial of low-risk p16+ OPC (AJCC 7e T1-T2 N1-N2b or T3 N0-N2b, ≤10 pack-year) randomized to de-escalated RT vs. CRT to 60 Gy; HPV ctDNA at pre-RT and ~4 wk post-RT. HPV ctDNA was measured by HPV-seq, targeting 38 HPV types. Correlations were assessed by Spearman coefficient (r). Associations with LRC/PFS were assessed by Fisher exact test (2-sided $\alpha=0.05$).

RESULT

Pre-RT HPV ctDNA was detected in 228/237 (96.2%) of Cohort 1 and 126/126 (100%) of Cohort 2 (range: 0.2 to 408147 copies/mL). Across both cohorts, dominant HPV types were HPV-16 (87.1%), 33 (5.0%), 35 (4.8%), 18 (2.0%), 26 (0.6%), 38 (0.3%), and 59 (0.3%). Pre-RT HPV ctDNA was correlated with GTV in both Cohort 1 ($r=0.46$ [0.34, 0.56]) and Cohort 2 ($r=0.25$ [0.08, 0.41]). In a multivariable model, baseline HPV ctDNA was associated with N category in both Cohort 1 ($p<0.001$) and Cohort 2 ($p=0.0125$) and not with T category or site (tonsil vs. other). At post-RT, HPV ctDNA clearance occurred in 189/237 (79.7% [74.2-84.4]) in Cohort 1 and 88/126 (69.8% [61.3, 77.2]) in Cohort 2. Pts with post-RT HPV ctDNA clearance vs. detection had 2-year LRC of 98% vs. 80% ($p < 0.001$) in Cohort 1 and 97% vs. 87% ($p = 0.0550$) in Cohort 2. Similarly, 2-year PFS was 94% vs. 52% ($p < 0.001$) in Cohort 1 and 95% vs. 84% ($p = 0.0659$) in Cohort 2. Negative predictive value (NPV) of post-RT HPV ctDNA clearance in Cohorts 1 and 2 respectively was 97.8% [94.5, 99.1] and 96.6% [90.3, 99.3] for 2-year LRC and 94.1% [89.7, 96.6] and 95.4% [88.6, 98.7] for 2-year PFS.

CONCLUSION

This study provides prospective clinical validation of the prognostic value of HPV-seq in two high quality independent cohorts. Pre-RT HPV ctDNA was detected in >96% of pts with p16+ OPC and correlated with GTV and N-category. Post-RT HPV ctDNA clearance was associated with favorable outcomes. Cohort 1 showed more clearance and stronger association with LRC and PFS, possibly due to test timing (3 vs. 1 month post-RT) and sample size.

UTDRO/STARS21 RESEARCH DAY ABSTRACTS – ORAL PRESENTATIONS

Oral Presentations: Section 4

21

Uncovering the Mechanism of HDAC3-Mediated Radiosensitization in Small Cell Lung Cancer

Ujas A. Patel, Mary Shi, Lifang Song, Vivek Philip, Troy Ketela, Hansen He, Benjamin H. Lok

PURPOSE

Small-cell lung cancer (SCLC) is a highly aggressive malignancy with a median overall survival (OS) of <10 months for extensive stage (ES) patients. Thoracic radiotherapy (TRT) to ES patients after chemotherapy improves OS however, many experienced disease recurrence. A strategy to improve tumor control is the addition of novel radiosensitizers. We conducted a CRISPR knockout screen against druggable gene targets for radiosensitizers and found the loss of Histone Deacetylase 3 (HDAC3) sensitized SCLC cells to ionizing radiation (IR). Our study aims to determine the mechanism and translational potential of HDAC3-mediated radiosensitization in SCLC.

METHOD

We generated HDAC3 loss in SCLC cells by either genetic knockdown (KD) using small-hairpin RNA constructs, or an HDAC3-selective inhibitor (HDAC3i), RGFP966. In vitro radiosensitization was evaluated using clonogenic survival (CS) and long-term cell viability (CV) assays. To investigate the mechanism of radiosensitivity, we performed ATAC-seq to determine changes in chromatin accessibility by HDAC3 loss. Immunofluorescence (IF) against γ H2AX and DDR proteins was used to assess the effect of HDAC3 loss on double-strand break (DSB) generation and persistence, and DNA DSB repair (DDR) after treatment with IR. To assess the therapeutic potential of HDAC3-mediated radiosensitization in SCLC, we evaluated mice treated with the combination of HDAC3 loss and radiation, compared to radiation alone, in cell-line derived xenografts (CIDX).

RESULT

Compared to HDAC3 wildtype (WT) cells treated with IR, cells with HDAC3 loss treated with IR demonstrated reduced CS and CV. The dose modification factor (DMF) for a 10% surviving fraction (SF) was found to range between 1.2 and 1.7 in cells with HDAC3 loss compared to the control (DMF >1.0 indicates radiosensitization). ATAC-seq demonstrated an increase in more accessible chromatin regions in cells with HDAC3 loss, and in accordance, IF against γ H2AX showed an increase in the average number of DSBs (DSBavg) 0.5 hours after IR (HDAC3 KD = 28.0, $p < 0.0001$; HDAC3i = 26.0, $p < 0.0001$) and persisting damage 48 hours after IR (HDAC3 KD = 10.0, $p < 0.0001$; HDAC3i = 15.0, $p < 0.0001$), compared to HDAC3 WT cells (DSBavg was 21.5 and 4.0 at 0.5 and 48 hours post-IR, respectively). Our in vivo studies demonstrated radiosensitization and improved tumor growth inhibition in one of two HDAC3 KD CIDX and in a third CIDX model treated with the combination of HDAC3i and radiation.

CONCLUSION

We show that HDAC3 loss sensitizes SCLC cells to IR in vitro and improves tumor growth inhibition in some SCLC xenografts. At a mechanistic level, HDAC3 loss increases chromatin accessibility, and the generation and persistence of DSBs following IR. Taken together, our work provides a foundation for understanding HDAC3-mediated radiosensitization and its potential as a therapeutic avenue in the treatment of a deadly disease known for its grim patient survival and limited therapeutic progress.

UTDRO/STARS21 RESEARCH DAY ABSTRACTS – ORAL PRESENTATIONS

Oral Presentations: Section 4

22 Cross-Cancer Analysis Reveals Distinct Pattern of Immune Modulation during Curative Radiotherapy: Preliminary Findings from the SCIPER study

Badr Id Said, Giselle Boukhaled, Benjamin Lok, Jelena Lukovic, Aruz Mesci, John Waldron, Philip Wong, Ben X. Wang, David Brooks, Michael Milosevic

PURPOSE

Radiation therapy (RT) is a cornerstone in the curative treatment of solid tumors, yet its complex effects on the immune system are not fully understood. The prospective SCIPER study aimed to examine these effects by analyzing changes in the immune profiles of patients undergoing RT for various solid cancers.

METHOD

Patients with a new diagnosis of head and neck cancer (HNC), non-small cell lung cancer (NSCLC), rectal cancer, or extremity soft tissue sarcoma (STS) treated with curative intent RT (>45 Gy, 1.8-3 Gy per fraction) were enrolled. Baseline and post-RT (after 45 Gy) blood samples were collected for multiplex Luminex cytokine analysis and high-dimensional CyTOF of immune cell populations. Immune alterations during treatment were identified and correlated with patient outcomes.

RESULT

Overall, 37 patients treated with curative RT for HNC (n=8), NSCLC (n=8), rectal cancer (n=7) and STS (n=14) were enrolled. Approximately 50% of patients received concurrent chemotherapy. With a median follow-up of 16.5 months, there were no local recurrences and nine distant recurrences. Cytokine analysis (available in only 17 patients) demonstrated significant increases in GCSF (p=0.025) and MCP-1 (p=0.029) during treatment, both important in the mobilization and trafficking of monocytes and other myeloid-derived cell populations. Conversely, there was a significant reduction in IL-12B (p=0.004), an effector cytokine important for CD8 T cell priming, effector cell differentiation and anti-tumor activity. Consistent with the increases in GCSF and MCP-1, CyTOF data (37 patients) demonstrated a significant increase in monocyte populations (p<0.001) and a reduction in NK cells (p<0.001) during treatment. Intriguingly, the abundance of circulating CD4 and CD8 T effector cells decreased in patients that subsequently developed distant metastases (p=0.055 and p=0.027 respectively), whereas no significant difference was observed for patients who remained recurrence-free. These observations were independent of tumor type and receipt of chemotherapy, suggesting conserved responses to therapy with tumor outcome and metastasis.

CONCLUSION

This early analysis of the SCIPER study identified a distinct pattern of immune modulation during RT across all tumor types, with increases in pro-tumoral myeloid cell populations and a reduction in effector T cells and NK cells. These findings are consistent with evolution towards an immune suppressed phenotype, which may be associated with a higher risk of distant recurrence. Further analysis and longer patient follow-up will improve our understanding of the relationships between immunoregulatory cytokines, specific cell populations and patient outcome.

UTDRO/STARS21 RESEARCH DAY ABSTRACTS – ORAL PRESENTATIONS

Oral Presentations: Section 4

23 Comparison of the Localisation of Phototheranostic PORPHYSONE Nanoparticles in Rodent and Nonrodent Models of Prostate Cancer

Michael S Valic, Carl Fisher, Mark Zheng, Celina Li, Alyssa Goldstein, Nicholas Bernards, Alexander Gregor, Abdullah El-Sayes, Jenny Ma, Lili Ding, Michael Halim, Pamela Schimmer, Juan Chen, Robert Weersink, Brian C Wilson, Gang Zheng

PURPOSE

Prostate cancer (PCa) is the most prevalent cancer in men. For early-stage PCa localised to the prostate, there is growing interest in minimally invasive light-based therapies such as photothermal therapy (PTT) that can precisely target the intraprostatic lesion while sparing healthy surrounding organs from damage. Our group has previously demonstrated focal PTT ablation of PCa xenografts using phototheranostic PORPHYSONE (PS) nanoparticles with selective tumour uptake and enhanced photothermal energy conversion. In the present study, we evaluate if the localisation of PS in larger, more anatomically relevant rat and canine models of orthotopic PCa exhibit similar uptake and tumour-to-prostate selectivity as observed in mice.

METHOD

PS nanoparticles were physicochemically characterised for size and morphology. Models of orthotopic prostatic adenocarcinoma were established in three animal species: (1) PC-3 human xenografts in nude mice (0.025 kg), (2) syngeneic MAT-Ly-Lu rat allografts in ACI rats (0.300 kg), and (3) syngeneic ACE-1 canine allografts in immunosuppressed mongrel canines (~30 kg). For in vivo studies PS were radiolabelled with positron-emitting Copper-64 (specific activity > 3.1 MBq/mg) and injected intravenously at scaled PS doses (mg/kg). Plasma was collected for pharmacokinetic and chelation stability analyses. 24 hours post-injection the uptake in the tumour, healthy prostate, and surrounding organs was evaluated using PET/MRI, ex vivo fluorescence imaging and γ counting. Fluorescence microscopy of frozen tissue sections was also performed.

RESULT

The plasma pharmacokinetics of PS in all three models were similar. Mice had the highest weight adjusted volume of distribution (184 mL/kg) and clearance (8.9 mL/h·kg) whereas canines had the lowest values (62.9 mL/kg, 3.0 mL/h·kg). The circulatory half-life of PS was 14~19 hours in all three animal species. PS uptake in the prostate tumour 24 hours post-injection was highest in the ACE-1 canine model (2.46 SUV), followed by the MAT-Ly-Lu rat model (2.27 SUV) and PC-3 mouse model (1.23 SUV). However, when compared to PS concentration in the healthy prostate, the tumour-to-prostate selectivity of PS was lowest in the canine model (1.35 ratio) and highest in the rat (3.75 ratio) and mouse (5.71 ratio) models. Fluorescence microscopy of PS localisation in MAT-Ly-Lu rat tumours confirmed selective uptake of PS in tumour cells along the lesion margin, whereas fluorescence imaging of cross-sections of ACE-1 canine tumours revealed unexpectedly high uptake by the healthy prostate gland not observed in the prostates of rats or mice.

CONCLUSION

PS demonstrated unexpected variability in tumour uptake and tumour-to-prostate selectivity depending on the type of PCa model used: mouse and rat models exhibited the most favourable tumour selectivity whereas the canine model did not. Which of these three preclinical models of orthotopic PCa will be most predictive of PS localisation (and responses to PS-PTT treatments) to human disease remains to be seen.

UTDRO/STARS21 RESEARCH DAY ABSTRACTS – ORAL PRESENTATIONS

Oral Presentations: Section 4

24 Determining DNA Damage Sensitivity and Synthetic Lethal Vulnerabilities of FBXO11 Loss in Small Cell Lung Cancer

Tony Yu, Violet Xiong, Mansi Aparnathi, Lifang Song, Benjamin Lok

PURPOSE

Small cell lung cancer (SCLC) is a high-grade, neuroendocrine carcinoma comprising 15% of lung cancers. First-line treatment with platinum and etoposide chemotherapy—with radiotherapy for limited stage disease—produces good initial response, but most patients suffer relapse within 2 years. This regimen has changed minimally in 3 decades, fueling a dire need for more effective therapies. PARP inhibitors (PARPi) have potential in this setting, but response varies with some SCLC cases being resistant. Previously, we conducted a CRISPR KO screen to identify gene deficiencies mediating PARPi resistance. One top hit was FBXO11, coding for a substrate recognition component of the SCF E3 ubiquitin ligase. Furthermore, a study identified FBXO11 loss in 17% of cisplatin-treated relapse patients, implicating this gene in cisplatin resistance. Our current model is that FBXO11 loss promotes homologous recombination and reduces sensitivity to DNA damaging therapies, potentially extending to radiotherapy. To combat this, I aim to identify a synthetic lethal vulnerability of FBXO11 deficient SCLC as a novel therapeutic opportunity.

METHOD

Cancer cell line pairs with and without FBXO11 were generated by lentiviral transduction using either CRISPR-Cas9 KO or overexpression depending on wildtype cell line status. Validation was done by Sanger sequencing, quantitative PCR, and Western blot. Cells were treated with cisplatin, olaparib, talazoparib, or radiation and assayed for viability in 96 well plate format or clonogenicity in 6 well plate format. Drug screening was conducted in 384 well plate format at 1 μ M and 10 μ M concentrations using the NIH oncology library and mechanistic set. Cisplatin, olaparib, and talazoparib were used as control drugs. Top hits were validated by viability or clonogenicity. Validated top hits will be tested in vivo by engrafting cells in immunodeficient mice and comparing treatment against the delivery vehicle.

RESULT

Six pairs of cell lines have been generated with and without FBXO11: SBC5, SHP77, H82, H69, H446, and HPB-ALL. FBXO11 deficient cell lines exhibit greater viability or clonogenicity when treated with cisplatin, and four of these (SBC5, H69, H446, and HPB-ALL) also show PARPi resistance. Both drug libraries have been screened in SBC5 and the oncology library has been screened in SHP77. Major drug classes identified among top hits include nucleoside analogues (mercaptopurine, gemcitabine, formycin A), microtubule inhibitors (paclitaxel, docetaxel), receptor tyrosine kinase inhibitors (pemigatinib, afatinib), and mTOR inhibitors (sirolimus). Paclitaxel and docetaxel have been validated in SHP77, while gemcitabine, pemigatinib, afatinib, and everolimus have some level of validation in SBC5.

CONCLUSION

FBXO11 loss confers resistance to PARPi and cisplatin in the cell lines constructed and tested, in concordance with our model. Drug hits targeting FBXO11 loss have been identified, and fall into four major drug classes. Investigation of radiation resistance following FBXO11 loss and validation of drug hits are ongoing.

UTDRO/STARS21 RESEARCH DAY ABSTRACTS – ORAL PRESENTATIONS

Oral Presentations: Section 4

25 Early Apparent Diffusion Coefficient (ADC) Changes During Concurrent Chemoradiation: An Imaging Biomarker for Treatment Response and Recurrence Prediction in Glioblastoma

Daniel Moore-Palhares, Liam Lawrence, Hany Soliman, James Stewart, Sten Myrehaug, Hanbo Chen, Mark Ruschin, Jay Detsky, Deepak Dinakaran, Pejman J. Maralani, Chia-Lin Tseng, Angus Lau, Arjun Sahgal.

PURPOSE

Diffusion-weighted imaging (DWI) enables in vivo diffusivity measurement through the apparent diffusion coefficient (ADC). Aggressive hypercellular tumours exhibit restricted water diffusion and low-ADC values. We hypothesized that during concurrent chemoradiation (CRT), areas of glioblastoma displaying radioresistance and a higher likelihood of recurrence will exhibit smaller increases in ADC values compared to those areas more responsive to treatment. Consequently, our study aims to compare ADC changes within the areas of the gross tumour volume (GTV) that developed recurrence compared to those that remained recurrence-free.

METHOD

We retrospectively reviewed patients with glioblastoma who were prospectively imaged with DWI at planning (Fx0), fraction 10 (Fx10), fraction 20 (Fx20), and 1 month after the completion of a standard 6-week course of concurrent CRT (P1M). We included patients 1) with in-field failure (>80% of the recurrence covered by the 95% isodose line) and a partial GTV recurrence (defined as recurrence confined to <2/3 of the GTV), and 2) those with no in-field failure over a minimum 36-month follow-up. The GTV was contoured at all time points and included the surgical cavity and any residual enhancing tumour. The recurrence was contoured at the first magnetic resonance imaging timepoint showing progression per RANO criteria. The intersection of the GTV and the recurrence volume was labelled as resistant-GTV, while the GTV that did not intersect with the recurrence was labelled as sensitive-GTV. For patients without in-field failure, the entire GTV was labelled sensitive-GTV. Absolute ADC values within resistant- and sensitive-GTV and ADC changes (%) at each time point relative to Fx0 were measured. The surgical cavity was contoured at each time point and excluded from all regions to avoid biasing ADC values.

RESULT

A total of 27 patients were included; most had undergone subtotal resection (59%) and had MGMT-methylated tumours (56%). The median absolute ADC values for resistant- and sensitive-GTV were 1.0 (IQR: 0.9-1.1) vs 0.9 (IQR: 0.9-1.1) at Fx0 ($p=0.651$), 1.0 (IQR: 0.9-1.23) vs 1.2 (IQR: 0.9-1.3) at Fx10 ($p=0.054$), 1.2 (IQR: 0.9-1.3) vs 1.2 (IQR: 1.0-1.4) at Fx20 ($p=0.167$), and 1.2 (IQR: 1.1-1.4) vs 1.4 (IQR: 1.2-1.5) at P1M ($p=0.075$), respectively. The median relative ADC change for resistant- and sensitive-GTV was 0.1% (IQR: -1.6-12.9) vs 15.3% (IQR: 7.5-28.5) at Fx10 ($p=0.007$), 6.9% (IQR: 3.4-19.1) vs 23.1% (IQR: 11.8-27.8) at Fx20 ($p=0.046$), and 19.9% (IQR: 8.9-31.4) vs 33.3% (IQR: 21.1-50.2) at P1M ($p=0.016$), respectively. The linear mixed-effects model revealed a significant difference in relative ADC changes between resistant- and sensitive-GTV ($p=0.002$).

CONCLUSION

Early ADC changes during CRT are a potential biomarker for treatment response and recurrence prediction in glioblastoma. Regions exhibiting smaller ADC changes during CRT indicate potential sites of recurrence, suggesting utility as a biomarker for biologically adapted radiation clinical trials.

UTDRO/STARS21 RESEARCH DAY ABSTRACTS – POSTER PRESENTATIONS

Poster Presentations: Section 1

01

Investigating Micro-Environmental Changes in a Syngeneic Radio-Recurrent Prostate Cancer Model

Stephanie D. White, Xiaoyong Huang, Daniel Djayakarsana, Greg Stanisz, Ian Mills, Stanley K. Liu.

PURPOSE

Approximately 1 in 8 men in Canada will be diagnosed with prostate cancer (PCa) in their lifetime, with ~20% presenting with high-risk disease. A standard treatment is radiotherapy (RT) and while many patients respond well to RT, up to 40% of men with high-risk disease can recur, often within the prostate. The tumour micro-environment (TME) is altered after radiotherapy, and therapies capitalizing on these changes in the TME might provide an advantage to tackling radiation-recurrent cancer. Identifying these TME changes in radio-recurrent PCa is the first step, however existing PCa animal models do not sufficiently model the TME. Our collaborator's lab at Oxford University (Professor Ian Mills), has created the DVL3 mouse model with a clinically relevant TME, making this model an innovative tool for investigating radio-recurrence. My project aims to create a radio-recurrent DVL3 PCa model and investigate changes in the TME.

METHOD

The first aim is to create, validate, and characterize the radio-recurrent cell line. To generate the radio-recurrent model, the DVL3 Parental cells (DVL3-Par) were irradiated with a clinical RT schedule, herein referred to as DVL3-CF cells. Validation of their radio-resistance was done using the clonogenic assay. Characterization of the phenotype of DVL3-CF cells involved evaluating changes in proliferative capacity, cell cycle, senescence, and invasion and metastatic potential.

The second aim evaluates the radio-recurrent model established with DVL3-CF cells grown in a mouse prostate (orthotopic) as this best emulates the TME and clinical tumour progression. This will be done in comparison to subcutaneous tumours (the most common experimental model). Parental and CF cells will be grown orthotopically or subcutaneously in C57BL/6 mice and monitored for growth via T2-weighted MRI in collaboration with Dr. Stanisz and his lab. Histological, transcriptional (RNA seq), and proteomic analyses of the tumours and draining lymph nodes will be compared across the radio-recurrent model and its parental model in both the subcutaneous and orthotopic tumours to evaluate environmental changes and potentially implicated mechanisms.

RESULT

For the first aim, the DVL3-CF cells were validated for their radiation resistance using the clonogenic assay which demonstrated a significant increase in clonogenic survival compared to DVL3-Par cells. For characterization of the DVL3-CF cell line, we found that the cells maintain a radio-recurrent phenotype with increased proliferation, decreased senescence, and increased invasion and migration. The DVL3-CF cells did not show any statistical difference in their cell cycle. For the second aim, we have confirmed the cells are able to be grown orthotopically, and our pilot MRI trial has been successful in visualizing subcutaneous and orthotopic tumour growth.

CONCLUSION

The DVL3 radio-recurrent model increases our repertoire of clinically relevant animal models and will have profound impacts on our understanding of the mechanisms of radio-recurrence.

UTDRO/STARS21 RESEARCH DAY ABSTRACTS – POSTER PRESENTATIONS

Poster Presentations: Section 1

02 Characterizing the Microcirculatory System Using Light: Towards Studying the Effects of High-Dose Radiation Therapy in the Tumor Microcirculatory System

Hector A. Contreras-Sanchez, W. Jeffrey Zabel, Edward Taylor and Alex Vitkin

PURPOSE

The microvascular system consist of highly organized blood vessels that distribute blood throughout a specific tissue. The architecture and blood flow pattern of the healthy microvascular network are optimized for an efficient delivery of nutrients and oxygen to the surrounding tissue cells. In cancer, solid tumors develop their own vasculature, commonly a very disorganized system of immature and weak vessels that exhibit remarkable differences from healthy tissue in both morphology and functionality. Comprehensive imaging of the tumor microcirculatory system is thus required to understand the vascular role in tumor growth and response to cancer therapy. Here, we implemented a non-invasive approach using two Optical Coherence Tomography (OCT) extensions: speckle variance (svOCT) and Doppler OCT (DOCT) for imaging microvascular architecture and blood flow velocity simultaneously in a xenograft model of pancreatic cancer. This methodology will further allow longitudinal studies of tumor vascular and blood flow response to various cancer treatments. Particularly, Stereotactic Body Radiation Therapy (SBRT), towards studying the effects of SBRT in the tumor microcirculatory system in a pre-clinical setting.

METHOD

A custom-made OCT (20 KHz A-scan rate) was used in this study. A phantom experiment consisting of a 305- μm inner diameter tube surrounded by static tissue-like gelatin was performed first, and a 1% intralipid solution was injected using a syringe pump at different flow rates (0-30 $\mu\text{l}/\text{min}$) to determine OCT resolution capacities. Then, the morphological (svOCT) + blood velocity (DOCT) microvascular maps in healthy mouse skin and the pancreatic tumor model (Bx-PC3 cancer cell line) were acquired (6x6 mm² field-of-view) using the dorsal skin window chamber model (NRG mice). The acquired 3D microvascular images were quantitatively compared by obtaining the diameter and velocity histogram, and the combined diameter-velocity plot.

RESULT

Blood velocity in small vessels such as capillaries are within the order of 1000 $\mu\text{m}/\text{sec}$, and minimum detectable velocity for this OCT system was found to be ≈ 200 $\mu\text{m}/\text{sec}$. From the quantitative analysis between healthy and tumor microcirculation, a larger mean diameter (51.12 ± 0.35 μm) and mean velocity (1.26 ± 0.02 mm/sec) was found for the tumor compared with healthy skin (21.80 ± 0.11 μm), and (0.47 ± 0.01 mm/sec). Further, the diameter-velocity plot for healthy skin shows a weak positive linear correlation ($r=0.48$) whereas a larger deviation from this trend was observed for the tumor ($r=0.23$). The Pearson correlation coefficient can then be used as a goodness-of-fit parameter to discriminate between both microvascular networks.

CONCLUSION

OCT enables a non-invasive approach to simultaneously study vascular architecture and blood flow in a preclinical tumor model. The established OCT workflow will provide a better understanding of tumor microcirculatory system and its physiological role in radiobiology. Longitudinal experiments of tumors exposed to SBRT are currently being pursued using the proposed OCT approach.

UTDRO/STARS21 RESEARCH DAY ABSTRACTS – POSTER PRESENTATIONS

Poster Presentations: Section 1

03

Cumulative Incidence of Sarcoma Brain Metastases: Report from a High-Volume Cancer Center

Ayah Erjan, Kurl Jamora, Enrique Gutierrez, Anna Santiago, Barbara-Ann Millar, Normand Laperriere, Tatiana Conrad, Dana Keilty, Philip Wong, Peter Chung, Charles Catton, David Kirsch, David Shultz

PURPOSE

While carcinomas commonly metastasize to the brain, the incidence, and predictors of Brain metastases (BrM) in sarcoma patients remain poorly understood given their rarity. We aimed to determine the cumulative incidence (CI) and clinical factors associated with BrM in sarcoma patients.

METHOD

We retrospectively analyzed data from all sarcoma patients who presented to our center between 2006 and 2023. The CI function was used to analyze time to BrM, with incidence stratified by key variables. Univariable (UVA) and multivariable analyses (MVA) were conducted to evaluate factors associated with BrM incidence.

RESULT

Among 3,766 sarcoma patients, 101 developed BrM. CI rates were 2.2%, 2.9%, and 3.3% at 24, 48, and 72 months, respectively, with a median time to BrM of 17 months. On UVA, intrathoracic and uterine primary locations, alveolar soft part sarcoma (ASPS), epithelioid and intimal histologic subtypes, and metastatic stage at diagnosis were associated with increased CI of BrM. In contrast, age ≥ 59 , primary retroperitoneal location and liposarcoma subtype were associated with a decreased CI. On MVA the following predictors remained significant: intrathoracic and uterine primaries (HR 18.0, 95% CI 8.52–38.0, $P < 0.001$; HR 6.72, 95% CI 2.56–17.6, $P < 0.001$), ASPS and Epithelioid Sarcoma (HR 4.89, 95% CI 2.17–11.0, $P < 0.001$; HR 2.77, 95% CI 1.02–7.54, $P = 0.047$), age ≥ 59 years (HR 0.45, 95% CI 0.27–0.73, $P = 0.001$) and liposarcoma (HR 0.12, 95% CI 0.03–0.60, $P = 0.009$).

CONCLUSION

This report provides valuable insights into the CI of BrM among sarcoma patients, highlighting the impact of age, tumor location, and histologic subtype on BrM incidence. These findings underscore the importance of tailored surveillance for high-risk patients, potentially leading to improved outcomes.

UTDRO/STARS21 RESEARCH DAY ABSTRACTS – POSTER PRESENTATIONS

Poster Presentations: Section 1

04 Pituitary Adenomas Treated with Gamma Knife Radiosurgery: A Retrospective Analysis within University Health Network

Inhwa Kim, Michael Yan, Colin Faulkner, Michel Sourour, Michael Cusimano, Aristotelis Kalyvas, Normand Laperriere, David Payne, Dana M Keilty, Gelareh Zadeh, Derek S. Tsang

PURPOSE

Pituitary adenomas that recur or persist following medical or surgical management can be treated with stereotactic radiosurgery (SRS). The aim of our study was to describe outcomes of patients with pituitary adenomas treated with SRS at Toronto Western Hospital and Princess Margaret Cancer Centre within University Health Network (UHN) in Toronto, Ontario.

METHOD

In this retrospective study, patients with pituitary adenomas treated with SRS at UHN between 2005 and 2023 were identified. Patients were treated with a Leksell Gamma Knife 4C (prior to 2012) or Perfexion (2012 onwards). The primary outcome was local tumour control. Overall survival was evaluated using the Kaplan-Meier method. This study was approved by the UHN Research Ethics Board.

RESULT

A total of 88 pituitary adenomas in 83 patients were included. The mean age of patients was 53 years at the time of SRS treatment. Of all patients, 43 were female (52%) and 40 were male (48%). The majority of tumors were functioning (63%). The median tumor volume was 1.74 cm³ (range, 0.1-6.4). The median prescribed dose was 18 Gy (range, 12-25) prescribed to the 50% isodose line (range, 40-65). The median dose rate of Co-60 was 2.54 Gy/min (range, 1.4-3.7). The median distance of tumor from the optic nerve was 4.0 mm (range, 0.5-12.0); tumours adjacent to optic structures were underdosed with no cases of optic neuropathy. Two patients had repeat SRS to out-of-field recurrence in the contralateral sella/cavernous sinus. Median follow-up was 4.7 years. There was excellent local control of all treated tumors (100%). Five- and ten-year overall survival estimates were 95% and 87%, respectively; five patients who died had passed from non-pituitary causes.

CONCLUSION

Radiosurgery for pituitary adenomas is a highly effective modality at attaining local tumour control, including for some patients whose tumours are close to optic structures.

UTDRO/STARS21 RESEARCH DAY ABSTRACTS – POSTER PRESENTATIONS

Poster Presentations: Section 1

05 MR-guided HDR brachytherapy boost in localized prostate cancer – results of a Phase II trial

Carlton Johnny, Alejandro Berlin, Robert Weersink, Srinivas Raman, Rachel Glicksman, Charles Catton, Alexandra Rink, Bernadeth Lao, Cynthia Menard, Peter Chung

PURPOSE

Dose escalation in localized prostate cancer using brachytherapy combined with external beam radiation (EBRT) has demonstrated improved biochemical control compared to EBRT alone. However, ultrasound guided LDR brachytherapy might be associated with increased GU toxicity. We report the results of a prospective study of MR-guided HDR brachytherapy (MRgHDR) in combination with EBRT for localized prostate cancer.

METHOD

Intermediate- (IR) and high-risk (HR) prostate cancer patients were eligible. Patients received either 15Gy single fraction or 10Gy x 2 fractions using MRgHDR technique, followed by EBRT (37.5 Gy, [prostate only] -IR or 45–46 Gy – [prostate + pelvic nodes] -HR). Toxicity (CTCAE v4) and HRQoL (EPIC) were recorded at 1, 3 and 6 months, then at 1, 2, 3, and 5 years. Androgen deprivation therapy (ADT) was used according to the appropriate disease risk category. Biochemical failure was defined according to Phoenix definition (nadir+2).

RESULT

From 2010-2018, 120 patients were enrolled, 53 (44%) had IR and 67 (56%) had HR disease. Median age was 69 years (range, 46-78), median PSA was 12.1 ng/ml (3.2-148). ADT was used in 84 (70%) of patients, of whom 51 (60%) patients received <1 year and 33 (40%) received >1 year of ADT. A single fraction of 15Gy was given to 94 patients (78%) and the remaining 26 patients (22%) received 10Gy x 2 fractions. EBRT dose was 37.5Gy in 52 (43%) patients while 67 (56%) received 45-46Gy. One patient received only the first fraction of 10Gy, declined the second fraction and subsequently received 60Gy EBRT to the prostate. The median follow up was 58 months (11-134). Overall 5-year biochemical control was 90% while it was 95% and 86% for IR and HR, respectively. At 5 years 7% patient had nodal or distant relapse or both. While the 5-yr distant control rates were 95% and 91% in the IR, HR, respectively. Acute grade >2 GU and GI toxicity was 6.7% and 5% respectively. Acute toxicity trended back to baseline by 6 months in all patients except one. Late grade > 2 GU and GI worst toxicity was seen in 10% and 4.2%, respectively. As with acute toxicity, late toxicity tended to improve over time. Only one patient experienced severe toxicity (Grade 3 GU - frequency) at 6 months but subsequently this resolved. HRQoL will be reported separately.

CONCLUSION

MRgHDR brachytherapy boost in conjunction with EBRT provides comparable biochemical outcomes compared to the literature. Severe toxicity rates were minimal. Further follow-up will determine if these outcomes are sustained.

UTDRO/STARS21 RESEARCH DAY ABSTRACTS – POSTER PRESENTATIONS

Poster Presentations: Section 1

06

Clinical Outcomes of Neuroendocrine Carcinoma of the Cervix: Retrospective Review from a Large Academic Cancer Center

Jason Fernandes, Anjelica Hodgson, Kathy Han, Mike Milosevic, Jelena Lukovic, Stephanie L'heureux, Sarah Ferguson, Anna Santiago, Jennifer Croke

PURPOSE

Neuroendocrine cervical cancers are a rare but aggressive malignancy associated with a poor prognosis and limited evidence to guide clinical decision-making. Our objective was to evaluate the patterns of practice and clinical outcomes of patients diagnosed with neuroendocrine cervical cancer at a large academic cancer center.

METHOD

This was a retrospective chart review of patients between January 2007 and December 2023 with biopsy positive neuroendocrine cervical cancer. Demographic, treatment, and clinical outcome data were extracted from the medical records and summarized using descriptive statistics. Overall survival (OS) was analyzed using the Kaplan-Meier method and was compared between those receiving primary surgery and primary radiotherapy using the Log-rank test. The Wilcoxon rank-sum test and Fisher's exact test were used to evaluate patient factors associated with primary treatment.

RESULT

In total, 32 patients were diagnosed with primary cervical neuroendocrine carcinoma between 2007 and 2023 and were included in our analysis. Median follow-up was 14.5 months, and median age at diagnosis was 52 (range 21-89), most (31.3%, 10/32) were stage IVB at time of diagnosis and 15.6% (5/32) were node-positive without evidence of distant metastases. Primary treatment consisted of surgery in 10 patients (31.3%) and chemo-radiation in 15 patients (46.9%), with the remainder of patients (7/32, 21.9%) unfit for radical therapy. The overall stages of those treated with primary surgery were 1A2-2A1, whereas primary chemo-radiotherapy was offered to patients from stages IB1-IVB. Among patients treated with primary surgery, 70% (7/10) received adjuvant concurrent chemo-radiotherapy followed by adjuvant chemotherapy. Of those treated with primary radiotherapy, 100% received concurrent cisplatin chemotherapy, 73.3% (11/15) received brachytherapy and 86.7% (13/15) received adjuvant chemotherapy. Adjuvant chemotherapy was a combination of cisplatin and etoposide, except in cases where either of the drugs may have been contraindicated. Median OS for the full cohort was 19 months (2-year OS 39%). Patients treated with primary surgery had significantly higher median OS compared to those treated with primary radiotherapy (39 vs 19 months, $p=0.04$). Patients treated with primary radiotherapy had significantly larger tumor size on diagnostic MRI compared to those treated with primary surgery (4.3cm vs. 1.8cm; $p=0.029$). No other patient factors were significantly different between the surgery and radiotherapy groups, including stage; however, this is likely due to the limited sample size. There was only a single long-term survivor among patients treated with primary chemo-radiation.

CONCLUSION

In our single institution review of neuroendocrine cancer of the cervix, primary surgery was associated with improved OS, however our sample size was quite limited highlighting the rarity of this malignancy and the importance of prospective, multi-institutional studies. Comprehensive molecular profiling is underway to help guide systemic therapy.

UTDRO/STARS21 RESEARCH DAY ABSTRACTS – POSTER PRESENTATIONS

Poster Presentations: Section 1

07 The Contribution of Inflammasomes and cGAS-STING in RT-Induced Cell Fate

Cindy Ha, Shirony Nicholson-Puthenveedu, Shane M. Harding

PURPOSE

Radiotherapy (RT) is a curative treatment modality for many solid cancers. Our group has previously demonstrated that activation of the cGAS-STING pathway by RT induces inflammatory cytokine production and subsequent stimulation of anti-tumour immunity in concert with immune checkpoint blockade treatment. We have identified three other proteins that contribute to inflammatory signalling after RT: AIM2 (Absent in Melanoma 2), NLRP3 (NOD-Like Receptor Pyrin Domain-Containing 3), and IFI16 (Interferon Gamma Inducible Protein 16). Each of these proteins contribute to form distinct protein complexes called inflammasomes that, like cGAS-STING, sense cytoplasmic DNA. Little is known about how inflammasome signalling may change after RT, or how inflammasomes may influence RT-ICB induced anti-tumour immunity. We hypothesize that RT induces inflammasome signalling to influence specific gene expression and cytokine profiles, in tandem with alterations in cellular fate with implications for systemic anti-tumour immunity triggered by radiotherapy.

METHOD

We will present ongoing work in which we show that pharmacological or genetic disruption of inflammasomes alters cytokine production post-RT. We also demonstrate that manipulation of cell fate through senolytic therapy or manipulation of caspase activity alters the balance of cytokine production post-RT.

RESULT

Together our data strongly implicates the role of several inflammasome complexes in the response of epithelial cells to RT.

CONCLUSION

Our work will also highlight the possible crosstalk between the cGAS-STING pathway and inflammasome complex pathway, both triggered by RT. Understanding and subsequent manipulation of cell fate, in part through inflammasome and cGAS-STING mediated activity, may be a therapeutic strategy to influence treatment responses, such as anti-tumour immunity, in cancer.

UTDRO/STARS21 RESEARCH DAY ABSTRACTS – POSTER PRESENTATIONS

Poster Presentations: Section 1

08

Machine Learning based Quality Assurance Optimization of Breast Radiation Therapy Peer Review

Christy Wong, Thomas G. Purdie

PURPOSE

Radiation therapy (RT) treatment planning is a rigorous and time-intensive process that involves simulating RT dose delivery to the patient with the goal of safety treating the target site while minimizing radiation to surrounding organs. This collaborative effort involves input from various professionals, including oncologists, radiation therapists, and medical physicists. In compliance with quality assurance (QA) protocols, each RT plan is presented at peer review QA rounds where it is evaluated by the multidisciplinary site team. This allows for the integration of multiple perspectives and opens discussion for pertinent issues and recommendations to avoid RT treatment errors. However, the efficacy of peer review QA rounds is hindered by increasing case numbers, demanding clinician schedules, and increasing complexities of plans that necessitate discussions. To address these inefficiencies, we propose utilizing innovative machine learning (ML) techniques to proactively identify complex RT cases and streamline the peer review process.

METHOD

We have access to over 2000 complete breast RT treatment plans with ongoing complexity evaluations performed by experts during weekly peer review QA rounds. Each RT plan is assigned a binary complexity score, with those necessitating a discussion labeled as complex (score=1) and those not initiating a discussion labeled as non-complex (score=0). We also document the sources of the complexities such as challenging patient anatomies and poor organ segmentation. Using this data, we will train an ML isolation forest classifier to identify outlier RT plans as complex cases. Subsequently, we will deploy and evaluate the efficacy of the model in a prospective peer review setting, assessing its ability to identify errors and prioritize cases necessitating discussion or replanning.

RESULT

The future ML classifier will proficiently identify and rank complex breast RT plans and their sources of errors, thereby facilitating efficient prioritization for review. ML performance will be evaluated using the true and false positive rates to calculate area under the curve (AUC) statistics related to accurate prediction of complexity scores by ML. In addition, we also be able to quantify the improvement of using ML for assigning the order of cases presented in peer review rounds by comparing it to our current, uninformed methods of patient order.

CONCLUSION

Our proposed ML platform aims to streamline the RT treatment planning process by optimizing multidisciplinary discussions during breast peer review QA rounds. By accurately flagging and prioritizing RT plans that require extensive review, it will enable earlier detection of potential RT treatment errors and allow the multidisciplinary team to render more efficient, objective clinical decisions. Further, the optimization of the peer review process will enhance collaboration within the multidisciplinary team, leading to improved standardization of clinical practice and faster and higher quality RT treatments for patients.

UTDRO/STARS21 RESEARCH DAY ABSTRACTS – POSTER PRESENTATIONS

Poster Presentations: Section 1

09

Dosimetric Outcomes of SBRT to Ultracentral Lung Tumors: Lessons from the SUNSET Trial

Rohan Salunkhe, David A. Palma, Andrew Warner, Houda Bahig, Joanna M. Laba, Pencilla Lang, George B. Rodrigues, Marie-Pierre Campeau, Marie Duclos, Thi Trinh Thuc Vu, Benjamin H. Lok, Srinivas Raman, Alexander V. Louie, Andrew Hope, Andrea Bezjak, Scott B

PURPOSE

The SUNSET phase I trial investigated the maximum tolerated dose for ultracentral (UC) lung tumors treated with stereotactic body radiotherapy (SBRT). Here we report a detailed spatial and dosimetric secondary analysis of the treatment plan and assess relationships between doses to targets, organs-at-risk (OARs) and clinical outcomes.

METHOD

Five Canadian institutions enrolled patients with UC primary lung cancer, cT1-3N0M0, and all received SBRT to a dose of 60 Gy in 8 daily fractions. Maximum dose (Dmax) was limited to 120% of the prescription. Targets were delineated as internal target volume (ITV) (combining gross tumor volume (GTV) across respiratory phases) expanded by 5 mm to form a planning target volume (PTV). All OARs including great vessels and bilateral proximal bronchial tree up to segmental bronchus were contoured at baseline. To evaluate OAR and target doses, planning datasets and treatment plans were imported into a central repository. Descriptive statistics were generated for baseline characteristics and dosimetry metrics. Univariable logistic regression and Cox proportional hazards regression modelling were performed to identify significant dosimetric predictors for related adverse events grade ≥ 2 (CTCAE v4.0), overall survival (OS) and local control (LC).

RESULT

All 30 enrolled patients (13 males, 17 females) were included in this sub-study. At median follow-up of 36.5 months, 9 patients (30.0%) experienced grade 2 adverse events and 1 patient (3.3%) each with grade 3 (dyspnea) and 5 (infection) attributed to treatment. Median ITV and PTV sizes were 11.3 cc (IQR: 6.2-26.8) and 34.4 cc (IQR: 21.9-62.2), respectively. PTV overlapped with at least one OAR for all patients, most commonly the proximal bronchial tree (PBT) or trachea (27/30). Additionally, a second overlapping structure was identified in 26/30 patients, most commonly the pulmonary artery (14/26) and esophagus (9/26). The mean overlap of first and second OAR with PTV were 0.95 cc (range: 0-4.2) and 0.7 cc (range: 0-4.7), respectively. The mean Dmax was 69.4 Gy (range: 64-72.5 Gy); all were within the PTV. Mean (\pm SD) PTV D98 was 56.1 \pm 7.8Gy, while D0.1cc of PBT, esophagus and pulmonary artery were 53.1 \pm 12.6Gy, 26.5 \pm 10.5Gy and 57 \pm 8.6Gy, respectively. On analysis, combined overlap volume (cc) of the two primary overlapping OARs with PTV was associated with statistically significant inferior LC (hazard ratio [HR] per 1 cc increase: 2.86, p=0.012); however, overlap volume was not associated with an increase in grade ≥ 2 adverse events (odds ratio [OR] per 1 cc increase: 1.17, p=0.49). There was no association between OAR doses (D1cc/D0.1cc) with toxicity. PTV under-coverage (D98) was not associated with worse LC (HR per 5 Gy increase: 1.54, p=0.68).

CONCLUSION

Within the dose constraints used in the trial, there was no relationship identified between OAR doses and toxicity. Local control decreased with increasing overlap of PTV with OARs, however, this was not associated with dosimetric under-coverage of the target.

UTDRO/STARS21 RESEARCH DAY ABSTRACTS – POSTER PRESENTATIONS

Poster Presentations: Section 1

10

Artificial Intelligence for Identification of Radiation-Related Toxicities from the Electronic Health Records of Patients with Head and Neck Cancer

Faisal Alfadli, John Mohan Mathew, John Waldron, Jennifer Kwan, Steven Aviv, Michelle ML Nguyen, Viktoia Mokriak, Christopher Pettengell, Philip Wong

PURPOSE

Radiotherapy-related late toxicities (RLT) impact the quality of life of head and neck cancer (HNC) patients. Progression of RLT is often subtle and its recognition is dependent on multiple visits, recorded within unstructured electronic health records (EHR).

This study details the process of tuning existing Artificial Intelligence (AI) platforms to identify RLT.

METHOD

The validated AI platform, DARWENTM, pre-trained on general clinical data, was fine-tuned and validated using data from HNC patients referred to a RLT clinic.

DARWENTM employed four models: relevance model (eliminates irrelevant sentences), subject detection model (determines RLT is related to the specific patient), assertion status model (determines presence of RLT), and query model (triangulates RLT, fine-tuned to adapt the engine to the concept of interest).

A rulebook defining each toxicity (dysphagia, fibrosis, osteoradionecrosis (ORN) and trismus) and the toxicity status (ground truth) was provided by a radiation oncologist. Data was split into a training and an unseen cohort.

Model queries were fine-tuned using the training cohort and run against an unseen cohort to determine toxicity status. Output was validated by comparing against manually curated ground truth clinical outcomes. The ground truth outcomes were reviewed by a second trained reviewer and discrepancies in the manually curated data were adjudicated. Models were further fine-tuned after adjudication. Overall accuracy, precision (positive predictive value), and F1 scores (harmonic mean of sensitivity and positive predictive value) were generated.

RESULT

Patients (n=207) were split into training (n=167) and unseen (n=40) cohorts.

Prior to adjudication, DARWENTM AI achieved overall accuracy of 53% (F1=0.66) for all toxicities. Precision of 42% for dysphagia (F1=0.33), 70% for fibrosis (F1=0.74), 86% for ORN (F1=0.88) and 53% for trismus (F1=0.50) was achieved.

After adjudication and further fine-tuning, DARWENTM AI achieved overall accuracy of 87% (F1=0.92) across all toxicities. Precision of 92% for dysphagia (F1=0.88), 100% for fibrosis (F1=0.93), 93% for ORN (F1=0.93) and 94% for trismus (F1=0.91) was achieved.

Running refined models on unseen cohort (759 notes with >1 million characters) took a mean (SD) of 4.01 (0.42) seconds for each toxicity.

CONCLUSION

This study demonstrates the feasibility and accuracy of fine-tuning existing AI to find patients experiencing RLT from EHR. For future work, AI should be tested on EHR from a real-world HNC cohort, with or without RLT. Automation of the adjudication process is yet another potential step towards optimizing the process for clinical settings. Further testing is warranted to train and deploy DARWENTM on fewer EHR documentation for continuous RLT monitoring and early detection.

UTDRO/STARS21 RESEARCH DAY ABSTRACTS – POSTER PRESENTATIONS

Poster Presentations: Section 1

11

Validating MR Hypoxia Detection in Prostate Cancer using pimonidazole and GLUT1

Martin Swinton, Michael Dubec, Damien McHugh, Ashwin Sachdeva, Christopher Moore, Diego F Sanchez, Pedro Oliveira, Claire A Hart, Vijay Ramani, Maurice Lau, Jeremy Oates, Noel Clarke, Gareth Price, Alan McWilliam, Marcel van Herk, Peter Hoskin, David Buck

PURPOSE

Intra-tumoral hypoxia is associated with a worse prognosis in prostate cancer. We aimed to develop a MR hypoxia detection protocol with the intent of identifying men with hypoxia who may benefit from treatment intensification.

METHOD

An MR hypoxia detection protocol was performed at 2 timepoints prior to radical prostatectomy in the Hyprogen trial (NCT05702619). Sequences were acquired on both a diagnostic 1.5 T MR and 1.5 T MR Linac and included Blood oxygen level-dependent (BOLD) sequences on room air (T2*air) and after breathing 100% O2 (T2*O2).

Patient-specific 3D-printed prostate moulds guided prostate whole organ dissection. Histological sections through the dominant lesion were stained for GLUT1 expression with a rabbit monoclonal antibody (clone EPR3915). GLUT1 staining intensity was quantified on HALO software as a tumour GLUT1 H-score (0-300). Median GLUT1 H-score defined the cut-off between low (LG) and high GLUT1 (HG) tumours.

Dominant prostatic lesion (DL) and non-malignant prostate (NP) regions were defined on T2W images and contours applied to T2* maps. Median T2* values within DL and NP were reported, averaged across both timepoints and compared using a two-sided paired t-test. A two-sided unpaired t-test compared LG and HG regions.

RESULT

11/13 patients received 2 MR scans. GLUT1 H-scores available for 9/13 patients and ranged from 95.8 – 194.7 with a median of 144.5.

Across all patients, T2*O2 values were higher than T2*air in both NP ($p<0.01$) and DL ($p<0.01$). In the HG population, T2*O2 was higher than T2*air in both NP ($p=0.02$) and DL ($p=0.02$). In the LG population T2*O2 values were higher than T2*air in the NP ($p<0.01$) but not in DL ($p=0.38$).

NP values for both T2*air and T2*O2 were higher in the LG population than HG ($p<0.01$ and $p=0.02$ respectively). DL values of T2*air and T2*O2 did not differ between the HG and LG populations ($p=0.43$ and $p=0.88$ respectively).

CONCLUSION

Our analysis used the GLUT1 intrinsic biomarker to define intraprostatic hypoxia. We provide evidence T2* sequences with oxygen challenge can differentiate hypoxic regions as more hypoxic (HG) tumours had lower T2*air and T2*O2 values in NP than less hypoxic (LG) tumours. Further analysis will compare the ability of T2* sequences to discriminate hypoxic tumours against other MR parameters; OE, IVIM and DCE, using both GLUT1 and the extrinsic hypoxia marker pimonidazole.

UTDRO/STARS21 RESEARCH DAY ABSTRACTS – POSTER PRESENTATIONS

Poster Presentations: Section 1

12 Prognostic value of baseline 18-FDG/PET parameters for disease burden in small cell lung cancer

Hillary Ho, Danielle Sacdalan, Benjamin Lok

PURPOSE

Small cell lung cancer (SCLC) is an aggressive disease characterized by early metastases and overall survival of less than 12 months. Clinically, SCLC is described as either limited stage (LS) or extensive stage (ES) depending on whether disease can be safely encompassed in a single radiation field. Treatment strategies that lead to durable remission in SCLC remain elusive. These challenges underpin the need for novel biomarkers to better guide clinical decision-making.

18-F fluorodeoxyglucose (FDG) positron emission tomography (PET) functionally images glucose metabolism rates in the body in the form of standardized uptake values (SUV). Total lesion glycolysis (TLG) reflects volumetric metabolism and is the product of maximum SUV (SUVmax) and MTV. MTV and TLG have been correlated with worse overall survival and could be a candidate for disease prognostication. The aim of this study was to investigate if MTV and its corresponding TLG is predictive of nodal burden extent and the number of distant metastatic sites.

METHOD

Patients with SCLC were prospectively accrued for a parallel epigenetics study and this study retrospectively analyzed 35 SCLC patients who received PET-CT scans before first line chemotherapy with approval from our institution's research ethics board. PET-CT scans were all contoured and analyzed for MTVs and SUVs using Raystation 10B. MTVs were quantified using an absolute SUV threshold value of 3.0g/mL to determine tumor and involved regional nodal (ntMTV), adrenal (aMTV) and liver (IMTV) metastatic volumes. TLG was computed as the product of MTV and SUVmax. The MTVs were stratified into "high TLG" and "low TLG" using a threshold TLG value and the two TLG groups were compared for correlation with extent of nodal involvement and number of distant metastatic sites. The comparison was done separately for ntMTV, aMTV, and IMTV.

RESULT

The study population was male (57%), former or current smokers (94%), with a median age at diagnosis of 70 (ranging from 50 to 85), median pack years of 50 (ranging from 0-100) and staged as LS-SCLC (14%) or ES-SCLC (86%) at diagnosis. It is hypothesized that higher TLG and MTV values will correlate with higher extent of regional nodal burden and more sites of metastatic disease.

CONCLUSION

PET-CT imaging features can be extracted and quantified in patients with SCLC. Ongoing work to correlate these PET-CT imaging features with clinical variables and outcomes is underway.

UTDRO/STARS21 RESEARCH DAY ABSTRACTS – POSTER PRESENTATIONS

Poster Presentations: Section 1

13

Deciphering Radioresistance Mechanisms in Head and Neck Cancer: A Genome-Wide CRISPR Exploration

Jacqueline H. Law, Pierre-Antoine Bissey, Isabella Kojundzic, Wei Shi, Kenneth W. Yip, Fei-Fei Liu

PURPOSE

Head and neck cancer (HNC) affects over 1 million individuals annually and is the seventh most common cancer worldwide. Radioresistance poses a significant challenge in HNC treatment. While some genes associated with radioresistance in HNC have been identified, a comprehensive assessment is lacking. This project aims to use genome-wide CRISPR screens to identify genes and pathways responsible for radioresistance in HNC.

METHOD

Genome-wide CRISPR screens were performed using the TKOv1 library on HPV-negative HNC cell lines. Cells were challenged with a radiation dose of 10 Gy and sequenced using the Illumina NextSeq 500 platform. MAGeCK analysis was used to identify significantly depleted gRNAs after irradiation. TCGA Pan-Cancer database was used to determine candidate genes where transcript expression negatively correlated with overall survival (OS). Candidate genes were validated through colony formation, DNA repair protein immunofluorescence, and migration assays.

RESULT

117 potential radioresistance genes were identified, with MMP14, CD44, and CALR ranking as the top hits. Transcript levels of these genes were inversely correlated with OS in radiation-treated HNC patients in the TCGA Pan-Cancer Atlas. Colony formation assays confirmed that the loss of these candidate genes increased radiosensitivity. Additionally, downregulation of at least one gene impaired cellular migration. Immunofluorescence analysis reveals that cells with downregulated candidate genes exhibit a deficiency in DNA repair.

CONCLUSION

This study enhances our understanding of the underlying mechanisms of radioresistance in HNC, a significant cause of mortality among HNC patients. Future investigations involving transcriptome analysis and functional characterization of pathways may reveal additional therapeutic targets, ultimately improving the outcomes of HNC patients receiving radiation treatment.

UTDRO/STARS21 RESEARCH DAY ABSTRACTS – POSTER PRESENTATIONS

Poster Presentations: Section 1

14

Serial 4DPET/4DCT imaging to predict long-term response after chemo-radiotherapy for locally-advanced non-small cell lung cancer

Daniel Tong, Alexander Sun, Andrea Bezjak, Mei Ling Yap, Xiang Y Ye, Jean-Pierre Bissonnette

PURPOSE

Potentially curative chemoradiotherapy (CRT) is the treatment of choice in locally-advanced inoperable non-small cell lung cancer (NSCLC). Locoregional relapse is common but potentially salvageable in the absence of distant disease. 4DPET/4DCT image features during a course of CRT have been shown to predict clinical outcomes, two years post-CRT completion, including overall survival (Bissonnette et. al, 2018, Radiother Oncol.). The impact on five-year outcomes and the predictive power of these image features 3-month post-CRT are not clear.

METHOD

In this prospective, REB-approved study, patients with LA-NSCLC receiving curative intent CRT had 4DPET/4DCT scans at 0, 2, 4, 7 weeks during CRT, and 3-month post-CRT. These patients were treated pre-Durvalumab approval (2010-12). Image features including V3SUV (volume represented by voxels with SUV>3), SUV50 (SUV>50% of SUVmax), Gross tumour volume on CT (GTV_CT) were analyzed and correlated with clinical outcomes (locoregional relapse-free survival (LRRFS), overall survival (OS)) at 2 years and 5 years using mixed-effect models for longitudinal data. The predictive power of the features identified associated with the outcomes were further assessed by area under ROC curve using logistic regression.

RESULT

Of 29 patients recruited, 25 completed all scans and were included for analysis. Median follow-up was 32 months. Median OS was 32 months and median LRRFS was 23.9 months. At 2 years, 15 were alive, 11 disease-free. At 5 years, 8 were alive and 6 disease-free. Five out of 6 that were relapse-free at 5 years remained disease-free at their last follow-up (median follow-up=120 months). Multiple image features at weeks 0 and 2 reached statistical significance for OS and LRRFS at 2 years, including V3SUV_tumor and nodal disease volume(V3SUV_t+n), V3SUV_nodal disease volume(V3SUV_n) and GTV_CT_n(LRRFS only). V3SUV_t+n and V3SUV_n at week 2 of CRT most strongly predicted LRRFS ($p=0.003$, AUC 0.80) and OS ($p=0.018$, AUC 0.76) at 2 years. No features at 3-month post-CRT were predictive of outcomes. No features were predictive of 5-year LRRFS and OS.

CONCLUSION

In this study of CRT without adjuvant immunotherapy, 5-year OS of 32% and LRRFS of 24% were observed, and the 3-month follow-up 4DPET/4DCT was not predictive of outcomes. 4DPET/4DCT at week 2 CRT has a potential to guide earlier salvage treatment in CRT non-responders.

UTDRO/STARS21 RESEARCH DAY ABSTRACTS – POSTER PRESENTATIONS

Poster Presentations: Section 1

15 Exploring Family Physician Training Needs to Improve Cancer Patient Care

Marissa Sherwood, Janet Papadakos, Kulamahan Kulasegaram, Maria A. Martimianakis, Edward Kucharski, Meredith Giuliani

PURPOSE

Family physicians have multifaceted roles in cancer patient care and oncology education among this group is unfortunately inadequate. This study explored the needs and perspectives of family physicians regarding their oncology training and experiences. As well, physician cancer care experiences, knowledge use, and continuing education practices were elucidated.

METHOD

The authors employed a qualitative approach with family physicians participating in semi-structured interviews. General practitioners in oncology were excluded. Purposeful sampling was used, with recruitment through Ontario regional primary cancer care leads and social media. Interviews were transcribed, and thematic analysis was conducted.

RESULT

Thirteen participants were interviewed-1.6:1 female: male, ages 30-39, practicing for an average of 9 years (0.5-30 years), with urban and suburban practices. Most trained in Canada as undergraduates and completed their residency in Ontario; 62% had participated in at least one oncology continuing medical education session. Three major themes emerged: delineation of roles, oncology knowledge and education, and palliative care. Participants reported role uncertainty after cancer diagnosis, with oncology teaching at all levels described as lacking relevance. Palliative care rotations were an avenue for oncology education and where participants returned to cancer care.

CONCLUSION

Changing existing teaching, information access, and avenues of oncology experiences may be the next step to supporting successful cancer care by family physicians.

UTDRO/STARS21 RESEARCH DAY ABSTRACTS – POSTER PRESENTATIONS

Poster Presentations: Section 1

16

Reduction of Radiation Induced Bone Fracture incidence using bone avoidance objectives for Radiotherapy planning of Lower Extremity Soft Tissue Sarcoma: Retrospective Chart Review

Hiba Othman, Anthony Griffen, Amy Parent, Charles Catton, Peter Chung, David Shultz, Colleen Dickie, Peter Ferguson, Jay Wunder, David Kirsch

PURPOSE

Evidence based bone avoidance objectives were established at our institution to try to reduce the incidence of bone fractures. Our objective is to evaluate the effectiveness of these objectives in radiotherapy planning on the incidence of radiation-induced fractures in LE-STS patients, utilizing modern image-guided radiotherapy delivery techniques and planning systems.

METHOD

: This is a retrospective chart review. All patients with LE-STS who received radical course of radiotherapy planned using evidence-based bone avoidance objectives between January 2005 and December 2020 at our institution were evaluated. The following radiotherapy (RT) planning objectives were extracted for fractured patients: Mean dose to bone, RT treatment volume (TV), maximum dose to a 2cc volume of bone, and volume of bone irradiated to ≥ 40 Gy (V40). Fracture site dose was determined by comparing radiographic images and surgical reports to fracture location on the RT dose distribution. Patient and tumor factors, treatment details, and patient survival and functional outcomes were extracted from medical records and compared between the fracture and non-fracture patient cohorts with findings displayed using descriptive statistics. The Chi-square test was used to analyze categorical variables and a student T-test was used to analyze continuous variables and T-test was used to compare means. Survival was estimated using the method of Kaplan-Meier

RESULT

Between January 2005 and December 2020, 700 eligible patients were assessed, 594 patients (84.9%) received preoperative RT, 103 (14.7%) received postop RT, and 3 (0.4%) both. At a median follow-up of 55 months, 10 patients (1.4%) developed radiation-induced fracture. Of the full cohort, 15 patients (2.1%) had an intramedullary nail, there was one fracture in this group and 20 patients (2.8%) had bone resection replacement with a prosthesis or an allograft. The mean time to fracture was 41.7 months. Fracture management varied from conservative treatment to amputation. Local recurrence occurred in 44 patients (6.3%) and 248 patients (35.4%) developed metastasis

CONCLUSION

The overall fracture risk is reduced with modern RT techniques and planning methods focused on bone protection.

UTDRO/STARS21 RESEARCH DAY ABSTRACTS – POSTER PRESENTATIONS

Poster Presentations: Section 1

17

Therapeutic Index Improvement with Use of Rectal Spacer and Focal HDR Boost for Localized Prostate Cancer in an MR-guided Brachytherapy Setting

Chopade P, Johnny C, Weersink R, Rink A, Lao B, Simeonov A, Di Tomasso A, Ballantyne H, Borg J, Beiki-Ardakani A, McPartlin A, Catton C, Raman S, Glicksman R, Chung P, Berlin A.

PURPOSE

Brachytherapy (BT) boost to the whole-gland (i.e., clinical target volume [CTV]) improves oncological outcomes in prostate cancer patients, albeit with higher likelihood of genitourinary (GU) and gastrointestinal (GI) toxicities. Magnetic resonance (MR) imaging can unveil the gross tumour volume (GTV) with high sensitivity and specificity (i.e., 86% (CI 82-89%) and 99% (CI 98-99%), respectively) in patients with localized disease, which also correlates with the most common area of local recurrence after radiation treatment. To improve the therapeutic index of BT boost, one potential approach is circumscribing it to the MR-depicted GTV (i.e., focal BT boost). Another approach is the use of rectal spacers, which significantly decrease the occurrence of radiation-related toxicities. However, their use is limited in ultrasound-guided BT given their echogenic noise limiting visualization of prostate and catheters. An MR-guided BT setting can converge the benefits of improved soft-tissue resolution and rectal spacers in the absence of device-related imaging artifacts. Herein, we present the results of a prospective study using rectal spacers for MR-guided focal BT boost combined with stereotactic body radiotherapy (SBRT) to the prostate

METHOD

Patients with localized prostate cancer and visible GTV on MR were enrolled in a prospective study (NCT00913939). All patients underwent insertion of rectal spacer under ultrasound guidance. Subsequently, patients received MR-guided HDR BT boost (15Gy in 1 fraction), followed by SBRT to prostate (33Gy to CTV, 30Gy to PTV, in 5 fractions). The present study reports on the first 73 patients enrolled.

RESULT

Seventy-three patients are included in this analysis, with a median follow-up of 42 months (IQR 30-57). Most patients (47/73; 64.4%) had Grade Group 2 disease; while 37 (50.7%) and 27 (37%) were respectively categorised as NCCN favourable and unfavourable intermediate-risk, and 9 (12.3%) high-risk disease. Thirty percent of patients received combinatorial ADT for a median duration of 6 months (IQR 6-20). Median number of BT catheters were 5 (IQR 4-7). Acute Grade 1 GI and GU toxicities were seen in 22 (30.1%) and 66 (90.4%) of patients, respectively. Only one case reported Grade 2 acute GU toxicity (dysuria). Late (i.e., 3-months after treatment) Grade 1 GI and GU toxicities were observed in 4 (5.5%) and 29 (39.7%) cases, respectively. There was a single case of late Grade 2 GU toxicity (haematuria). No incidence of acute or late Grade 3-4 toxicities was observed. Seven (9.6%) biochemical recurrence events were recorded, with an associated BCR-free survival of 83.7% at 5 years. Among those with BCR, 6 cases had recurrence localization by imaging: two local recurrences alone (both intra-prostatic outside the focal boost volume), while four had regional and/or distant recurrences.

CONCLUSION

MR-guidance allows the incorporation of rectal spacers to the BT treatment paradigm, which together with the use of focal BT boost combined with SBRT renders a favourable therapeutic index for men with localized prostate cancer.

UTDRO/STARS21 RESEARCH DAY ABSTRACTS – POSTER PRESENTATIONS

Poster Presentations: Section 1

18

Investigating PLOD2 as a Therapeutic Target to Overcome Metastasis in Radiorecurrent Prostate Cancer

Gavin Frame, Hon Leong, Roni Haas, Xiaoyong Huang, Jessica Wright, Michelle Downes, Paul C. Boutros, Thomas Kislinger, Stanley K. Liu

PURPOSE

Prostate cancer (PCa) is the second most common cancer in males, with 1 in 8 men developing the disease in their lifetime. For PCa, a common treatment strategy is external beam radiation therapy to the prostate. However, when cancer recurs (radiorecurrent PCa), it often behaves aggressively by invading into surrounding organs or spreading distantly. Radiorecurrent PCa metastasis is therefore a significant cause of morbidity and mortality that must be overcome to improve survival of advanced PCa patients. Proteomic analysis revealed the procollagen enzyme Lysyl Hydroxylase 2 (PLOD2) to be upregulated in our radiorecurrent, and highly aggressive, conventionally fractionated DU145 (DU145-CF) PCa cell line. Given its established function as a mediator of invasion in various other cancers, we sought to characterize the role of PLOD2 in the aggressive phenotype of our radiorecurrent PCa cells.

METHOD

Bioinformatic analysis was conducted using CPC-GENE and TCGA PCa patient datasets. In vitro invasion of PCa cells was assessed using Matrigel-coated transwells, and migration was assessed using uncoated transwells. The Chick Chorioallantoic Membrane (CAM) model was performed in collaboration with Dr. Hon Leong's lab to assess in vivo extravasation of PCa cells. PCa cells were treated with siRNA or the drug PX-478 24hrs prior to invasion, migration, or extravasation assay. Protein levels were detected by western blot. For RNA analysis, RNA sequencing was conducted on PLOD2 knockdown DU145-CF cells; results were validated by qRT-PCR.

RESULT

Bioinformatic analysis of clinical data revealed PLOD2 genomic amplification to be significantly associated with biochemical recurrence in PCa patients. Upon further examination in vitro, it was revealed that PLOD2 knockdown significantly reduces matrigel invasion and migration in our radiorecurrent DU145-CF cell line, in addition to numerous other PCa cell lines, including primary cells we derived directly from PCa patients. Using the in vivo chick Chorioallantoic Membrane (CAM) model, we confirmed that PLOD2 knockdown significantly reduces the ability of DU145-CF cells to extravasate from the CAM vasculature into the surrounding stroma, a critical step of the metastatic cascade. Since PLOD2 is known to be regulated by hypoxia-induced protein HIF1a, we explored whether PLOD2 expression could be inhibited by the HIF1a inhibitor, PX-478. Treatment with PX-478 reduced both HIF1a and PLOD2 protein expression, and significantly reduced invasion, migration, and in vivo extravasation in DU145-CF cells, thereby indicating its potential as a pharmacological inhibitor of HIF1a-associated PLOD2 in radiorecurrent PCa. Finally, RNA sequencing of PLOD2 knockdown DU145-CF cells revealed the long non-coding RNA LNCsRLR to be a novel downstream target of PLOD2, involved in promoting the invasive phenotype associated with PLOD2.

CONCLUSION

Together, our results demonstrate for the first time the role of PLOD2 in radiorecurrent PCa invasiveness, and point towards its potential as a therapeutic target to reduce metastasis and improve survival outcomes in PCa patients.

UTDRO/STARS21 RESEARCH DAY ABSTRACTS – POSTER PRESENTATIONS

Poster Presentations: Section 2

19

Computational and Experimental Investigation of the Applicability of X-ray PDT Using Gold Nanoclusters

Etain Davidson, Juan Chen, Greg Bootsma, Steve Ansell, Kevin Stampelcoskie, Cathleen Crudden, Gang Zheng, Catherine Coolens

PURPOSE

Photodynamic therapy (PDT) is a clinically approved treatment for different types of cancer. However, it ultimately faces limitations due to the shallow penetration depth of light. X-ray induced PDT has potential for the treatment of deep tissue cancer due to its better penetration depth through soft tissue. In previous studies different nanomaterials have been explored for X-ray PDT, but there is currently a knowledge gap surrounding the physical mechanisms of this proposed therapy and how they can be related to properties of nanomaterials. Gold nanomaterials have shown potential due in part to their biocompatibility and heavy metal cores. Nanomaterials made with heavy metals are attractive on account of their high atomic numbers, corresponding to higher X-ray attenuation coefficients. Nanoclusters have become a source of investigation, offering advantages over nanoparticles; they are atomically precise with known molecular weights and better characterized compared to nanoparticles, giving us more control over the system. This project aims to establish the x-ray and photophysical properties of novel gold nanoclusters using computational (Monte Carlo) simulations and absorbance/emission measurements.

METHOD

A polychromatic cone beam CT benchtop system has been adapted for x-ray and light emission measurements to quantify absorption of x-rays by the gold nanoclusters and their subsequent emissions. This is done using a movable x-ray spectrometer setup that can evaluate spherical effects, and the addition of a moveable optical spectrometer system with a fibre optic cable to pick up light emissions from the sample upon x-ray irradiation. The radioluminescence will be measured by the optical fibre and spectrograph setup while under x-ray irradiation, with the x-ray emission spectra collected simultaneously.

RESULT

Theoretical simulations have been done using the Monte Carlo toolkit EGSnrc and show emission spectra characteristic of gold for the first water soluble gold nanoclusters; Au₂₂(Lys-Cys-Lys)₁₆ and [Au₁₃(bisNHC-TEG)₅Br₂]_{Br}₃. Simulations have been run for pure gold as a control to compare the spectra and attenuation. Both simulations and experiments are run at 50, 80, 100, 120, and 225keV energies for comparison of energy effects on absorbance. A concentration of 400uM of gold cluster was used. Preliminary theoretical results show attenuation by the clusters matching the predications for attenuation by the NIST database. Currently the experimental setup for measuring scintillation has been tested with optical reference standards, and the x-ray spectrometer is being optimized.

CONCLUSION

Following this, we expect to analyze and obtain x-ray absorbance and light emission spectra for these different gold nanoclusters. These results will help elucidate the mechanisms behind X-ray PDT and their relationship to the structural properties of the gold nanoclusters. Furthermore, the system provides a foundation to screen nanomaterials for scintillation and other properties. Curating a library of nanomaterials and their photophysical properties will allow for selection of agents depending on the application.

UTDRO/STARS21 RESEARCH DAY ABSTRACTS – POSTER PRESENTATIONS

Poster Presentations: Section 2

20

Quantification of the Tumor Microvascular Response to Stereotactic Body Radiation Therapy Using Optical Coherence Tomography Angiography and Dynamic Contrast-enhanced MRI

W. Jeffrey Zabel, Hector Alejandro Contreras Sanchez, Warren D. Foltz, Costel Flueraru, Edward Taylor, Alex Vitkin.

PURPOSE

Stereotactic Body Radiation Therapy (SBRT) is a cancer treatment that involves the delivery of much higher doses of radiation in fewer fractions than conventional radiation therapy. Preliminary evidence has suggested that the high doses associated with SBRT lead to vascular ablation and thus the tumor vascular response to SBRT may be an important determinant of treatment outcome.

Speckle Variance Optical Coherence Tomography (svOCT) allows for high resolution (~10 μm) 3D imaging of the vascular network in a tumor xenograft window chamber mouse model enabling longitudinal vascular quantification. Dynamic Contrast Enhanced Magnetic Resonance Imaging (DCE MRI) is a more clinically applicable imaging modality however its limited spatial resolution (mm scale) may not be able to image the tumor microvasculature (μm scale). To overcome this 'resolution gap', we directly correlated high-resolution svOCT images of the microvasculature to the comparably lower resolution DCE-MRI in the same animals. The successful discovery of correlates between svOCT-derived microvascular information and DCE-MRI macrovascular metrics will support the use of DCE-MRI in the clinic for SBRT microvascular response monitoring potentially enabling personalized SBRT treatment adaptations.

METHOD

$n = 42$ mice were subcutaneously injected with human pancreatic cancer cells (BxPC3 cell line) and plastic window chambers were installed. Mice were exposed to several fractionation schedules: 20 Gy in 1 fraction ($n = 10$ mice), 30 Gy in 3 fractions ($n = 10$ mice), and 45 Gy in 3 fractions ($n = 10$ mice). $n = 12$ mice were kept as unirradiated controls. svOCT and DCE-MRI were performed at regular intervals before, during, and up to 2.5 months after SBRT. Tumor volume (TV) and the vascular volume fraction (VVF) were extracted from the OCT structural and microvascular images respectively and were longitudinally monitored.

RESULT

Control mice exhibited a consistent rise in TV and VVF. The TV for mice exposed to 20 Gy in 1 fraction exhibited a sharp drop after irradiation and then regrew back to their baseline values 2 months post-irradiation. TV for 30 Gy in 3 fractions showed a significant decrease with no signs of regrowth. VVF for 20 Gy in 1 fraction and 30 Gy in 3 fractions was not significantly different than VVF changes in unirradiated control mice. Experiments and data analysis for 45 Gy in 3 fractions are ongoing. For MR imaging the strongest correlation was found between svOCT's mean intervascular distance and DCE-MRI's time to peak contrast enhancement metric (Spearman correlation coefficient, $r = -0.81$, $P < 0.0001$).

CONCLUSION

The microvascular insights afforded by svOCT are important for understanding what role the microvasculature plays in determining treatment response during SBRT. Furthermore, linking svOCT micro-vascular metrics to DCE-MRI macro-vascular metrics provides a 'bridge' to the clinic so that microvascular information may be used to personalize/optimize a patient's treatment plan.

UTDRO/STARS21 RESEARCH DAY ABSTRACTS – POSTER PRESENTATIONS

Poster Presentations: Section 2

21

Leveraging hybrid PET/MR imaging to distinguish progression from radionecrosis post-radiosurgery

Michael Maddalena, Adam Farag, Paula Alcaide-Leon, David Schultz, Catherine Coolens

PURPOSE

Despite excellent local control of brain metastasis patients treated with stereotactic radiosurgery (SRS), potential tumour progression (TP) is observed during follow-up in up to 20% of cases. The lesion may also contain radionecrosis (RN), a by-product of SRS which appears indistinguishable from TP via MRI yet warrants a distinct treatment regimen. Proper diagnostic protocols are key in prolonging patient survival post-SRS, as up to 20% of all cancer patients develop brain metastases, a condition currently associated with a dismal 24-month overall survival rate of 8.1%. Currently, invasive post-surgical histopathology remains the only gold-standard confirmation of TP/RN. Thus, non-invasive imaging techniques with strong diagnostic accuracy are urgently required to improve patient stratification while minimizing harm. To address this requirement, we hypothesize that a novel image-based PET/MR classification protocol will distinguish tumour progression from radionecrosis in lesions post-SRS at a $\geq 80\%$ diagnostic accuracy/sensitivity/specificity threshold across all implemented classification methods.

METHOD

To date, eight adult patients with histopathologically confirmed TP or RN have been enrolled in an ongoing ethics board-approved clinical trial. All image datasets were co-acquired using a hybrid PET/MR platform. PET imaging utilizes the nuclide-based radiotracer 18-F-Fluorothymidine (FLT). Acquired static and dynamic FLT-PET datasets were analyzed using two methods: (i) a static PET standard uptake value (SUV_{bw}) estimation and, (ii) compartmental modelling of a 20-minute dynamic PET acquisition (dPET). dPET time-activity curves were fitted to a two-compartment model of tracer diffusion. Two parallel AI networks will be trained to classify lesion ROIs in each selected functional MRI (fMRI) sequence based on TP/RN prevalence: a feature-based machine learning approach utilizing normalized image radiomics as input, and a feature-independent deep learning approach utilizing direct imaging dataset input. AI classification results will be surveyed to assess accuracy, specificity, and sensitivity in TP/RN differentiation for each acquired fMRI sequence.

RESULT

The FLT-dPET derived kinetic parameters K_i and P_f suggest that dPET analysis can distinguish TP from RN in post-SRS lesions (0.063 ± 0.043 ; 0.304 ± 0.204 and 0.002 ± 0.0 ; 0.004 ± 0.001 respectively, $p < 0.05$), whereas RN cannot be separated from background FLT uptake in healthy tissues ($p > 0.05$). The best-performing radiomic features as selected by ANOVA f-score feature selection ($f = 185.06$, $p < 0.05$) as well as the top-3 most significant features were related to textural metrics, hinting at the importance of intensity-based image data for TP/RN classification and corroborating the relative inefficacy of geometrical features at distinguishing TP from RN.

CONCLUSION

Our study examined the accuracy of FLT-PET and DWI-MR protocols in classifying TP/RN of post-SRS brain metastasis lesions. Direct comparison of co-acquired PET/MR differentiation accuracy can advise future development of image-based protocols to favour patient stratification. Although effective treatments exist for both TP and RN cases, robust stratification is crucial due to the substantial divergence in treatment approaches.

UTDRO/STARS21 RESEARCH DAY ABSTRACTS – POSTER PRESENTATIONS

Poster Presentations: Section 2

22

Molecular Heterogeneity in Radiation Resistance and Metastatic Ability of NSCLC

Marina Martínez Cruz, Sebastian Urban, Johann Matschke, Alexander Schramm, Verena Jendrossek, Barbara M. Grüner

PURPOSE

Tumor cells possess the ability to adapt to diverse selection pressures. Related to this, it was seen that both metastatic ability and radiotherapy (RT) resistance require increased metabolic plasticity and antioxidant defense mechanisms. Non-small cell lung cancer (NSCLC) is characterized by a high degree of inter- and intratumor heterogeneity, due to both genetic and non-genetic sources. However, its impact on RT failure and cancer relapse remains unclear.

Own previous work showed that NSCLC cells with distinct metastatic abilities differ in their metabolic phenotypes, metastatic cells being the ones with the highest metabolic plasticity and resistance against oxidative stress. Thus, we suspect this specific subpopulation of cells might overlap with the one that displays RT resistance.

The overall hypothesis is that non-genetic intratumor heterogeneity and (metabolic) plasticity of cancer cells determine both metastatic ability and radiation response. We further hypothesize that distinct subclones respond differently to radiation and might mediate therapy resistance through clonal evolution.

METHOD

Therefore, our goal is to identify tumor cell subpopulations that confer resistance to radiation with distinct metastatic abilities, decipher the relationship between radiation response and metastasis and determine the underlying molecular mechanisms of this complex setting. To do so, we are going to do a sub-clonal analysis of two different cell subpopulations, primary tumor-derived and metastasis-derived cells, under radiation using barcoding technology.

RESULT

We have already seen some differences between these two subpopulations regarding their response to radiation, being metastasis-derived cells less tolerant to radiation than primary-tumor derived cells. We will expand this characterization in relation to DNA damage repair and metabolic changes.

CONCLUSION

In addition, and to help us to investigate whether resistance to radiation is inherent or acquired and if it has an impact on metastatic ability, we are going to perform a sub-clonal analysis of cells under radiation using barcoding technology combined with single cell transcriptome sequencing, which allows us to unravel the molecular mechanisms behind.

UTDRO/STARS21 RESEARCH DAY ABSTRACTS – POSTER PRESENTATIONS

Poster Presentations: Section 2

23

Spatial Dynamics of Cell States and the Tumour Microenvironment in Glioblastoma

Lombard Phoebe, Zaidi Mark, Wu Ronald, Mansouri Sheila, Zadeh Gelareh, Wouters Bradley.

PURPOSE

Glioblastoma (GBM) is a highly aggressive disease with poor overall survival rates that have not changed substantially in decades. One feature contributing to treatment resistance is the intricate morphological and phenotypic diversity inherent in GBM. Previous single-cell sequencing studies have demonstrated this phenotypic diversity and attempted to define core transcriptional states of GBM cells. This study proposes to characterize the spatial organization of these cellular states relative to hypoxia in GBM and identify potential mechanisms by which hypoxia may drive cellular state.

METHOD

Twelve samples from surgically resected GBM tumor masses were obtained as part of a clinical trial of patients administered the hypoxia marker pimonidazole prior to surgery. Spatial transcriptomics sections were processed with the Visium Spatial Gene Expression assay. Resulting data were integrated with public datasets and analyzed in Python and R. After quality control, Leiden clustering and Gene Set Enrichment Analysis identified enriched pathways per cluster. The degree of enrichment overlap (Jaccard distance) between Leiden clusters was then used for consensus clustering to determine groups of Leiden clusters with similar pathway enrichment.

To investigate mechanisms by which hypoxia may influence cell state, patient-derived glioma stem cells (GSCs) were cultured under normoxic and hypoxic conditions. ATAC-seq, ChIP-seq, and bulk RNA-seq were performed in GSCs to identify changes in chromatin, epigenetic, and transcriptomic state.

RESULT

By overlaying spatial transcriptomics sections with serial pimonidazole-stained sections, we constructed a pimonidazole-based hypoxia signature from differential gene expression in stained areas. This signature was used to identify hypoxic regions in spatial transcriptomic datasets, which spatially correlated with mesenchymal-like cellular states characterized previously in scRNA-seq studies.

Given the spatial transcriptomics resolution of 1-10 cells per spot, where each spot may contain a mix of cell states and types, a pathway-based computational approach was employed to validate the analysis of scRNA-seq derived states. This approach grouped per-sample clusters by similar gene set enrichment, revealing recurring cancer cell, neuronal, and immune programs characterizing transcriptional heterogeneity in the GBM microenvironment.

In GSCs, hypoxia was found to drive significant changes in epigenetic state. Interestingly, chromatin regions that close and result in reduced transcriptional output were enriched for neurodevelopment and differentiation related transcription factors. A set of genes was derived demonstrating differential accessibility (at the chromatin level) and expression (at the transcript level) under hypoxia. This signature showed strong spatial correlation with hypoxic regions in spatial transcriptomics data and was prognostic in TCGA data.

CONCLUSION

This work demonstrates that hypoxia spatially correlates with mesenchymal-like states and remodels the transcriptional and epigenetic landscape in GBM. Hypoxia-driven remodelling represses neurodevelopment programs, which may explain the emergence of mesenchymal-like states in hypoxic regions. The spatial associations of these states with hypoxia-driven gene regulation suggest a potential link between microenvironmental conditions and transcriptional phenotypes.

UTDRO/STARS21 RESEARCH DAY ABSTRACTS – POSTER PRESENTATIONS

Poster Presentations: Section 2

24

Elucidating the Drivers of Tumour Hypoxia: a Focus on PDAC

Ji Zhang, Pedro Boasquevisque, Anna Dvorkin-Gheva, Patrick Policicchio, Nicole Rapallo, Sabrina Ge, Nikolina Radulovich, Neesha Dhani, Ming-Sound Tsao, David Hedley, Faiyaz Notta, Marianne Koritzinsky, Rob Cairns, Bradly G. Wouters

PURPOSE

Hypoxia is present in most tumours and has been linked to poor prognosis, disease aggressiveness, and therapy resistance in a variety of cancers including pancreatic ductal adenocarcinoma (PDAC). The overall level of hypoxia within an individual tumour is also highly variable across patients and the underlying drivers of this diversity are currently unknown. To elucidate these potential drivers, we propose that the steady-state levels of hypoxia across patient tumours are strongly influenced by underlying genetic and/or transcriptional cell states that impact oxygen metabolism and hypoxia tolerance. The development of hypoxia gradients around perfused vessels is determined by oxygen metabolism, whereas tolerance to hypoxia determines how long cells can survive in oxygen-depleted environments.

METHOD

In collaboration with the Princess Margaret Living Biobank, we established a matched panel of 22 primary PDAC, PDX, and patient-derived-organoid (PDO) models that span the range of hypoxia observed in patients. Oxygen metabolism and glycolytic rates were characterized in PDOs using Seahorse XFe96. Hypoxia tolerance was measured by assessing PDO growth and regrowth under defined levels of oxygenation. We created a comprehensive immunofluorescence (IF) image analysis workflow to characterize microenvironment features including perfusion in the matching PDXs. Single-cell RNA sequencing was performed on 8 pairs PDOs following organoid formation, cultured under normoxia or exposed to 48h of 0.2% O₂.

RESULT

Across the PDOs there were significant and striking variations in both oxygen consumption and hypoxia tolerance. IF image analysis of PDXs confirmed the hypothesis that higher oxygen consuming PDAC have steeper hypoxia gradients, however a trend was observed for these tumours to have lower total hypoxia, potentially due to more severe hypoxic stress. Strong trend was observed for more hypoxia tolerant PDACs to have greater tumour hypoxia, and tolerance can influence the distance at which viable hypoxic cells can be found away from perfused blood vessels. These phenotypic characterizations will be combined with transcriptomic features and subtypes for classification and identification of features predictive of tumour hypoxia.

CONCLUSION

Using this dataset, we are evaluating the impact of phenotypic and genetic drivers of individual tumour hypoxia. These tumour-specific vulnerabilities can be targeted as potential hypoxia-directed therapies.

UTDRO/STARS21 RESEARCH DAY ABSTRACTS – POSTER PRESENTATIONS

Poster Presentations: Section 2

25 Investigating Interstitial Fluid Pressure: Analyzing Drug Transport through Cross Voxel Exchange Model and Dynamic Contrast Enhanced MRI

Janny Y. Kim, Noha Sinno, Warren Foltz, Michael F. Milosevic, Catherine Coolens

PURPOSE

Despite immense progress in cancer treatment, drug resistance in cancer patients remains a challenge due to tumour heterogeneity. Among various factors in the tumour microenvironment, interstitial fluid pressure (IFP) has been indicated as a main cause of drug resistance. Growing solid tumours accumulate IFP at their core due to defective vasculature and lymphatics. This pressure gradient induces fluid convection in surrounding normal tissues, creating a barrier obstructing the entry of large therapeutic molecules. To comprehend the interplay between IFP and drug resistance, a thorough investigation into their transport mechanisms is needed. Dynamic contrast-enhanced magnetic resonance imaging (DCE-MRI) and the novel Cross-Voxel eXchange Model (CVXM) offers the means to derive image-derived transport parameter maps (ImTPs). Augmenting the Tofts Model (TM), CVXM allows the measurements of both intra-voxel exchange (extravasation) and cross-voxel transport (diffusion and convection). It is hypothesized that the ImTPs from DCE-MRI and CVXM will help explore the intricate mechanisms between drug delivery, IFP, and the tumour microenvironment.

METHOD

The ME180 human cervical carcinoma xenograft model (n=9) was used for in vivo studies since IFP of ME180 has been extensively investigated. DCE-MRI was performed using a 7T pre-clinical scanner (Bruker) and Gadolinium-DTPA (Gadovist, Bayer) was used as a contrast agent. IFP measurements were taken immediately after DCE-MRI using a Millar microtip pressure transducer (SPR-1000, Millar) under ultrasound guidance. The dynamic change in concentration across timepoints was processed to generate the pharmacokinetic parameters using both the TM and CVXM.

RESULT

Tumour extravasation from both CVXM and TM showed high values near the periphery and small values in the center with poor vasculature, indicating lack of blood flow. Convection map from CVXM illustrated higher velocity at the tumour periphery than the center. Using the microtip pressure transducer, the range of actual IFP was determined to be from 3.5 to 24mmHg, with a mean of 11.8 ± 6.9 mmHg at the tumour center and 1.12 ± 0.8 at the periphery, which agrees with the reported range of IFP. The results indicated that the convection map from CVXM accurately illustrated the IFP gradient, showing increased velocity flow at the periphery and decreased velocity at the center. This characteristic of IFP gradient was further confirmed by microtip pressure transducer measurements.

CONCLUSION

IFP influences drug resistance in solid tumors. DCE-MRI combined with CVXM, aids in exploring cross-voxel mechanisms of drug transport, including extravasation, convection, and diffusion. Convection map from CVXM accurately illustrated the IFP gradient, showing increased velocity flow at the periphery and decreased velocity at the center. The findings from CVXM can help understand the heterogeneity in tumours and the aggressiveness of the tumour. This comprehension will pave the way for personalized treatments, such as immunotherapy or drug delivery through nanoparticles, customized to the unique characteristics of each patient's tumour microenvironment.

UTDRO/STARS21 RESEARCH DAY ABSTRACTS – POSTER PRESENTATIONS

Poster Presentations: Section 2

26 Automated Segmentation of Pancreatic Tumour Vascular in Optical Coherence Tomography Images

Elham Abouei, Yuheng Li, Jeffrey Zabel, Hector Contreras, Xiaofeng Yang, Alex Vitkin

PURPOSE

Speckle variance OCT (svOCT) provides 3D tissue microvasculature in vivo, thereby offering insights into the tumor microenvironment and enabling longitudinal monitoring of vascular response to radiotherapy (RT). We developed an automatic segmentation framework with the objective of enabling quantitative assessment of tumor microvascular network properties, such as vessel lengths and tortuosity to investigate pancreatic tumor response to both conventional RT and stereotactic body RT (SBRT).

METHOD

We propose a deep learning framework for automatic vascular segmentation in pancreatic tumor. For our algorithm, we adopted an encoder-decoder network which is well-suited to spatially aggregate feature maps across several scales. We developed a large-kernel convolutional neural network (CNN), utilizing the flexible STU-Net architecture. In the encoder of our network, we implemented 13x13x13 kernels instead of the traditional 3x3 x3 convolution kernels, allowing capturing larger spatial contexts for accurate segmentation. We also added squeeze-and-excitation modules to facilitate feature recalibrations. svOCT images were obtained with OCT system resulting in 8 μm and 15 μm axial and lateral resolution in air, respectively. 3D OCT images were acquired over a 6x6 mm² area with 800 A-scans per frame with 1.5 mm imaging depth in tissue over 7 weeks at different time points. We only employed a small dataset consisting of 10 svOCT images for the fine-tuning and testing of our proposed model since obtaining semi-manual segmentations is laborious task. These semi-manual segmentations were obtained using MATLAB to generate ground truth segmentations. Evaluation of automatic deep learning framework in comparison to ground truth segmentation was conducted using the Dice score.

RESULT

The average value of Dice scores were 0.79 ranging from 0.74 to 0.84. These relatively low Dice scores could likely be due to the challenges in accurately defining vessel boundaries inherent in svOCT images and the limited size of the dataset. Since the svOCT studies focus on relative changes in the derived microvascular metrics between control and experimental groups, and/or within the same group over time, the observed low Dice scores will likely suffice for practical applications.

CONCLUSION

The integration of OCT imaging with deep learning framework for automatic vascular network segmentation provides a promising approach for automating analysis of tumor vasculature, potentially facilitating the understanding of tumor progression and response to RT. Our next endeavor will focus on implementing our deep learning framework on a comprehensive svOCT dataset to refine our model and improve segmentation accuracy. Afterward, we will apply our segmentation results for quantitative analysis of control and irradiated mice to study tumor response to conventional RT and SBRT.

UTDRO/STARS21 RESEARCH DAY ABSTRACTS – POSTER PRESENTATIONS

Poster Presentations: Section 2

27

Prostate External Beam Radiation Therapy Treatment Planning on Deep Learning Enhanced Diagnostic CT Imaging

Aly Khalifa, Sangwook Kim, Junghyun Roh, Yunkyoung Jun, Christy Wong, Marc Vincent N. Barcelona, Jeff Winter, Tony Tadic, Alejandro Berlin, Chris McIntosh, Thomas G. Purdie

PURPOSE

Delays between diagnostic CT (dxCT) and radiation therapy (RT) simulation CT (simCT) imaging can be up to several weeks. Using standard-of-care dxCT imaging for RT planning can accelerate the diagnosis to treatment pathway, but differences in imaging parameters, couch top, patient pose, and anatomy exist. This study demonstrates the feasibility of RT planning on synthetic simulation CT (synCT) generated from dxCT to expedite RT timelines.

METHOD

We trained a deep learning model to produce a synCT from dxCT that replicate simCT image features. The model, based on the state-of-the-art CycleGAN architecture, was trained using registered dxCT and simCT image slices from 81 RT patients with prostate cancer. The trained model was used to generate synCT images for a separate test set of 11 patients. The dxCT, simCT, and synCT images of each test patient were all manually contoured, followed by RT planning on each image using a clinical automated RT planning model. The dxCT and synCT plans were compared to the ground-truth simCT plan of each patient based on institutional dose-volume acceptance criteria (paired t-tests; $p < 0.05$).

RESULT

Our deep learning model successfully replicated dxCT image features such as the treatment couch top and image field of view. RT plans for the three image types achieved all institutional acceptance criteria, except for PTV D1cc in which 91% dxCT and synCT plans passed. However, there were statistically significant increases in mean bladder D30 and D50 doses of dxCT and synCT plans of 718 cGy and 437 cGy, respectively, compared to the simCT plans. This discrepancy is a result of the full bladder preparation for simCT and no set bladder preparation for dxCT and resultant large simCT volume and smaller dxCT volume.

CONCLUSION

This study shows the feasibility of producing clinically acceptable RT plans on synthetic simulation images generated using deep learning and the potential to eliminate the requirement for redundant RT simulation imaging to expedite the RT process.

UTDRO/STARS21 RESEARCH DAY ABSTRACTS – POSTER PRESENTATIONS

Poster Presentations: Section 2

28

CRISPR Screen of Druggable Targets in Small Cell Lung Cancer Identified ATM Inhibitor (AZD1390) as a Radiosensitizer

Xiaozhuo Ran, Bell Xi Wu, Mary Shi, Lifang Song, Kevin Nixon, Vivek Philip, Housheng Hansen He, Ming-Sound Tsao, Benjamin H Lok

PURPOSE

Small cell lung cancer (SCLC) is an aggressive and lethal form of lung cancer and the overall 5-year survival (OS) for patients is a dismal 7%. Radiation therapy (RT) provides some benefit for selected patients with SCLC but could be improved with radiosensitizing agents. In this study, we identified novel radiosensitizers for SCLC by a CRISPR-Cas9 screen and evaluated the efficacy of ATM inhibitor AZD1390 as a radiosensitizer of SCLC.

METHOD

We transduced the SCLC cell line SBC5 with a custom CRISPR sgRNA library focused on druggable gene targets and treated cells with RT. Cells collected at multiple timepoints were subjected to next-generation sequencing. We determined radiosensitization both in vitro with cell lines assessed by short-term viability and clonogenic assays, and in vivo mouse models by tumor growth delay. Pharmacodynamic effects of AZD1390 were quantified by ATM-Ser1981 phosphorylation, and RT-induced DNA damage by comet assay.

RESULT

Using a CRISPR dropout screen, we identified multiple radiosensitizing genes for SCLC at various timepoints with ATM as a top determinant gene for radiosensitivity. Validation by ATM knockout (KO) demonstrated increased radiosensitivity by short-term viability assay (dose modification factor [DMF]₅₀ = 3.25-3.73 in SBC5 ATM-KO) and clonogenic assays (DMF₃₇ 1.25-1.65 in SBC5 ATM-KO). ATM inhibition by AZD1390 effectively abrogated ATM Ser1981 phosphorylation in SCLC cell lines and increased RT-induced DNA damage. AZD1390 synergistically increased the radiosensitivity of SCLC cell lines (cell viability assay: SBC5 DMF₃₇ = 2.19, SHP77 DMF₃₇ = 1.56, H446 DMF₃₇ = 3.27, KP1 DMF₃₇ = 1.65 at 100nM; clonogenic assay: SBC5 DMF₃₇ = 4.23, H1048 DMF₃₇ = 1.91), and in vivo murine syngeneic, KP1, and patient-derived xenograft (PDX) models, JHU-LX108 and JHU-LX33.

CONCLUSION

In this study, we demonstrated that genetically and pharmacologically (AZD1390) inhibiting ATM markedly enhanced RT against SCLC, providing a novel pharmacologically tractable radiosensitizing strategy for patients with SCLC.

UTDRO/STARS21 RESEARCH DAY ABSTRACTS – POSTER PRESENTATIONS

Poster Presentations: Section 2

29 Synthesis and Characterization of Auger Electron (AE)-Emitting [197Hg]Hg-NS4-TCO-Panitumumab Radioimmunoconjugates.

Arthur Chu, Conrad Chan, Parmissa Randhawa, Shaohuang Chen, Neil Weatherall, Valery Radchenko, Caterina Ramogida, Raymond Reilly

PURPOSE

Triple Negative Breast Cancer (TNBC) is an aggressive and poor prognosis subtype of breast cancer that lacks estrogen and progesterone receptors and HER2. There are few targeted therapies for TNBC. However, overexpression of EGFR is found in 60-90% of TNBC, thus panitumumab (Pmab), a high affinity ($KD=10^{-11}$ M) anti-EGFR monoclonal antibody may be used as a vector to target therapeutic radionuclides to TNBC. ^{197}Hg ($t_{1/2}=64.1$ h) emits abundant subcellular range Auger electrons (AEs) that cause lethal DNA double-strand breaks in BC cells due to their high linear energy transfer (LET). A novel bifunctional chelator NS4-Tz for ^{197}Hg that harbors a tetrazine (Tz) side-chain may be conjugated to Pmab via click chemistry after transcyclooctene (TCO)-modification of Pmab. Our aim was to synthesize and characterize [197Hg]Hg-NS4-TCO-Pmab as an AE radioimmunotherapeutic agent for TNBC.

METHOD

Reaction conditions for Pmab with TCO-NHS ester were optimized to yield 8-10 TCO per Pmab. These immunoconjugates (ICs) were purified by ultrafiltration on a 30 kDa MWCO Amicon filter. The number of TCO per Pmab was determined by MALDI-TOF mass spectroscopy (MS). Reaction conditions for conjugation of NS4-Tz to Pmab-TCO were optimized to yield at least 4 NS4 per Pmab. These ICs were purified by ultrafiltration and buffer exchanged into H₂O containing 1% DMSO. The number of NS4 per NS4-TCO-Pmab was determined by MALDI-TOF MS. NS4-TCO-Pmab (40 μg) were labeled with 10 MBq of [197Hg]HgCl₂ in 400 μL of 1 M NH₄OAc, pH 7 and purified by ultrafiltration into PBS, pH 7.0. The radiochemical purity (RCP) of [197Hg]Hg-NS4-TCO-Pmab was measured by instant Thin-Layer Chromatography (iTLC) in 50 mM DMSA, pH 4.5–5. The binding of [197Hg]Hg-NS4-TCO-Pmab (40 nM) to EGFR-overexpressing MDA-MB-468 human TNBC cells was determined with/without a 100-fold excess of Pmab to measure total binding (TB) and nonspecific binding (NSB), respectively. Specific binding (SB) was obtained by subtracting NSB from TB.

RESULT

Pmab (30 mg/mL in PBS, pH 9.5, 25°C, 1 h) reacted with a 100-fold excess of TCO-NHS-ester yielded 8.1 ± 1.3 TCO per conjugate. Pmab-TCO (3 mg/mL in PBS, 37°C, 1 h) reacted with a 30-fold excess of NS4-Tz yielded 4.1 ± 0.1 NS4 per conjugate. The RCP measured by iTLC was $49.9\% \pm 3.4\%$ and $68.7\% \pm 0.6\%$ before and after purification, respectively. [197Hg]Hg-NS4-TCO-Pmab binding to MDA-MB-468 cells was competed by excess Pmab. SB of [197Hg]Hg-NS4-TCO-Pmab to EGFR was $91.0\% \pm 2.0\%$.

CONCLUSION

[197Hg]Hg-NS4-TCO-Pmab was synthesized and bound specifically to EGFR-overexpressing MDA-MB-468 human TNBC cells. RCP measurement by iTLC may underestimate the true RCP of [197Hg]Hg-NS4-TCO-Pmab post-purification. Future research will include further optimization of RCP assays, studies of binding and internalization of [197Hg]Hg-NS4-TCO-Pmab into TNBC cells and in vitro clonogenic assays to determine the cytotoxic effects of AE emitted by [197Hg]Hg-NS4-TCO-Pmab.

UTDRO/STARS21 RESEARCH DAY ABSTRACTS – POSTER PRESENTATIONS

Poster Presentations: Section 2

30

Identifying Immune Resistance Mechanisms in Locally Advanced Anal Cancer - Preliminary Results from the GRECIAN Study

Robert Samuel, Fay Ismail, Karen Scott, Emma West, Andrew Renehan, Natalie Cook, Sarah Brown, David Sebag-Montefiore, Adel Samson

PURPOSE

Chemoradiotherapy (CRT) is a common standard of care treatment for localised squamous cell carcinoma of the anus (SCCA). Patients with locally advanced disease have a risk of treatment failure of 20-30%. It is recognised that immune-mediated tumour cell death contributes significantly to the efficacy of radiotherapy. There is a strong scientific rationale for why immunotherapy may be able to reduce treatment failure in locally advanced SCCA. The IdentifyinG Radiotherapy and Immune ResistanCe Mechanisms In Anal CaNcer (GRECIAN) study investigated the expression of various immune cell subtypes and checkpoint proteins in peripheral blood mononuclear cells (PBMCs) in patients with locally advanced SCCA undergoing CRT.

METHOD

40 patients were recruited across 3 centres (Leeds, Manchester, Oxford). Bloods were taken at 6 timepoints before, during and after CRT and PBMCs isolated. Immunophenotyping by flow cytometry was performed. Differences between patients with complete response and treatment failure were assessed on CD4+, CD8+ and Regulatory T-cells (Tregs).

RESULT

Select preliminary results from 13 patients are presented - 7 with complete response and 6 with treatment failure. Patients with treatment failure had higher Tregs at baseline, maintaining this difference throughout treatment. For all patients, expression of PD-L1 and CTLA-4 increased during treatment, peaking at the end of treatment before returning towards baseline by 3 months. Patients with treatment failure had statically significant higher expression of PD-1 and PD-L1 at baseline on CD4+ cells and PD-L1 and TIGIT on CD8+ cells. Similar trends were seen for other markers, but differences did not reach significance due to low numbers.

CONCLUSION

Preliminary results from the GRECIAN study suggest that immune resistance mechanisms may explain some differences in treatment response to CRT for SCCA. Further analysis of more patients and confirmatory analysis of baseline tissue is required

UTDRO/STARS21 RESEARCH DAY ABSTRACTS – POSTER PRESENTATIONS

Poster Presentations: Section 2

31

Characterization of a Dual-Energy CT Protocol for Radiation Treatment Planning

Heather M Young, Catherine Coolens, Harry Keller, Hedi Mohseni

PURPOSE

Dual-energy CT (DECT) has many potential applications in radiation oncology including metal artifact reduction [Bamburg et al. Eur Radiol. 2011], improved visualization of iodine contrast [Lam et al. Am. J. Neuroradiol. 2015], and calculating stopping power ratios for improved proton dosimetry [Zhu and Penfold. Med Phys. 2016]. Before DECT can be used in CT simulation and treatment planning, there is a need to characterize the DECT imaging protocols and compare them to current single-energy CT (SECT) protocols.

METHOD

A Sun Nuclear multi-energy phantom and a Catphan 500 phantom were imaged on a Canon Aquilion CT simulator using a clinical SECT (120 kV) simulation protocol and two dose-matched DECT (80 and 135 kV) protocols. The dual-energy images were acquired using a helical acquisition and a step-and-shoot volume acquisition, both with 40 mm beam collimation to match the clinical protocol. All DECT protocols were evaluated using a 120kV-equivalent scan generated on the CT scanner workstation using a blend of the 80 kV and 135 kV images. All image analysis was completed using Matlab code developed in our institution. In the multi-energy phantom, the measured CT numbers of the density inserts in the phantom were compared across all protocols. In the Catphan phantom, uniformity, high-contrast spatial resolution and low-contrast resolution were analyzed and compared across all protocols.

RESULT

The measured CT number of high-density inserts was up to 40 HU higher in the DECT images as compared to the SECT images (Iodine 15 mg/mL, Iodine 10 mg/mL, Calcium 300 mg/mL and cortical bone). For all other inserts, the CT number agreed within 10 HU (1%) across all protocols. Uniformity was better in the SECT image (1.6 HU) than the helical DECT (1.8 HU) and the volume mode DECT (2.4 HU) images, but difference this is not expected to be clinically significant. High-contrast spatial resolution was higher in the SECT protocol (7.7 line pairs/cm) than the helical DECT (7.0 line pairs/cm) and volume mode DECT image (5.3 line pairs/cm). Low-contrast resolution in the DECT images was visually decreased as compared to the SE images; 11 1% contrast objects were counted in the SECT image, as compared to 7 in the DECT helical image and 10 in the DECT volume acquisition image. Visually, there were no streaking artifacts present in any of the images.

CONCLUSION

The DECT protocols studied here resulted in lower image quality than a dose-matched SECT protocol. More work is needed to determine the clinical and dosimetric impact of these differences, and to optimize DECT protocols for CT simulation.

UTDRO/STARS21 RESEARCH DAY ABSTRACTS – POSTER PRESENTATIONS

Poster Presentations: Section 2

32

Evaluation of EZFluence for 2-field Breast Tangents Field-in-field Planning

Jie He, Raxa Sankreacha, Mithunan Modchalingam

PURPOSE

Adjuvant radiotherapy post-lumpectomy using field-in-field breast tangents plays an important role in the clinical management of breast cancer. These plans are often “forward planned” by manual generation and weighting of MLC segments. EZFluence, a tool developed by RADformation, can generate MLC segments based on set objectives and automate the segmentation process. The purpose of this work was to evaluate EZFluence for 2-field breast tangents planning in terms of plan quality and time savings.

METHOD

A total of 91 patients’ 2-field breast tangent plans were reviewed and replanned using EZFluence. The original beam arrangement was maintained for all replans. The evaluation was then conducted in three progressive phases. Phase I (40 patients) maintained the same number of segments and global max dose as the manual plans. Phase II (32 patients) simulated a more realistic planning process by allowing EZFluence to determine the number of segments while meeting the clinical protocol hotspot constraint of 105%. Finally, phase III (19 patients) was performed on “difficult” plans. A paired t-test was performed on the difference between paired plans for the following metrics: PTV V95%, V103%, V105%, and global max dose. The ipsilateral lung dose and heart dose were also compared. A total of 41 EZFluence plans were timed and compared to an average time of segmentation obtained through a survey of 10 planners to determine the time savings.

RESULT

For the phase I evaluation, EZFluence-generated plans showed a statistically insignificant change in the PTV V95% of +0.18% ($p=0.2952$). The V103% however, showed a significant reduction of 6.15% ($p<0.0001$). For phase II, EZFluence-generated plans again showed an insignificant change in the V95% by +0.29% ($p=0.15$). The V103% and global max dose, however, were reduced by 9.03% ($p<0.0001$) and 0.55% ($p<0.0001$). For phase III, EZFluence-generated plans again showed an insignificant change in V95% of -0.27% ($p = 0.27$), while showing a significant reduction in V103% and global max dose of 7.74% ($p = 0.0034$) and 1.45% ($p < 0.0001$). There was <1% change in the ipsilateral lung and heart doses across all plans, which was clinically insignificant. The average time of segmentation using EZFluence was 4 minutes, which was an 84.5% reduction of the 25.8 minutes required for manual segmentation.

CONCLUSION

Using EZFluence, there is a statistically significant improvement in the plan’s homogeneity. This was marked by a reduced V103% and global max dose for the same PTV V95% of manual plans. Owing to substantial time savings, EZFluence can increase planning efficiency, which greatly benefits a busy community cancer center that treats over 800 breast cancer patients using this technique every year.

UTDRO/STARS21 RESEARCH DAY ABSTRACTS – POSTER PRESENTATIONS

Poster Presentations: Section 2

33

Evaluation of bladder filling variability for cervical cancer patients undergoing radical radiotherapy

Claire Nelder, Cynthia Eccles

PURPOSE

Bladder volume (BV) variability is difficult to replicate for cervical cancer patients undergoing radiotherapy and has potential to impact dose to both target and organs at risk (OARs). Challenges in replicating a consistent BV, can include anatomical mismatch, increased time on treatment couch and need for a replan. This work assessed variation in bladder filling from planning CT (pCT) to on treatment imaging following the introduction of a bladder filling protocol. The dosimetric impact of BV variability was investigated.

METHOD

An ethics approved clinical trial (NCT03617133) for patients undergoing radical radiotherapy for cervical cancer required the introduction of a “comfortably full” bladder protocol. To achieve this, patients were asked to empty their bladder, drink 350mls of water and wait 30 minutes before scanning/treatment. Patients undergoing planning computed tomography (pCT) during the first month of the new drinking protocol were included in this retrospective analysis. pCT scans and daily cone-beam computed tomography (CBCT) were exported to Monaco treatment planning system. Bladder was contoured by a single observer, and BV variations from pCT were calculated for all fractions. Time from initial CBCT to beam-on, and annotations regarding details of the daily image registration (e.g., manual match or intervention from a senior radiographer (RTT) were included in the analysis. The prescribed treatment plan was overlaid on the daily CBCT to establish how often maximum bladder dose was exceeded, and to investigate dose to target and OARs. Descriptive statistics were used to determine trends.

RESULT

Nine pCT (including 2 rescans) and 175 CBCT for 7 patients were evaluated. Mean BV on pCT was 157.1cm³ (range 41.9–335.4). For all patients and fractions, the mean BV change from pCT of + 35 % (range + 164 % to -24 %). BVs varied from pCT \geq 50 % in 41 % of all fractions for all patients. At least 1 repeat CBCT was required on 38 of 175 fractions, with > 2 required on 4 fractions. Mean time from CBCT to beam-on was 21 minutes (range 5-171 minutes). Reasons for longer appointments included the need for patients to get off the bed to adjust bladder filling (#28), or to wait for image review by an RTT (n=199 fractions, range 3-24 fractions per patient). 6 of 7 patients spent > 45 minutes in the department \geq 1 treatment day. A trend in decreased BV variation and overall time to treat (from CBCT1 to beam-on) was seen from patients 1 to 6. To date repeat plan calculations have been completed in 4 patients.

CONCLUSION

This work confirms new patient bladder filling instructions requires a period of adaption. Work continues to assess the dosimetric impact of bladder filling variability.

UTDRO/STARS21 RESEARCH DAY ABSTRACTS – POSTER PRESENTATIONS

Poster Presentations: Section 2

34 Investigating NRF2-Mediated Radioresistance in HPV-Negative Head and Neck Squamous Cell Carcinoma Preclinical Models

Aakshi Puri, Meghan Lambie, Scott V. Bratman

PURPOSE

Head and neck squamous cell carcinomas (HNSCC) that are not driven by human papillomavirus (HPV) are associated with a higher likelihood of treatment resistance and recurrence compared to HPV-positive HNSCC. There are currently no genomic-guided treatments for HPV-negative HNSCC, meaning that patients do not benefit from precision medicine approaches. Thus, it is critical to understand the mechanisms underlying HNSCC progression to identify molecular targets and better stratify therapeutic options for patients. NFE2L2 encodes for nuclear erythroid 2-related factor 2 (NRF2), a transcription factor that plays a crucial role in responding to oxidative stress by regulating the expression of genes associated with cellular defense mechanisms. Mutations in NFE2L2 and its negative regulator, KEAP1, make up 25% of HPV-negative HNSCCs. Additionally, constitutive activation of NRF2 confers a growth advantage and causes resistance to chemotherapy and radiotherapy. We will elucidate the role of NRF2, identifying novel radiosensitizers to better guide therapeutic strategies for HPV-negative HNSCC patients.

METHOD

Using clonogenic and long-term viability assays measuring radiation response, we identified radioresistant and radiosensitive cells in a panel of 19 HPV-negative SCC cell lines. An area-under-the-curve (AUC) metric was used to measure cellular response to multiple doses of ionizing radiation. Reactive oxygen species (ROS) and DNA double strand breaks (DSBs) were quantified using DCFDA and γ H2AX assays, respectively. Radiosensitization was measured using the Δ AUC of varying drug doses of NRF2 inhibitor, ML385. NFE2L2 and KEAP1 were knocked down using RNA interference in radioresistant and radiosensitive cells, respectively.

RESULT

We identified 13 radiosensitive and 6 radioresistant cell lines out of the 19 HPV-negative SCC cell lines. There was a strong correlation between AUCs of the clonogenic and long-term viability assays (Pearson $r=0.74$, $p=3.0 \times 10^{-4}$). Six cell lines were consistently radioresistant ($AUC > 3.5$) in both assays. None of the cell lines contained mutations in the NRF2 pathway, and only 1/6 were radiosensitized by ML385 ($\Delta AUC=2$); this effect was not correlated with ROS or DSBs, yet was abrogated by NFE2L2 knockdown. KEAP1 knockdown cell lines were generated for ongoing functional characterization and for genetic screens to identify radiosensitizers in HPV-negative HNSCC.

CONCLUSION

We aim to identify the role of NRF2 in the treatment response of HPV-negative HNSCC. Although NRF2 is an important pathway in driving a radioresistant phenotype, the majority of radioresistant cell lines were not sensitized by NRF2 inhibition. Therefore, elucidating the molecular underpinnings of NRF2-mediated therapeutic resistance will be critical to identifying novel radiosensitizers with activity in HPV-negative HNSCC.

UTDRO/STARS21 RESEARCH DAY ABSTRACTS – POSTER PRESENTATIONS

Poster Presentations: Section 2

35 DNA Methylation Subgroup and CNV Mediates Response to Radiotherapy in Chordoma

Andrew Ajisebutu, Jefferey Zuccato, Vikas Patil, Jeffrey Liu, Justin Wang, Farshad Nassiri, Mohammed Hasen, Gelareh Zadeh

PURPOSE

Chordomas are rare aggressive primary bone cancers affecting the skull-base and spine. Standard of care treatment includes radical surgical resection and radiotherapy. Despite this, the overall survival at 10 years is only 40%, with most patients experiencing disease recurrence. Radiotherapy is a cornerstone in the treatment of chordomas, however the impact of radiotherapy remains incompletely described: not all patients appear to benefit, and many studies fail to replicate the finding of improvement in overall survival. Herein, we utilized our previously described DNA Methylation subgroups to examine sensitivity to radiation.

METHOD

We utilized a well annotated dataset of 68 patients from a multi-institutional 20-year series who had undergone whole genome DNA methylation profiling on the Illumina EPIC array. Copy number variance (CNVs) were extracted from the raw methylation data after normalization, with median intensity values calculated and converted to amplification and deletions defined as a log2 copy number ratio of over .3. Multivariable cox analysis and Kaplan Meyer analysis were then completed.

RESULT

Within our cohort we found that patients with a cellular molecular subtype who had received radiation had a significantly improved overall survival on cox multivariate analysis (median survival 17.3 years, $p=0.0208$) when compared to patients with an immune-infiltrative (median survival 6.0 years). The favourable nature of the cellular molecular subtype appeared to diminish if radiation was not given (median survival 1 year). This improvement in survival did not appear to be fully explained by simply delayed progression, as progression-free survival between irradiated immune-infiltrative and cellular subtypes did not differ significantly ($p=0.65$). A panel of 30 target genes were investigated through CNV analysis for association with this phenomenon, for which 3 were identified: ERBB2 deletion ($p<0.0001$), ERBB4 deletion ($p=0.00029$) and KRAS homozygous amplification ($p=0.0134$).

CONCLUSION

Overall, molecular subtype predicted through DNA methylation influenced the response to radiotherapy: patients with a cellular subtype have improved survival overall, which appears to be partially mediated through response to and enhanced response to radiotherapy which does not appear to be shared with their immune-infiltrative counterparts. Moreover, three target genes have been identified as potential targets that may be exploited to improve potentiate radiosensitivity in chordoma.

UTDRO/STARS21 RESEARCH DAY ABSTRACTS – POSTER PRESENTATIONS

Poster Presentations: Section 2

36 Comparison of Online Adaptation Strategies for Patients with Prostate Cancer Undergoing MR-Guided Radiation Therapy Using Dose Accumulation

Iymad R. Mansour, Chris D. Johnstone, Daniel Letourneau, Victor Malkov, Tony Tadic, and Jeff D Winter

PURPOSE

The advent of the integrated magnetic resonance linear accelerator (MRL) platforms has provided an opportunity to develop of treatment workflows that allow for adaptation of the radiation treatment plan on a fractional basis immediately before treatment delivery. Considering the Elekta Unity MRL, two workflows for adaptive therapy exist: 1. Adapt-to-Position (ATP) can be performed quickly and adapts treatment plans based solely on fractional changes in isocentre translation shifts between the reference and daily images; 2. Adapt-to-Shape (ATS) takes substantially more time and resources to adapt plans based on daily changes in patient anatomy and target/OAR contours, but is able to account for rotations and deformations between fractions. This works compares the ATP versus ATS online daily adaptive workflows by evaluating both target and organ-at-risk cumulative dose differences across the full course of treatment using dose accumulation.

METHOD

Dose accumulation was performed for 30 patients undergoing adaptive prostate stereotactic body radiation therapy on a 1.5 T Elekta Unity MRL. All patients were treated using ATS with either 3000 cGy in 5 with 110% Rx to CTV (3000/5; N= 19) or 4270 cGy in 7 (4270/7; N= 11). The ATP approach was retrospectively simulated for comparison for all 30 patients. For each adapted plan, the dose was mapped to the reference image using a hybrid image-intensity and structure-based deformable image registration algorithm. Accumulated dose volume histogram metrics for ATS and ATP were compared using corrected Wilcoxon signed-rank tests.

RESULT

For both fractionations, no statistically significant differences in accumulated D95 and D98 CTV coverage existed between ATP and ATS plans. However, some statistically significant differences in OAR metrics were observed. For the 3000/5 cohort, population average D5 to femur were 1167 +/- 74 and 1104 +/- 48 cGy for ATS and ATP, respectively (p-val: 1.24E-04) and average D50 to penile bulb were 470 +/- 383 and 370 +/- 249 cGy (p-val: 6.82E-04). Significant differences in bladder, rectum, or urethra differences were not observed which are the most clinically relevant OARs. Similar results were observed for the 4270/7 cohort.

CONCLUSION

Comparison of accumulated dose for ATP and ATS workflows reveal comparable target coverage and OAR doses. Although statistically significant differences in femur and penile bulb were observed, all other plan evaluation metrics were similar between ATP versus ATS workflows across 3000/5 and 4270/7 cohorts. Despite ATP generated plans performing more basic adaptations which do not explicitly consider individual anatomical variations, plans have comparable target coverage and OAR sparing to those created using ATS. Future work will investigate the impact of the planning target volume margin on the accumulated dose differences between ATP and ATS workflows.

UTDRO/STARS21 RESEARCH DAY ABSTRACTS – POSTER PRESENTATIONS

Poster Presentations: Section 2

37

Physical Dose Validation of Dynamic Treatment for Gamma Knife Radiosurgery

Benjamin Z. Tham, Dionne M. Aleman, Robert K. Heaton, Håkan Nordström, Catherine Coolens

PURPOSE

Dynamic treatment in Gamma Knife (GK) radiosurgery systems delivers radiation continuously with couch movement, and has the potential to give improved dose conformity and homogeneity, and faster treatment times. Existing GK dynamic treatment studies have focused only on computational simulations, and this study aims validate them with physical experimental measurements. The experiments aim to (1) address assumptions made with computational studies, such as treating a continuous path as discrete points, (2) investigate uncertainties in translating computed plans to actual dynamic treatment, and (3) determine ideal treatment planning parameters, such as interval distance for discretising paths, collimator change limitations, and minimum isocentre treatment times.

METHOD

A GK ICON radiosurgery machine is used, and a custom motion phantom is attached to the machine's mask adapter to move in one-dimensional superior-inferior motion. Phantom positioning accuracy is first verified through comparing against couch motion and computed doses. For dynamic treatment experiments, the phantom is moved with a program that reads the treatment plan's isocentre details, then carries out the motion continuously while the treatment machine delivers radiation. Measurements are done with increasing levels of motion complexity: varying speed, varying collimator sizes, varying both speed and collimator sizes, and finally extending the same measurements to simulated 2D motion by combining phantom and couch motion. Dose comparisons between phantom motion measurements and either couch motion measurements or dose calculations are analysed with 2 mm/2% and 1 mm/2% gamma indices, and both local and global gamma index calculations.

RESULT

Phantom positional experiments show a high accuracy, with global gamma indices for all dose comparisons $\geq 99\%$. Discretisation interval level, to approximate continuous paths as discrete points, give a close match with dose calculations when using 1 and 2 mm gaps. Complex 1D motion, including varying speed, collimator sizes, or both, as well as 2D motion with the same complexities, all show good dose matches with dose calculations: the scores are $\geq 92.0\%$ for the strictest 1 mm/2% local gamma index calculation, $\geq 99.8\%$ for 2 mm/2% local gamma index, and $\geq 97.0\%$ for all global gamma indices. Five simulated 2D treatments with optimised plans scored highly as well, with all gamma index scores $\geq 95.3\%$ when compared to stationary treatment, and scores $\geq 97.9\%$ when compared to plan calculated dose.

CONCLUSION

Dynamic treatment computational studies are validated, with dynamic treatment shown to be physically feasible and deliverable with high accuracy. A 2 mm discretisation level in treatment planning is proposed as the best option for shorter optimisation times while maintaining dose accuracy. Our experimental method enables dynamic treatment measurements using the existing clinical workflow, which may be replicated in other centres, and future studies may include 2D or 3D motion experiments, or planning studies to further quantify potential indication-specific benefits.

UTDRO/STARS21 RESEARCH DAY ABSTRACTS – POSTER PRESENTATIONS

Poster Presentations: Section 2

38

Liver Cancer Volume Changes during MR Guided SBRT

*Aisling M. Glynn, Saheli Saha, Michael Velec, Teodor Stanescu,
Juan Diaz Martinez, Pablo Munoz, Ali Hosni, Aruz Mesci, Cathy Rocca, Andrea Shessel, Tae Kyoung Kim, Laura A. Dawson*

PURPOSE

The MR-Linac (MRL) provides a platform for adaptive stereotactic body radiation therapy (SBRT). This study is aimed to 1) compare liver tumor volumes on multiphasic liver CT and MR simulation imaging to tumor volumes on MRL images and 2) measure changes in liver tumor volume during SBRT.

METHOD

A single center prospective MR imaging study was developed prior to implementation of MRL liver cancer SBRT. Patients with a diagnosis of hepatocellular carcinoma (HCC), cholangiocarcinoma or liver metastases, treated with SBRT using MRL or cone beam CT (CBCT) were eligible.

At the time of simulation, consenting patients underwent T2w and T1w multiphasic CT and multiphasic 3T MR liver imaging in exhale breath hold (standard of care 'gold standard'), as well as 1.5T MRL T2w-exhale navigator-triggered images (MRL0). Repeat MRL T2w images were acquired at the time of each SBRT fraction (up to 5).

Liver tumors were contoured twice on multiphasic simulation CT and MR imaging and on each MRL T2w image, by an GI radiation oncology fellow, with review from an experienced GI radiation oncologist. Liver tumor volumes on simulation imaging were compared to those from baseline MRL imaging (MRL0). Changes in liver volume from baseline MRL0 images to MRL T2w images obtained during SBRT were measured.

RESULT

From August 2019 to January 2023, liver tumors from 23 patients with 29 tumors, treated with MRL (22) or CBCT (7) guided SBRT were contoured on 23 multiphasic CT/MR images and 104 MRL images. Diagnoses included HCC without vascular invasion (6), HCC with vascular invasion (4), cholangiocarcinoma (2), mixed cholangiocarcinoma/HCC (1), liver metastases (11), from sarcoma (3), neuroendocrine (3), prostate (2), lung (1), colorectal (1) and parotid (1) cancers. Three patients had multiple tumors. The median gold standard MR/CT tumor volume was 39.3cc (range 2.8-346.1) and the median MRL0 tumour volume was 29.0cc (1.7-325.2). The mean time from MRL0 to MRL1 was 15 days (range 6-30).

All tumors were visible on all MRL images. Tumor volumes on MRL0 images were smaller than tumor volumes contoured on simulation MR/CT multiphasic images (gold standard) obtained on the same day, by an average of 9.5 cc ($p < 0.05$). Overall, there were no predictable tumor volume changes over SBRT. Data analysis is ongoing and expected to be completed by April 2024.

CONCLUSION

Liver tumor volumes based on T2wMRL images were systematically smaller than volumes based on multiphasic CT/MR images. This systematic difference needs to be considered when adapting to tumor changes during SBRT. There were no predictable trends in tumor volumes over the course of SBRT. The majority of tumor volumes were stable; however, unexpected tumor growth and shrinkage was seen.

UTDRO/STARS21 RESEARCH DAY ABSTRACTS – POSTER PRESENTATIONS

Poster Presentations: Section 2

39

Investigating the Role of Macrophages in Small Cell Lung Cancer to Enhance Immunotherapy Efficacy

Jalal M. Kazan, Vivek Philip, Tracy L. McGaha and Benjamin Lok

PURPOSE

The Inflamed subtype of small cell lung cancer (SCLC-I) differs from other subtypes (SCLC-A, -N and -P) by being highly infiltrated with immune cells and upregulating the expression of inflammatory genes. Current treatment for patients with metastatic SCLC involves platinum-based chemotherapy with anti-PD-1/-PD-L1 immunotherapy (IO), however IO efficacy is modest in all SCLC subtypes. Tumor-associated macrophages (TAMs) are the most abundant immune cells in SCLC tumors and exert an immunosuppressive activity. In this study, we aim to understand mechanisms driving TAMs' immunosuppressive functions in order to develop novel therapeutic approaches able to deplete immunosuppressive TAMs and to enhance IO efficacy.

METHOD

Polarization of monocyte-derived macrophages (from healthy blood donors) into either M1 (pro-inflammatory) or M2 (anti-inflammatory) states, upon culture with conditioned media (CM) from different SCLC cell lines of different subtypes, was assessed by qPCR. In addition, macrophage immunosuppressive activity was measured by T cell suppression assay, which assess T cell proliferation upon coculture with macrophages treated with different CM. Next, ligand-receptor interaction analysis was applied to the transcriptomic profiles of macrophages from two healthy blood donors, cultured with CM from three different SCLC cell lines of the -A, -P and -I subtypes, to infer which ligands/receptors might serve as a potential therapeutic target to deplete immunosuppressive macrophages.

RESULT

Upregulation of polarization genes (IL-1B, IL-6, TNF α , CCL22 and CD23) was only seen in macrophages cultured with SCLC-I CM. Although, T cell suppression was exerted by macrophages cultured with CM from all SCLC subtypes, the highest suppression was seen by macrophages cultured with SCLC-I CM. Ligand-receptor interaction analysis identified ADGRE5, CXADR and SDC2 as the most significant receptors upregulated in macrophages cultured with SCLC-I CM, which might be implicated in the observed immunosuppressive phenotype.

CONCLUSION

SCLC-I CM increases macrophage suppressive activity against T cells. Future experiments will validate if these receptors are associated with macrophage immunosuppressive phenotype and will be targeted/depleted in a syngeneic tumor mouse model aiming to enhance IO efficacy.

UTDRO/STARS21 RESEARCH DAY ABSTRACTS – POSTER PRESENTATIONS

Poster Presentations: Section 2

40

Investigating The Cell-Free Hydroxymethylome Of Small Cell Lung Cancer Patients Receiving Chemoradiation

Janice J.N. Li, Dangxiao Cheng, Gregory Schwartz, Scott Bratman, Geoffrey Liu*, Benjamin H. Lok*

*Co-supervisors

PURPOSE

Small cell lung cancer (SCLC) is an aggressive neuroendocrine carcinoma characterized by rapid tumour growth, early metastases, and poor prognosis. First-line treatments include various combinations of platinum-etoposide chemotherapy and radiation. Despite initial remission, most patients develop resistance and relapse within 2 years of treatment. Consequently, strategies for patient risk stratification and targeting mechanisms that underpin chemoradioresistance are vital for improving SCLC outcomes. Unfortunately, identifying biomarkers for SCLC remains a challenge due to the limited access to tumour tissue and the lack of targetable driver mutations. Investigating epigenetic mechanisms, such as dysregulated DNA hydroxymethylation (5-hydroxymethylcytosine, 5hmC), through a liquid biopsy approach offers a promising, non-invasive avenue for prognostication and understanding chemoradioresistance.

METHOD

In this study, blood plasma samples were collected from 102 SCLC patients seen at the Princess Margaret Cancer Centre at pre-treatment (N=102) and relapse (N=38) timepoints. Genome-wide profiling of cell-free 5hmC was examined using the 5hmC-selective chemical labeling (HMe-SEAL) assay. HMe-SEAL was also performed on sheared genomic DNA from peripheral blood leukocytes from 20 of the 102 SCLC patients and on 55 healthy, non-cancer controls (NCC) to refine the tumour-specific 5hmC signal. Samples will be sent in three batches for sequencing. Differential hydroxymethylation region (DhMR) analysis was used to compare 5hmC patterns between SCLC vs NCC, chemotherapy alone (N=23) vs chemoradiation (N=95), and pre-treatment vs relapse cohorts to delineate SCLC-specific, radiation-specific, and relapse-specific 5hmC patterns, respectively. Gene ontology and pathway enrichment analyses were conducted to further elucidate the biological relevance of the DhMRs.

RESULT

Of the 102 SCLC patients, 39 (38%) had limited-stage (LS-SCLC) disease and 63 (62%) extensive-stage (ES-SCLC) disease. 4 (10%) LS-SCLC and 19 (30%) ES-SCLC patients received chemotherapy only, whereas 33 (85%) and 41 (65%) received chemotherapy and radiation. Preliminary DhMR analyses comparing pre-treatment non-small cell lung cancer (NSCLC, N=70) and NCC (N=45) plasma samples revealed that enrichment of 5hmC at enhancers were important for differentiating between NSCLC and NCC. Enhancers are important distal DNA regulatory elements for transcriptional activation. We hypothesize that epigenetic reprogramming of enhancers via enrichment of 5hmC may be promoting cancer progression and treatment resistance, therefore driving differences observed in the hydroxymethylomes between SCLC vs NCC samples and pre-treatment vs relapse. Future directions include creating a cell-free 5hmC-defined prognostic classifier, using the DhMRs and unsupervised hierarchical clustering. Correlations will be examined between clusters and clinical outcomes, such as overall survival, to determine whether clusters have prognostic meaning.

CONCLUSION

This study elucidates how the SCLC hydroxymethylome contributes to tumorigenesis and chemoradioresistance. Importantly, the development of a 5hmC prognostic signature could improve SCLC patient risk stratification. This will allow clinicians to optimize treatment planning, as well as develop risk-adaptive, biomarker driven clinical trials to improve SCLC management and survival outcomes.

UTDRO/STARS21 RESEARCH DAY ABSTRACTS

01

A Machine Learning Tool for Prediction of Vertebral Compression Fracture Following Stereotactic Body Radiation Therapy for Spinal Metastases

Laura Burgess, Matthew Rezkalla, Geoffrey Klein, Batuhan Karagoz, Gonzalo Martinez Santos, Mobin Malmirian, Cari Whyne, Arjun Sahgal, Michael Hardisty

PURPOSE

Spine stereotactic body radiotherapy (SBRT) achieves impressive rates of overall pain response and local control. The most common complication following spine SBRT is vertebral compression fracture (VCF), this occurs at an estimated rate of 9% in a recent meta-analysis. Many clinical, radiographic and dosimetric factors have been found to be predictive of VCF including age, lytic disease, pre-existing fracture, spinal deformity, histology and radiation dose. There is interest in the development of a tool capable of predicting those at high risk for developing this potentially destabilizing condition, which may allow for prophylactic interventions. We aimed to develop a machine learning (ML) tool able to predict the development of VCF following spine SBRT.

METHOD

A retrospective review of a prospectively maintained database of spinal segments treated with SBRT was conducted. The database includes clinical, tumor and treatment information. ML models were compared to spine instability neoplastic scores (SINS), the current clinical standard for predicting spinal instability. Clinical, tumor and treatment factors were used as inputs in 4 ML models: logistic regression, neural network/multi-layer perceptron (MLP), support vector machine (SVM) and random forest (RF). Models were evaluated with respect to accuracy, precision, sensitivity and specificity in predicting VCF, and relative feature importance determined.

RESULT

Between 2008 and 2021, 1406 spinal segments were included within the database. Patients were followed by institutional protocol with clinical assessment and full spine magnetic resonance imaging every 2 to 3 months. The median age of patients was 63.8 years. The most common histologies were breast and non-small cell lung cancer. The most common dose fractionation was 24Gy in 2 fractions (47.1%). The majority of spines were SINS stable (53.2%). Most patients did not have a baseline VCF (81.1%); 7.4% of vertebrae went on to experience a VCF and 3.9% had progression of a VCF.

In predicting VCF, all machine learning models were more precise than SINS. Compared to SINS, RF, SVM and logistic regression models had improved sensitivity and MLP and RF models had improved specificity. Overall, the RF model outperformed SINS in all performance metrics. Based on the RF model, important factors increasing the risk of VCF were age at the time of treatment, extent of vertebral body collapse, performance status, pain, and spinal alignment.

CONCLUSION

Simple machine learning models using clinical, tumor and treatment specific data outperform SINS alone in the prediction of VCF following spine SBRT.

UTDRO/STARS21 RESEARCH DAY ABSTRACTS

02 Detection of Oligo-metastases in Oropharyngeal Carcinoma Following (Chemo) Radiation Therapy

Revadhi Chelvarajah, Ye Liu, Jie Su, Ali Hosni, Scott Bratman, John Cho, Ezra Hahn, Andrew Hope, John Kim, Brian O'Sullivan, Jolie Ringash, Jillian Tsai, John Waldron, Anna Spreafico, Enrique Sanz Garcia, David Goldstein, Christopher Yao, Li Tong, Shao Hui Huang, Andrew McPartlin

PURPOSE

The benefit of ablative therapy for oligometastases (oligo-DM) has been reported.¹ Early detection of oligo-DM vs polymetastases (poly-DM) may facilitate salvage treatment. This study investigates factors associated with detection of oligo-DM (≤ 5 lesions and ≤ 5 cm in size) vs poly-DM in oropharyngeal cancer (OPC) and subsequent disease outcomes.

METHOD

All OPC patients who developed DM ≥ 3 months after definitive (chemo)radiation (c/RT) in 2006-2019 were identified from an in-house prospective system. Tumor HPV status was ascertained by p16 staining. Frequency and timing of imaging surveillance after 3 months post c/RT was at clinician's discretion. DM detection was classified as symptomatic (DM or constitutional symptoms prompting imaging) vs asymptomatic. DM characteristic and outcomes were compared between oligo-DM vs poly-DM. Multivariable analysis (MVA) was performed for overall survival (OS) after DM.

RESULT

A total of 124/1666 (7.6%) consecutive OPC patients developed DM. Despite similar DM rate in HPV-positive (HPV+, 91/1287, 7.1%) vs HPV-negative (HPV-, 33/379, 8.7%) ($p=0.52$) patients, longer interval from c/RT to DM was observed for HPV+ vs HPV- (median 16.8 [range 4.3-93.8] vs 8.6 [4.6-60.4], $p<0.01$). There was a similar proportion of oligo-DM for HPV+ vs HPV- (46 [37%] vs 35 [38%], $p=0.75$). Oligo-DM was significantly more frequent in asymptomatic versus symptomatic patients (62% vs 42%, $p=0.049$). Scan intervals were shorter in oligo-DM vs poly-DM (median 7.9 vs 12.7 months, $p=0.03$) (Table 1). Thoracic metastasis (includes lung and mediastinum) was the most common DM site for both HPV+ vs HPV- (77 [85%] vs 30 [91%], $p=0.56$). Only patients with oligo-DM received DM-directed salvage ablative therapy (41% vs 0, $p<0.001$). Median follow-up from DM diagnosis was 2.6 years. OS at 3 years after DM was higher for patients diagnosed with oligo-DM vs poly-DM (32% vs 5%, $p<0.001$), and, among the oligo-DM subset, for those who received ablative salvage therapy (63% vs 7%, $p<0.001$). On MVA, salvage ablative therapy (Hazard Ratio [HR] 0.27 [95% CI 0.12-0.59], $p<0.01$) and HPV+ status (HR 0.52 [0.34-0.80], $p<0.01$) were associated with longer OS, while oligo-DM (HR 0.72 [0.45-1.16], $p=0.18$) and interval to DM detection (HR 1.00 [0.99-1.01], $p=0.51$) were not.

CONCLUSION

Lung is the most common DM site for both HPV+ and HPV- OPC. Despite similar DM rates, HPV+ DM tends to occur at a longer interval after primary treatment. Nearly one-third of OPC DM are oligo-DM regardless of tumor HPV status. Oligo-DM patients are more likely to be asymptomatic at time of diagnosis, and detected following a shorter surveillance scan interval. Patients with oligo-DM who received salvage ablative therapy, and HPV+ patients regardless of DM volume, had a longer OS following diagnosis of DM. Prospective studies assessing the utility of surveillance imaging to increase detection of oligo-DM in asymptomatic high risk OPC patients may help inform clinical practice.

UTDRO/STARS21 RESEARCH DAY ABSTRACTS

03

Role of Angiotensin Converting Enzyme Inhibitors in Genito-Urinary Toxicity Following Curative Radiotherapy for Bladder Cancer

Aarani Devi, Ananya Choudhury, Peter Hoskin

PURPOSE

Bladder preservation with transurethral resection of bladder tumour, neoadjuvant cisplatin-based chemotherapy followed by radiotherapy with a radiosensitiser is an established alternative to radical cystectomy for muscle-invasive bladder cancer (MIBC). Despite its efficacy, a subset of patients develop genitourinary (GU) and gastrointestinal (GI) toxicity, which can significantly impact the patient's quality of life. Recent studies involving men undergoing radiotherapy for prostate cancer have indicated that those taking angiotensin-converting enzyme inhibitors (ACEi) experience reduced GU toxicity. While ACEi demonstrated radioprotective effects in preclinical animal models, there is a lack of research focusing on patients treated for bladder cancer. We hypothesise that concurrent administration of ACEi diminishes the risk of GU toxicity in patients undergoing curative radiotherapy for bladder cancer.

METHOD

A comprehensive dataset of patients who underwent bladder preservation at a single large-volume cancer centre was collected, recording baseline demographics, drug history, treatment details, acute and late toxicity. Acute and late clinician-reported toxicity was assessed using CTCAE V5 grading weekly during treatment, as well as at 6 weeks and 12 months post-treatment. The statistical analysis was performed using Stata 18.0 SE with student t-tests for continuous variables and Chi-Square test for categorical variables to compare the outcomes. Multivariable logistic regression analysis was conducted to explore the association between ACEi use and GU toxicity outcomes while adjusting for potential confounding factors.

RESULT

All patients who underwent bladder preservation following the diagnosis of MIBC were identified between 2017 and 2022. A total of 387 patients were analyzed, with 103 receiving ACEi treatment and 284 not receiving ACEi treatment. Patient demographics reported no statistically significant differences in baseline characteristics, including age, Eastern Cooperative Oncology Group (ECOG) performance status (PS), tumour stage, and smoking status, between the two groups. On evaluation of acute GU toxicity of Grade ≥ 2 during treatment and at 6 weeks, there was no statistically significant difference between the ACEi and no ACEi groups, 40.5% vs 44.1%, $p = 0.81$ and 57.3% vs 55.6% $p = 0.92$. The late Grade ≥ 2 GU toxicity at 12 months post-radiation was also similar between the groups (ACEi vs no ACEi group, 18.6% vs 21.9%, $p = 0.56$), resulting in an odds ratio of 0.81 (CI 0.40 to 1.64, $p = 0.56$).

CONCLUSION

The study found no significant impact of ACEi administration on either acute or long-term GU toxicity. There were inherent limitations, including its retrospective nature and a relatively small sample size. Large, prospective studies are needed to investigate this hypothesis further.

UTDRO/STARS21 RESEARCH DAY ABSTRACTS

04

Re-designing PTV Margins for Proactive Planning Towards Adaptive Radiation Therapy for Bladder Cancer

Jie He, David Contella, Yongjin Wang, Jasper Yuen, Raxa Sankrecha, Grace Zeng

PURPOSE

Consistent bladder preparation is difficult to achieve for bladder cancer patients because of their disease. Traditionally, large PTV margins of at least 1.5 cm, suggested by literature, are employed in clinical practice to accommodate target variations. This results in a significant portion of the bowel being inside the PTV for many patients. In this study, we performed statistical analysis of inter-fraction bladder variations based on daily CBCT images and derived a new set of PTV margin options. This enables us to proactively prepare multiple plans with different PTV margins and perform adaptive plan selection, with the ultimate goal of reducing dose to the bowel as much as possible.

METHOD

Thirteen bladder cancer patients who received 44-50 Gy in 20-25 daily fractions between 2022-2023 at our center were included. Patients were instructed to empty bladder as much as they can prior to CT simulation and each treatment. CBCT was acquired daily and registered with planning CT by bony match, which resulted in a total of 278 CBCT image sets. The bladder was contoured in each CBCT, compared to that of the planning CT and the difference in 3D was calculated in six directions: Sup-Inf, Ant-Post and Rt-Lt. "Zero" was assigned to any negative expansion, i.e. when the CBCT bladder is smaller than the CT bladder. A new PTV margin was derived as mean expansion plus 2 standard deviations ($\mu+2\sigma$) in each direction, which corresponds to a 95% confidence level in normal distributions.

RESULT

The most significant expansion was observed in the superior direction with $\mu+2\sigma = 20$ mm. The inferior expansion's $\mu+2\sigma$ was only 11 mm since the bladder is constrained by the pubic symphysis. The posterior border varied more compared to the anterior, with $\mu+2\sigma = 14$ mm and 10 mm, respectively. This is expected considering the daily variations of rectum and sigmoid, both are located posteriorly to the bladder. Right and left directions' $\mu+2\sigma$ are 11 mm and 12 mm respectively. The slightly higher variation in left may be due to the descending bowel being on patient's left. Based on these results, we proposed a new PTV margin option with non-uniform expansion: [Sup, Inf, Ant, Post, Rt, Lt] = [20 mm, 11 mm, 10 mm, 14 mm, 11 mm, 12 mm].

CONCLUSION

Even with an empty bladder protocol, significant variations in bladder volume and shape are observed in bladder cancer patients undergoing radiotherapy. The variations are asymmetrical owing to pelvic anatomy. Our next step is to validate and determine a set of PTV margins for multiple plan preparation and perform adaptive plan selection in clinical practice in future.

UTDRO/STARS21 RESEARCH DAY ABSTRACTS

05

Dosimetric comparison of musculoskeletal sparing during breast radiotherapy with and without internal mammary nodal irradiation

Stephen Lowell Ciocon, Grace Lee, Mohammad Rahman, Leigh Conroy, Robert Bleakney, Jennifer Croke, Jennifer Jones, Emma Mauti, Eugene Chang, Melissa Weidman, Wey Leong, Phillip Ye, Amy Liu, Jennifer Kwan, Fei-Fei Liu

PURPOSE

Breast cancer is the most common cancer diagnosis among women in Canada. Up to 91% of women who undergo breast cancer treatment face shoulder-related complications including weakness, limited range of motion, stiffness, and discomfort. Integral to breast cancer treatment is radiation therapy (RT), which often includes targeting the internal mammary nodes (IMNs). However, the dosimetric impact of IMN irradiation on surrounding musculoskeletal (MSK) structures such as the chest wall, neck, and shoulder remains unclear. We aim to evaluate the impact of excluding IMN coverage on these MSK structures and optimize breast RT protocols to minimize patient toxicity. We hypothesize that omitting IMN coverage during breast RT will lead to a significantly reduced treatment volume and thereby dose to the neck, chest wall, and shoulder

METHOD

We are conducting a retrospective study at the Princess Margaret Cancer Center, involving 30 patients with biopsy-confirmed breast cancer who underwent lumpectomy and sentinel lymph node biopsy (SLNB) or axillary lymph node dissection (ALND), followed by whole breast radiotherapy (RT) with regional nodal irradiation (4005 cGy in 15 fractions), from January 1, 2022, to November 30, 2023. MSK structures such as the bones (ribs, scapula, humeral head, clavicle), muscles (sternocleidomastoid, trapezius, and others), and joints (glenohumeral, acromioclavicular) will be retrospectively contoured on the CT simulation images. Two radiation plans (with and without IMN coverage) will be generated for each patient using the RayStation system. Dosimetric parameters, including mean dose, maximum dose, minimum dose, near maximum dose, near minimum dose and volume receiving 20 Gy, will be recorded for each plan and compared to assess the effect of IMN exclusion on the MSK structures. Descriptive statistics will be used to describe the patient characteristics. Two-sided paired t-tests and Pearson's correlation coefficient will be used to compare dosimetric parameters and evaluate associations with patient and tumor characteristics.

RESULT

To date, a total of 7 patients (ages 45-82 years) have been included, comprising 4 patients (57.1%) with left-sided and 3 patients (42.9%) with right-sided breast malignancies. Tumor locations within the breast were distributed as lateral (n=4, 57.1%), central (n=2, 28.6%), and medial (n=1, 14.3%). Tumour categories were T1 (n=1, 14.3%), T2 (n=5, 71.4%), and T3 (n=1, 14.3%). Nodal categories were N0 (n=1, 14.3%) and N1 (n=6, 85.7%). Two radiotherapy plans (with and without IMN coverage) have been generated for the first 7 study patients. Data analysis is ongoing, anticipated for completion by May 2024

CONCLUSION

This study will investigate significant differences in radiation doses to MSK structures between breast radiotherapy plans with and without IMN coverage. The dosimetric impact of IMN coverage on the neck, chest wall, and shoulder will help inform the relative risks and benefits of IMN coverage.

UTDRO/STARS21 RESEARCH DAY ABSTRACTS

06

Cognitive Outcomes Following Proton versus Photon Radiotherapy for Children with Localized Non-Germinomatous Germ Cell Tumours: a Children's Oncology Group Study

David Y. Mak, Sunita Patel, Shannon MacDonald, Erin S Murphy, Arzu Onar-Thomas, Girish Dhall, Derek S. Tsang

PURPOSE

To determine if superior dosimetry with proton therapy (compared to photon therapy) is associated with better cognitive outcomes in children with non-germinomatous germ cell tumours (NGGCT) who are treated with radiotherapy.

METHOD

Dosimetric data for patients with non-germinomatous germ cell tumours (NGGCT) enrolled in stratum 1 of the Children's Oncology Group (COG) study ACNS1123 were obtained. Cognitive outcomes of these patients were examined at 9 and 30 months post-radiation treatment using the COG Standard Neuropsychological and Behavioral Battery (co-enrolled on COG study ALTE07C1), and compared between subgroups of patients who were treated with proton vs. photon radiotherapy.

RESULT

Current data demonstrates significantly lower mean doses to the supratentorial brain, cerebellum, and bilateral temporal, parietal and frontal lobes when treating with protons, compared to photons. Additional cognitive data has been acquired from participating COG sites at 9 and 30 months post-radiotherapy. It is currently being analyzed for measures of intelligence (IQ), processing speed, attention, memory, social/behavioural function, executive function, adaptive function, and quality of life. Subsequent statistical analysis and comparison between the proton and photon cohorts is currently underway.

CONCLUSION

Proton therapy for children with NGGCT currently demonstrates superior dosimetry, with the results of corresponding cognitive outcomes currently under investigation.

UTDRO/STARS21 RESEARCH DAY ABSTRACTS

07 Accelerated Hypofractionated Radiotherapy for the Definitive Management of Locally-Advanced Non-Small Cell Lung Cancer: A Systematic Review

Badr Id Said, Alexander Louie, Shahed Badiyan, Andrew Bang, Andrea Bezjak, Kevin Chua, Corinne Faivre-Finn, Yimin Geng, Feng-Ming Kong, Daniel Przybysz, Paul Martin Putora, Pablo Schuffeneger, Shankar Siva, Meng Welliver, Fiona McDonald, Stephen Chun

PURPOSE

Hypofractionated radiotherapy (RT) offers potential advantages over conventional RT in inoperable locally advanced non-small cell lung cancer (LA-NSCLC), including shorter treatment times and potentially enhanced biological effectiveness. However, systematic appraisals of its efficacy and safety are lacking.

METHOD

A systematic search was conducted on Ovid MEDLINE, Ovid Embase, Wiley Cochrane Library, and ClinicalTrials.gov for English publications from 2010 to January 26, 2023. Prospective studies and clinical trials investigating hypofractionated RT in LA-NSCLC (> 2 Gy per fraction) delivered alone or in combination with chemotherapy were included.

RESULT

We analyzed 30 studies with 1290 patients. The median RT prescription dose, fraction size and biologically effective dose BED(10) was 60 Gy (range 23-85.5), 3 Gy per fraction (2.2-8.5), and 82 Gy (41-118). The median OS for hypofractionated RT alone (reported by 10 studies) was 13.6 months (6-46), while the 1-, 2-, and 3-year OS was 77.2% (38-98), 50.9% (38-85), and 32.1% (29-61%), respectively. The median OS in patients treated with concurrent chemotherapy (in 12 studies) was longer at 25.85 months (13-38), with 1-, 2-, and 3-year OS rates reported as 74.75% (50-89), 56.15% (38-68), and 50% (49-61%). Rates of severe (grade 3+) esophageal and pulmonary toxicity were higher in patients receiving chemotherapy (range 0-17% and 0-17%, respectively) compared to hypofractionated RT alone (range 0-9% and 0-6%, respectively).

CONCLUSION

Hypofractionated RT for LA-NSCLC is a safe and viable treatment option in carefully selected patients unable to undergo standard treatment. However, its application requires careful patient selection and stringent dose constraints, especially when combined with chemotherapy. The integration of hypofractionated RT with emerging treatments, including immunotherapy and particle therapy, presents a promising area for future research, although optimal protocols remain to be established.

UTDRO/STARS21 RESEARCH DAY ABSTRACTS

08

Survival Analysis and Predictive Factors for Leptomeningeal Disease in Metastatic Breast Cancer

Badr Id Said, Katarzyna J. Jerzak, Veronika Moravan, Ellen Warner, Sten Myrehaug, Chia-Lin Tseng, Jay Detsky, Arjun Sahgal, Hany Soliman

PURPOSE

Leptomeningeal disease (LMD) is a fatal complication of metastatic breast cancer (MBC) characterized by the infiltration of cancer cells into the cerebrospinal fluid and leptomeninges of the brain and spinal cord. Despite advances in the management of MBC, the prognosis of patients with LMD remains poor. In this study, we aim to characterize the incidence, clinical characteristics and factors associated with the development and survival of LMD in MBC.

METHOD

We conducted a retrospective analysis of MBC patients treated with radiation therapy for brain metastases (BrM) between 2005 and 2019. LMD diagnosis was confirmed via magnetic resonance imaging (MRI). Multivariable analysis (MVA) was used to identify predictors of LMD, overall survival (OS), and brain-specific progression-free survival (bsPFS).

RESULT

Among 691 MBC patients, 161 (14%) developed LMD, with a significant number (31.1%) experiencing it as their first intracranial relapse. Younger age at breast cancer diagnosis, ER+ status, and previous surgical intervention for BrM were identified as significant predictors of increased LMD risk, with hazard ratios (HR) of 1.31 (95% CI: 1.11-1.54, $p=0.001$), 1.63 (95% CI: 1.10-2.40, $p=0.01$), and 3.04 (95% CI: 1.68-5.51, $p=0.0002$), respectively. Notably, HER2+ patients had better OS (HR 0.14, 95% CI: 0.04-0.48, $p=0.0003$) and bsPFS (HR 0.29, 95% CI: 0.13-0.63, $p=0.0008$) compared to HR+/HER2- patients. HER2+ systemic treatment, given either at or after LMD diagnosis, significantly improved long-term survival (>2 years) (Fisher's test both $p < 0.05$). Conversely, low Karnofsky Performance Status (KPS) (HR 10.55, 95% CI: 3.50-31.81, $p<0.0001$) and multiple BrMs (HR 7.0, 95% CI: 1.50-32.57, $p=0.01$) were associated with worse survival outcomes.

CONCLUSION

In the largest study of its kind in MBC, we identify younger age at breast cancer diagnosis, ER+ subtype, and prior surgical resection for BrM as key LMD predictors. These factors could inform targeted surveillance protocols for early LMD detection. Additionally, the significant benefits of HER2+ targeted treatments on long-term survivorship underscore the need for updated clinical protocols and further studies to integrate these treatments into standard care.

UTDRO/STARS21 RESEARCH DAY ABSTRACTS

09

Assessing the Hidden Curriculum in Medical Education – a Scoping Review and Residency Program’s Reflection

George J Li, Marissa Sherwood, Andrea Bezjak, May Tsao

PURPOSE

The hidden curriculum (HC) is becoming recognized as an important component of medical education. Despite this, the ideal method for measuring or assessing the HC, if one exists, remains unclear. The aim of this study was to review the literature for methods of assessing the HC either qualitatively or quantitatively in the context of healthcare education.

METHOD

We conducted a scoping review on methods to measure or assess the HC in accordance with the JBI Manual for Evidence Synthesis. Ovid MEDLINE, Ovid EMBASE, and Proquest ERIC databases were searched from inception until August 2023. Studies which focused on undergraduate and/or postgraduate healthcare education, including medicine, as well as other professions such as nursing, social work, pharmacy were included.

RESULT

Of the 141 studies included for full text review, 41 were included for analysis and data extraction. Most studies were conducted in North America and were qualitative in nature. Physician education was best represented with most studies set in undergraduate medical education (n = 21, 51%). Qualitative methods (n = 27, 66%) were more common than quantitative methods (n = 14, 34%). Assessment techniques included conducting interviews/focus groups (n = 19, 46%), cross section surveys (n = 14, 34%), review of written reflections (n = 7, 17%), and direct observation of the working environment by researchers (n = 2, 5%). Nine standardized quantitative assessments tools were identified, consisting of between 20 to 82 questions each. There were no examples of implementation into an educational program formally or longitudinally, and no studies reported on actions taken based on evaluation results.

CONCLUSION

While the HC has an increasing presence in the medical education community and literature, efforts to measure the HC in an actionable way have not been reported. We reflect on the HC’s impact on our residency program and discuss our quantitative and longitudinal approach.

UTDRO/STARS21 RESEARCH DAY ABSTRACTS

10

Comparative Insights into DNA Repair Pathways Responses in Proton versus Photon Radiation Therapy

Razan Hessenow, Xixi Lin, Carina Behrends, Aashish Soni, Emil Mladenov, Martin Stuschke, George Iliakis, Johann Matschke, Verena Jendrossek, Beate Timmermann

PURPOSE

Clinical radiation therapy (RT) constantly evolves to improve tumor treatment efficacy while minimizing damage to healthy tissues. An essential technical strategy is the use of particle beams, like proton beam therapy. Previous research, both external and internal, has hinted at variations in DNA damage and repair pathways, particularly double-strand breaks (DSBs). This study seeks deeper insights into the significance of specific DSB repair pathways, particularly homologous recombination repair (HRR), in cells exposed to SOBP proton RT compared to photon RT. Additionally, we aim to explore potential differences in metabolic requirements associated with cancer cell survival upon each type of radiation.

METHOD

To unravel HR's role in repairing photon or SOBP-induced DSBs, we created and utilized syngeneic cancer cells deficient in ATM (an essential DSB repair regulator by HR) and BRCA2 (a key HR factor), comparing them with their ATM- or BRCA2-proficient counterparts. Analysis included assessing γ H2AX foci accumulation (indicative of DSBs), Rad51 levels (an indicator of HR activation), cell survival, chromatid breaks generation, and cellular metabolic response (utilizing Seahorse technology and flow cytometry for reactive oxygen species and mitochondrial superoxide).

RESULT

Findings reveal a more pronounced role of HR in repairing proton-induced DSBs compared to photon RT, especially in cells exposed to SOBP RT. HR-deficient cells displayed slower chromosomal repair kinetics and reduced survival after proton radiation compared to photon radiation. Additionally, our data unveiled an increase in radiation-induced oxidative stress in cells exposed to proton RT, evident in both cellular and mitochondrial reactive oxygen species (ROS) generation. This heightened oxidative stress represents a novel facet in the comparative analysis between proton and photon radiation effects.

CONCLUSION

This study validates nuanced biological differences in DSB repair pathway preferences between photon and proton radiation, emphasizing the heightened importance of HR in repairing proton-induced DSBs. Additionally, it sheds preliminary light on potential variations in metabolic dependencies of HR-deficient cells exposed to proton RT, not observed with photon IR.

Acknowledgement:

This project received funding from the European Union's Horizon 2020 research and innovation program under the Marie Skłodowska-Curie grant agreement No 860245 (to BT), "Bundesministerium für Bildung und Forschung" (02NUK043B, COLLAR to GI; 02NUK061B to JM), Deutsche Forschungsgemeinschaft (DFG GRK2762/1 to VJ and JM), and (BMW: ESA-AO-IBER-2017, 50WB1836) (to GI).